

NACA TN 2801

NATIONAL ADVISORY COMMITTEE FOR AERONAUTICS

TECHNICAL NOTE 2801

INVESTIGATION WITH AN INTERFEROMETER OF THE
FLOW AROUND A CIRCULAR-ARC AIRFOIL AT
MACH NUMBERS BETWEEN 0.6 AND 0.9

By George P. Wood and Paul B. Gooderum

Langley Aeronautical Laboratory
Langley Field, Va.



Washington
October 1952

**CASE FILE
COPY**

NATIONAL ADVISORY COMMITTEE FOR AERONAUTICS

TECHNICAL NOTE 2801

INVESTIGATION WITH AN INTERFEROMETER OF THE
FLOW AROUND A CIRCULAR-ARC AIRFOIL AT
MACH NUMBERS BETWEEN 0.6 AND 0.9

By George P. Wood and Paul B. Gooderum

SUMMARY

The flow around a 12-percent-thick circular-arc airfoil at zero incidence was observed with an interferometer for small increments of free-stream Mach number from 0.609 to 0.896 with laminar and turbulent boundary layers. Mach number contours in the flow field and Mach number and pressure distributions on the airfoil were obtained. Conditions were determined along and at the bases of the shock waves that interacted with the turbulent boundary layer on the airfoil.

INTRODUCTION

Results of experimental investigations of the flow over airfoils at high subsonic Mach numbers have been reported in a number of papers. In some of these, pressure-distribution measurements on the surface of the model and schlieren photographs of the flow were obtained (refs. 1 and 2). In others (refs. 3 to 5), Mach number distributions in the flow field about the model were also obtained in addition to the distributions on the surface. Reference 6, however, indicates that there are some discrepancies among the data on the pressure distributions on the surface of circular-arc airfoils.

With regard to the flow fields, which have application to studies of interference phenomena and are useful in evaluating theoretical studies of the flow at high subsonic Mach numbers, available experimental data are limited. Most of the published results on the flow field were obtained by means of static-pressure orifices in the test-section walls, a technique by which it is difficult to obtain either a large number of test points or reliable data near shock waves. The interferometer technique offers the opportunity of obtaining greater detail in the flow field than could be obtained by wall pressure measurements.

An investigation of the flow past a 12-percent-thick biconvex circular-arc profile at zero angle of attack has been conducted in which

the interferometer technique was used. The purpose of the investigation was to obtain pressure distributions on the model and Mach number distributions in the field around the model with laminar and turbulent boundary layers and to study the conditions along and at the bases of the shock waves that occurred at the higher Mach numbers and that interacted with turbulent boundary layers. The range of free-stream Mach number was from 0.609 to 0.896. The range of Reynolds number per inch of model chord was from 0.39×10^6 to 0.60×10^6 .

SYMBOLS

c	chord
M	Mach number
p	static pressure
Δp	pressure difference across shock wave, $p_2 - p_1$
P	pressure coefficient, $\frac{p - p_0}{q_0}$
q	dynamic pressure
x	chordwise coordinate from leading edge of circular arc in direction of free-stream flow
y	coordinate normal to chord of circular arc
$y_{M=1.05}$	value of y at intersection of contour for Mach number 1.05 and shock wave
α	angle of attack
δ	angle of deviation of flow across shock wave
ϵ	angle of shock wave
ρ	density
Subscripts:	
o	free stream
1	ahead of shock wave
2	behind shock wave

APPARATUS AND METHOD

The wind tunnel in which the tests were made was a blow-down tunnel which was operated by use of dry compressed air from a storage tank. The air passed through an automatic pressure regulator, through a settling chamber, through a subsonic nozzle and test section, and then exhausted to atmosphere. The top and bottom of the test section were open to the atmosphere and the sides were closed and contained glass windows. The test-section height was 4 inches and the width was 5 inches. A cutaway view of the nozzle, test section, and model is shown in figure 1.

The basic model was a 12-percent-thick biconvex circular-arc airfoil with a chord of 1 inch and a span of 5 inches. The model was held in the tunnel by two struts that were attached to the lower surface of the model. In order to provide a larger field for the flow around the upper surface, on which observations were made, the model was placed off the center line of the tunnel, with the chord of the model 3 inches from the upper jet boundary and 1 inch from the lower. In order to reduce the intensity of the disturbances that were propagated forward from the wake of the model at the higher Mach numbers, a flat plate of 1 chord was attached to the rear part of the model for most of the tests at the higher Mach numbers. (See fig. 2.) For some of the tests a turbulent boundary layer was produced on the model. Two methods of producing turbulence were used. For one method a wire of 0.028-inch diameter was stretched across the test section about 1 chord ahead of the leading edge of the model. In the other method a different model was used, a plano-convex model (a profile formed by a circular arc and its chord), which was mounted on a flat plate, as shown in figure 2. The leading edge of the model was 1 chord behind the sharp leading edge of the plate. The Reynolds number of the present tests per inch of model varied from 0.39×10^6 at a free-stream Mach number of 0.609 to 0.6×10^6 at a Mach number of 0.880. The experiments were not carried to higher Mach numbers than 0.9 because structural limitations on the apparatus did not permit the use of higher stagnation pressures.

Observations were made by means of an interferometer that has previously been described (ref. 7) and that was used for taking the interferograms and also for taking a few shadowgraphs. (The shadowgraphs were made by blocking off one of the light paths through the interferometer.) The interferograms were analyzed to obtain contours of constant density by superposing flow and no-flow interferograms. During the analysis of the interferograms, two corrections were made. One correction was for the effect of the boundary layers on the walls. These boundary layers caused the effective path length of the light through the test section to be less than the actual geometric span of the test section. In order to determine the effective path length, static pressures

were read at a chordwise series of three static orifices in the model. From the pressures, the densities were calculated at the locations of the orifices. Then from the actual observed fringe shifts at these locations, the effective geometric path length was calculated and was found to increase with increasing free-stream Mach number from 4.5 inches at a Mach number of 0.6 to 4.7 inches at a Mach number of 0.9. The other correction was made to account for slight changes in reference, or no-flow, fringe spacing caused by vibration during a test. The correct reference fringe spacing was calculated for each interferogram from pressure measurements that were made at a static orifice in the model and at one in the glass window about $1\frac{1}{4}$ chords from the model.

The location of the orifice in the window, together with the pressure tube leading from it, is indicated in figure 1. These pressure measurements gave the ratio of the densities at the locations of the two orifices. From the ratio of the densities, the correct fringe shift between the locations of the orifices was calculated. An enlargement of the no-flow interferogram was made of the proper size (that is, proper fringe spacing) to give the correct fringe shift when superposed on an enlargement of the flow interferogram. The correction to the no-flow spacing, which was thus included in the analysis, was within the limits of ± 10 percent.

Because the airfoil was placed asymmetrically in the test section (3 chords from one boundary and 1 chord from the other), calculations were made to determine the magnitude of the effect of the jet boundaries. The airfoil was represented by a source-sink model and the first image of the model was used in the calculations. The calculations were made for a subcritical free-stream Mach number of 0.7 and showed that the effect of the asymmetrical location of the model was an induced camber of 0.1 percent. The magnitude of the effect of the proximity of the jet boundary on the velocity of the flow on the upper surface of the airfoil, which was 3 chords from the boundary, was also calculated and was found to be less than 1 percent.

All free-stream Mach numbers given herein should be understood to be "indicated Mach numbers" and were calculated as follows: Stagnation pressure in the settling chamber and atmospheric pressure were measured; from the ratio of stagnation to atmospheric pressure, the Mach number was calculated under the assumption that free-stream pressure was the same as atmospheric pressure.

RESULTS AND DISCUSSION

The results of this investigation are derived from interferograms of the flow about a circular-arc airfoil. In order to assist in the interpretation of the interferograms, a few selected shadowgraphs are compared in figure 3 with corresponding interferograms at the same flow conditions.

Mach Number Contours in the Flow Field

Interferograms of the flow about the basic 12-percent-thick biconvex circular-arc model at 0° angle of attack and about the modifications to the basic model are shown in figure 4 for a range of free-stream Mach numbers from 0.609 to 0.896. These interferograms have been analyzed to obtain contours of constant Mach number, which are also shown in figure 4. A few contours are shown in the region behind the shock waves. In determining these contours, the change in entropy through the shock wave was neglected. For the present investigation this approximation is very satisfactory, as the error in Mach number due to neglect of entropy increase is nowhere more than 1 percent on any of the contours actually shown in figure 4. On the interferograms that have a single, strong shock wave and, consequently, a large, abrupt pressure rise through the shock wave, the fringes bend sharply in the flow field just ahead of the shock wave. The bending indicates a rapid rise in density ahead of the shock wave but this rise is probably a spurious effect that is restricted to the neighborhood of the side walls and is due to the action of the pressure increase across the shock wave on the boundary layer on the side walls. When the interferograms were analyzed, the bending was eliminated by extrapolating the fringes from the unaffected region to the shock wave.

The free-stream Mach number at which sonic speed is first reached on the model lies between 0.725 (fig. 4(f)) and 0.761 (fig. 4(g)) at approximately 0.74. The steady increase in the size of the supersonic region as the Mach number of the free stream is increased is shown by figures 4(g) to 4(r). The contours also show the effects of a change in the character of the boundary layer on the shock waves and on the flow in the supersonic zone, effects that are generally well known after the work reported in references 1 and 2. In figure 4(l) the flow in the boundary layer on the airfoil has been made turbulent by a wire strung across the tunnel ahead of the leading edge of the model. Because the boundary layer is turbulent, the effect of the jump in pressure across the shock wave is not felt far forward of a small region near the base of the shock wave where the flow separates. A similar condition exists in figure 4(m) where the transition from a laminar boundary layer has been caused by a flat plate that extends ahead of the airfoil. In figures 4(l) and 4(m) the flow appears to separate near the base of the shock wave. In figure 4(n), however, the boundary layer is laminar and the flow appears to separate far ahead of the normal shock wave at the base of the oblique shock wave. Behind the region of separation of the laminar boundary layer is a region of nearly constant pressure, as shown by the very wide fringe. Recompression then takes place comparatively gradually through multiple shock waves. Similar comparisons can be made between figures 4(j) and 4(k) and figures 4(o) and 4(p). Figures 4(o) and 4(p), for example, show that with a laminar boundary layer the Mach number at the surface does not reach as high values as it does with a turbulent layer.

At the higher Mach numbers and when the boundary layer is turbulent, the flow expands all the way to the single shock wave. (See figs. 4(k), 4(l), 4(m), 4(p), 4(q), and 4(r).) The expansion, however, is not so large as it would be in Prandtl-Meyer flow that turned an equal amount around a corner. In the flow about the airfoil are compression waves from the sonic region that partially cancel the effect of the expansion waves from the surface. In figure 4(p), for example, the flow is turned 9° at the surface between the Mach number 1.00 and the Mach number 1.30 contours. If a flow at $M = 1.00$ is turned 9° by a pure Prandtl-Meyer turn, then a Mach number of 1.40 is reached.

The change in the shape of the Mach number contours in the supersonic zone from symmetric to asymmetric is shown by the series of plots in figure 4. Up to a free-stream Mach number of approximately 0.74 (figs. 4(a) to 4(f)), the flow is completely subsonic, and the contours are nearly symmetrical about a line at the midchord station perpendicular to the chord and the span of the airfoil. The small departure from symmetry is probably due to separation on the rear part of the airfoil. At $M_o = 0.784$ (fig. 4(h)), the contours in the supersonic region appear to be slightly asymmetrical and at $M_o = 0.821$ (fig. 4(i)), they are definitely asymmetrical as they are at all higher Mach numbers. Most theories for calculating the flow about an airfoil at high subsonic free-stream Mach numbers assume a symmetrical supersonic region. Because the assumption can be considered applicable for only a very short range of free-stream Mach numbers above the critical (in the present case only from about 0.74 to 0.78), theoretical attention should undoubtedly be given principally to the flow with the asymmetrical supersonic region, as was done in references 6 and 8, for example.

Mach Number and Pressure Distributions on the Surface

Mach number and pressure distributions on the surface of the airfoil have been calculated from some of the interferograms of figure 4. In order to obtain these distributions, fringe shifts must be obtained at the surface. The fringes, however, bend sharply in the boundary layer on the airfoil because of the density gradient through the boundary layer. Because the entropy variation through the boundary layer is not known, the entropy at the surface is not known, and the density at the surface cannot be converted to pressure at the surface. The fringes can, however, be extrapolated through the boundary layer to the surface to obtain what would have been fringe positions at the surface if there had been no boundary layer. When the boundary layer was made turbulent, however, by a flat-plate extension ahead of the airfoil, the boundary layer was thick and the distance that the fringes would have to be extrapolated was believed to be too great to give surface pressures accurately. Moreover, when the boundary layer was made turbulent by means of a wire placed

ahead of the model, the flow in the neighborhood of the model appeared to be considerably disturbed by the wake of the wire, as shown by the changes in the curvature of the fringes near the model. Again, it was believed that the fringes could not be properly extrapolated or corrected through this disturbed region. On the interferograms with laminar boundary layer, however, the boundary layer is very thin and the extrapolation is accurate. Pressure distributions and Mach number distributions, therefore, have been calculated only from the interferograms for which the boundary layer was laminar. The pressure distributions are shown in figure 5. Because interferograms cannot be used to obtain surface pressures where the flow is separated, the pressure distributions were terminated near the beginning of the separated flow, which was near the three-quarter chord station for the lower Mach numbers and near the midchord station for the higher Mach numbers.

In order to check on the magnitude of the random errors in the results of figure 5, figure 6 has been prepared. The pressure distributions shown in figure 6 include not only some of those of figure 5 but also others from additional interferograms that were taken during the course of the investigation. These pressure distributions show that the present results are reproducible and that the random errors are reasonably small, as the data from different interferograms at the same approximate Mach number agree fairly well.

Mach number distributions on the surface were calculated from pressure distributions given in figure 5 and are shown in figure 7.

Data from figures 5, 6, and 7 were used for plotting both figures 8 and 9. Figure 8 shows the variation with free-stream Mach number of the chordwise location of the point on the airfoil surface at which the pressure and the Mach number are equal to the free-stream pressure and Mach number. The point is seen to be constant only for Mach numbers for which the flow is entirely subsonic, as has previously been shown in reference 9 for a 10 percent bump. (In some theoretical investigations, however, the assumption has been made that the location of the point on the surface where free-stream conditions exist is constant also at supercritical speeds.) Figure 9 shows the variation with free-stream Mach number of the chordwise location of the point on the airfoil surface at which sonic speed is reached.

Conditions Along the Shock Waves

The interferograms in figure 4 of the flow around the plano-convex model have a single shock wave and offer an excellent opportunity to determine, by a method that does not disturb the flow, the variations of density, pressure, Mach number, and shock-wave angle along the shock waves. The conditions along the shock waves were found on four interferograms for which the model was the same, the boundary layer was

turbulent, and the supersonic Mach number contours were asymmetrical (figs. 4(k), 4(m), 4(p), and 4(r)). Thus, a small range of free-stream Mach numbers from 0.840 to 0.896 was covered. Because an airfoil of only one thickness ratio was used in the tests, an attempt to correlate conditions at the shock wave by means of the transonic similarity parameters was believed to be useless. Instead, the assumption was made that flow parameters should be plotted against the ratio of y to the value of y at the tip of the shock wave in order to show whether the variation of conditions at the shock wave was similar for various free-stream Mach numbers. Examination of the contours indicates that neither the tip of the shock wave nor the conditions in the region around the intersection of the shock wave and the sonic line could be determined exactly. Accordingly, the value of y at the intersection of the contour of Mach number 1.05 with the shock wave, designated $y_{M=1.05}$, was chosen for reducing the values of y . The value of $y_{M=1.05}/c$ as a function of free-stream Mach number was measured and is shown in figure 10.

The density ratio ρ_2/ρ_1 across the shock wave is shown by the open points of figure 11. The fringe shifts ahead of and behind the shock wave were used to obtain values of ρ_1 and ρ_2 , respectively. A plot for comparing the four curves is presented in figure 12. The solid symbols in figure 11 were obtained by using the fringe shifts ahead of the shock wave to obtain ρ_1 and M_1 from which the ratio ρ_2/ρ_1 was calculated as though the shock wave were normal to the flow. Large differences between the two sets of points indicate that the shock-wave angle ϵ was much less than 90° . The two sets of points are in good agreement except near the base of the shock wave where the shock-wave angle is considerably less than 90° . The actual variation of ϵ along the part of the shock wave near the airfoil was obtained from the data of figure 11. Measured values of ρ_2/ρ_1 were used to obtain the corresponding values of $M_1 \sin \epsilon$ from shock-wave tables (for example, see ref. 10) and the known values of M_1 were then used to find $\sin \epsilon$. The resulting values of ϵ are shown in figure 13. The values of ϵ are not accurately known when ϵ is greater than approximately 82° because $\sin \epsilon$ varies only 1 percent when ϵ varies between 82° and 90° . Inasmuch as the experimental error in ρ_2/ρ_1 is approximately 2 percent, the error in $\sin \epsilon$ determined from ρ_2/ρ_1 is approximately 1 percent. To determine ϵ accurately over the nearly normal part of the shock wave is, therefore, impossible and the experimental points for that part are not shown in figure 13.

The values of ρ_2/ρ_1 shown by the open points in figure 11 were used, together with shock-wave tables, to obtain values of the pressure ratio across the shock wave p_2/p_1 shown in figure 14.

The values of ρ_1 obtained from the interferograms were used to calculate the values of M_1 , the Mach number ahead of the shock wave. The variation of M_1 with $y/y_{M=1.05}$ is shown in figure 15. This figure indicates that perhaps some degree of correlation of the variation of Mach number ahead of the normal part of the shock waves can be obtained by this method of plotting.

Conditions at the Bases of the Shock Waves

The actual equilibrium conditions that are fulfilled at the base of a shock wave which interacts with a boundary layer have been the subject of considerable speculation. In reference 11 the hypothesis was made that the shock wave would occur at a Mach number close to unity. In reference 12 a Mach number of unity on the downstream side of the shock wave was proposed. In reference 8 the obliquity of the shock wave was proposed to be such that the deflection of the flow by the shock wave was a maximum. In reference 6 the tentative assumption was made that the pressure on the downstream side of the shock wave is equal to free-stream pressure.

The conditions at the base of the shock waves on the four interferograms shown in figures 4(k), 4(m), 4(p), and 4(r) were obtained from figures 11, 13, 14, and 15 and are shown in columns 7, 9, 13, and 4, respectively, of table I. These data were checked by a careful examination of the interferograms at the point where the shock wave intersected the outer edge of the boundary layer. Other data given in table I include the measured value of ϵ in column 5, the flow deviation δ in column 10, the maximum possible δ for the given value of M_1 in column 11, the value of M_2 in column 12, the value of $\Delta p/q_1$ in column 15, and the value of p_2/p_0 in column 16. The information given in table I can be used for discussing the boundary condition at the base of the shock wave. First, however, the configuration at the lowest free-stream Mach number of 0.840 seems to differ from those at the higher Mach numbers. The oblique part of the shock wave (fig. 4(k)) near its base either does not exist or is too small to be seen. Attention, therefore, is restricted to the three cases of higher Mach number. None of the ideas proposed in references 6, 8, 11, and 12 seems to be substantiated by the present experimental data. Column 4 shows that the shock wave does not occur at a Mach number very close to unity. A comparison of columns 10 and 11 shows that the flow deviation is not the maximum possible. Column 12 shows that the Mach number behind the shock wave is not constant at unity. Column 16 shows that the pressure behind the shock wave at its base is not free-stream pressure. Column 13 shows that the condition may be a nearly constant value of pressure ratio across the shock wave. Column 15 shows that the value of $\Delta p/q_1$ is nearly constant.

The shock-wave angles appropriate to the various boundary conditions proposed in references 6, 8, and 12 are shown in figure 16 and compared with the present experimental data. The curves show what the shock-wave angle would be, as a function of Mach number ahead of the shock wave (considered as given), for each of the several proposed boundary conditions. The experimental data do not fit any of the previously proposed boundary conditions. Also shown in figure 16 are two empirical conditions that are based on the present empirical results, either of which fits the data better than do the previously proposed conditions. The present data cover such a small range of variables (Mach and Reynolds numbers and airfoil contour) that a choice cannot be made between these two boundary conditions on the basis of the limited amount of data. The data indicate, however, that when the boundary layer is turbulent, a constant value of $\Delta p/q_1$ equal to 0.3 may be used as the boundary condition at the base of the shock wave, at least for the small range of variables covered by the present investigation.

CONCLUDING REMARKS

The flow around a 12-percent-thick circular-arc airfoil at zero incidence has been observed with an interferometer through a range of Mach numbers from 0.609 to 0.896 with both laminar and turbulent boundary layers. Mach number contours in the flow field and Mach number and pressure distributions on the surface of the airfoil have been obtained.

Sonic speed was found to be first reached at an indicated Mach number of approximately 0.74 and the contours of constant Mach number in the supersonic region changed from the symmetrical to the asymmetrical type at an indicated Mach number of approximately 0.78.

Conditions were investigated along the length of the shock waves that interacted with the turbulent boundary layer on the airfoil. Some degree of correlation of the variation of Mach number along the front of the normal part of the shock waves could be obtained. Also, the boundary condition at the bases of the shock waves that interacted with turbulent boundary layers could be taken to be $\Delta p/q_1 = 0.3$ over the limited range of variables that was covered by the experiments, where Δp is the pressure difference across the shock wave and q_1 is the dynamic pressure ahead of the shock wave.

Langley Aeronautical Laboratory,
National Advisory Committee for Aeronautics,
Langley Field, Va., July 8, 1952.

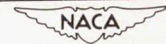
REFERENCES

1. Liepmann, Hans Wolfgang: Investigations of the Interaction of Boundary Layer and Shock Waves in Transonic Flow. Tech. Rep. No. 5668, ATI No. 34705, Air Materiel Command, U. S. Air Force, Feb. 9, 1948.
2. Liepmann, Hans Wolfgang, Askenas, Harry, and Cole, Julian D.: Experiments in Transonic Flow. AF Tech. Rep. No. 5667, Air Materiel Command, Feb. 9, 1948.
3. Lindsey, W. F., Daley, Bernard N., and Humphreys, Milton D.: The Flow and Force Characteristics of Supersonic Airfoils at High Subsonic Speeds. NACA TN 1211, 1947.
4. Daley, Bernard N., and Hanna, Lillian E.: Subsonic Two-Dimensional-Flow Conditions Near an Airfoil Determined by Static Pressures Measured at the Tunnel Wall. NACA TN 1873, 1949.
5. Bryson, Arthur Earl, Jr.: An Experimental Investigation of Transonic Flow Past Two-Dimensional Wedge and Circular-Arc Sections Using a Mach-Zehnder Interferometer. NACA TN 2560, 1951.
6. Perl, William: Calculation of Transonic Flows Past Thin Airfoils by an Integral Method. NACA TN 2130, 1950.
7. Gooderum, Paul B., Wood, George P., and Brevoort, Maurice J.: Investigation With an Interferometer of the Turbulent Mixing of a Free Supersonic Jet. NACA Rep. 963, 1950. (Supersedes NACA TN 1857.)
8. Tsien, Hsue-shen, and Fejer, Andrej: A Method for Predicting the Transonic Flow Over Airfoils and Similar Bodies From Data Obtained at Small Mach Numbers. GALCIT Rep., Dec. 31, 1944. (Submitted in Partial Fulfillment of Compressibility Effect Project, Contract No. W 33-038 ac-1717 (11592).)
9. Lindsey, W. F., and Daley, Bernard N.: Effects of Compressibility on the Flow Past a Two-Dimensional Bump. NACA TN 2484, 1952.
10. Burcher, Marie A.: Compressible Flow Tables for Air. NACA TN 1592, 1948.
11. Donaldson, Coleman duP.: Effects of Interaction Between Normal Shock and Boundary Layer. NACA CB No. 4A27, 1944.
12. Theodorsen, Theodore: A Condition on the Initial Shock. NACA TN 1029, 1946.

TABLE I

CONDITIONS AT BASE OF SHOCK WAVE

1	2	3	4	5	6	7	8	9	10	11	12	13	14	15	16
Figure	M_0	$y/y_{M=1.05}$	M_1 measured, from fig. 15	ϵ measured, deg	$M_1 \sin \epsilon$ from (4) and (5)	ρ_2/ρ_1 measured, from fig. 11	ρ_2/ρ_1 theoretical, from (6)	ϵ calculated, from fig. 13, deg	δ calculated from (4) and (5)	δ_{\max} for M_1 in (4), deg	M_2 calculated from (4), (5), and (10)	P_2/P_1 from fig. 14	P_2/P_1 theoretical, from (8)	$\Delta p/q_1$ from (13) and (4)	ρ_2/ρ_0 measured
4(k)	0.840	0.18	1.24	76.0	1.20	1.31	1.34	73	4° 28'	5.0	0.89	1.46	1.51	0.45	0.91
(m)	.859	.16	1.28	65.0	1.16	1.25	1.27	64	5° 41'	6.1	1.01	1.37	1.40	.32	.82
(p)	.880	.08	1.35	58.7	1.15	1.26	1.26	59	6° 00'	8.0	1.10	1.38	1.38	.30	.77
(r)	.896	.08	1.37	56.4	1.14	1.265	1.24	57	5° 49'	8.6	1.14	1.39	1.35	.30	.76



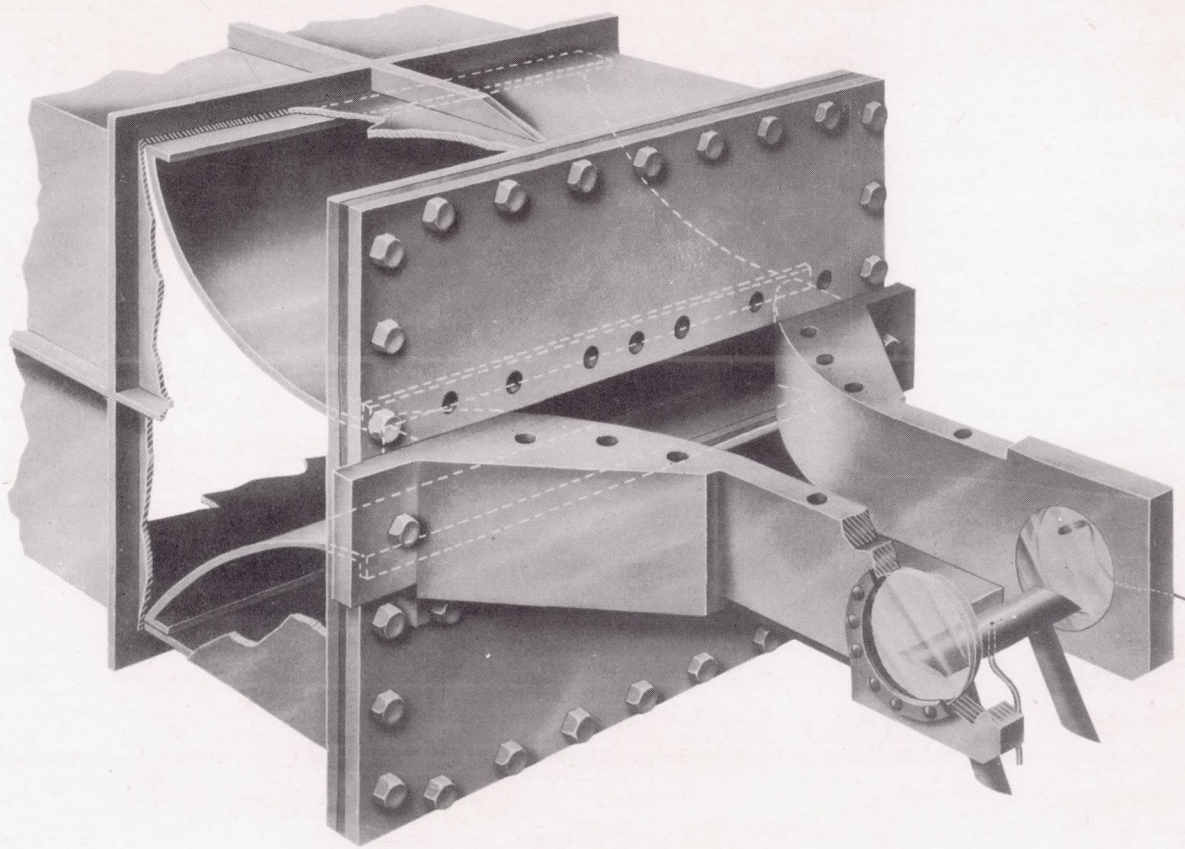
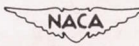
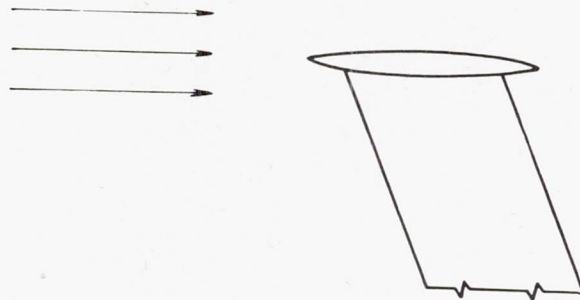
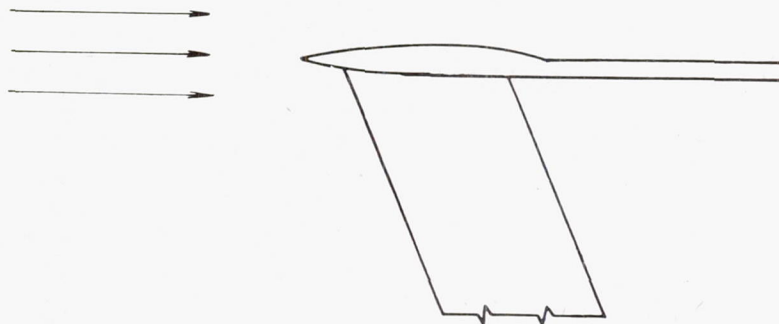


Figure 1.- Nozzle and test section showing model installation.

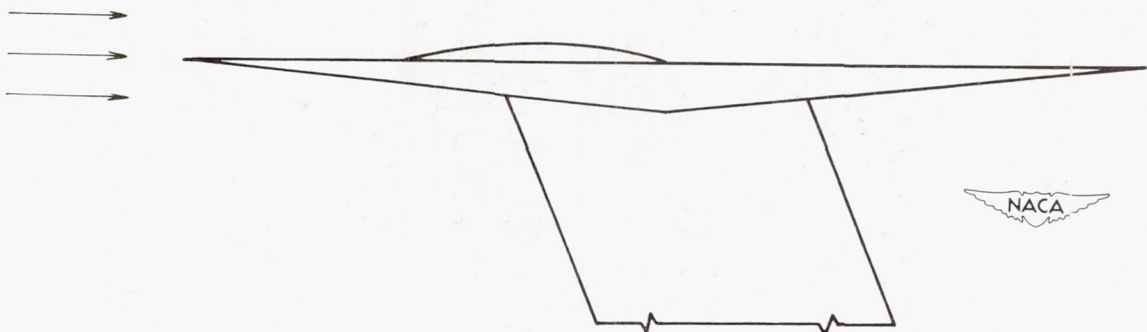

L-72522.1



(a) Biconvex model.

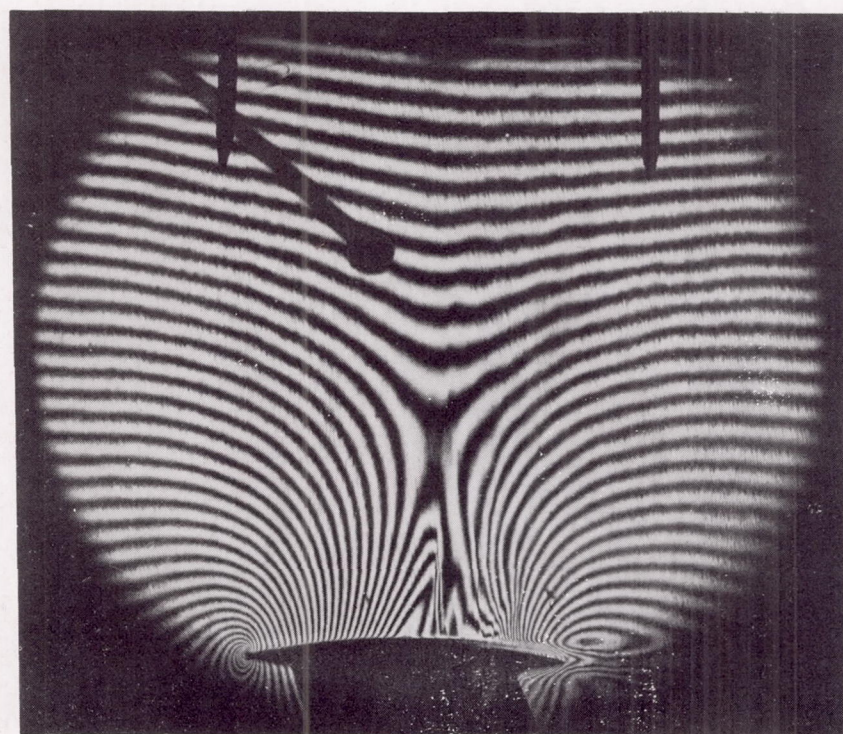
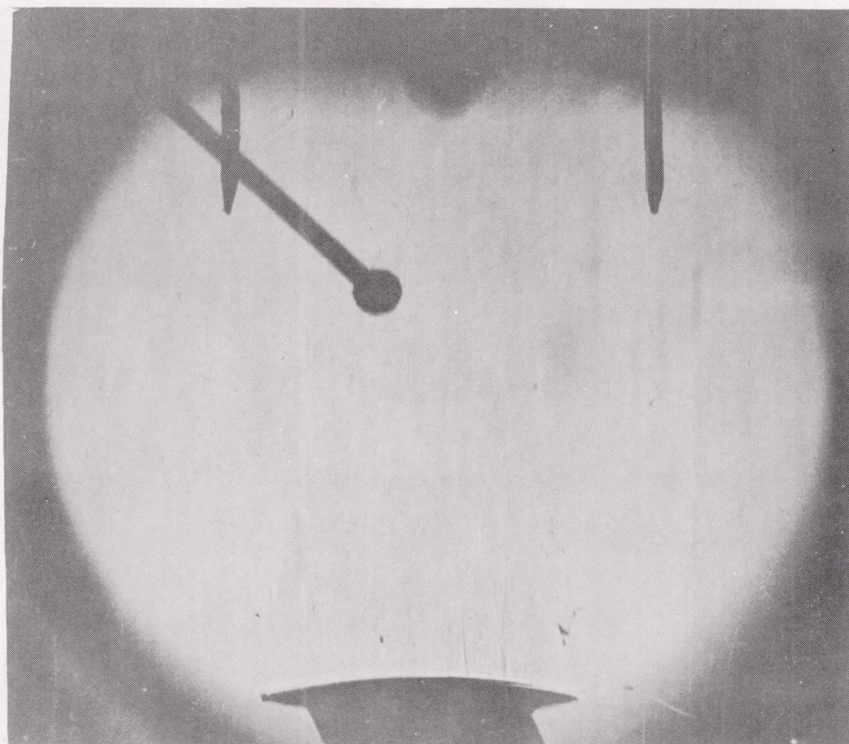


(b) Biconvex model with flat plate.



(c) Plano-convex circular-arc model.

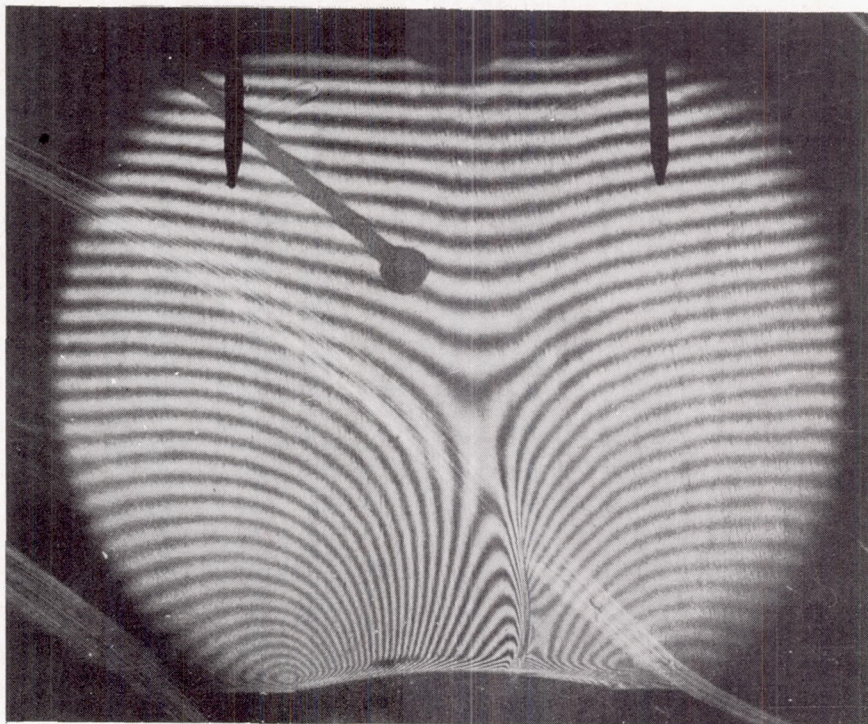
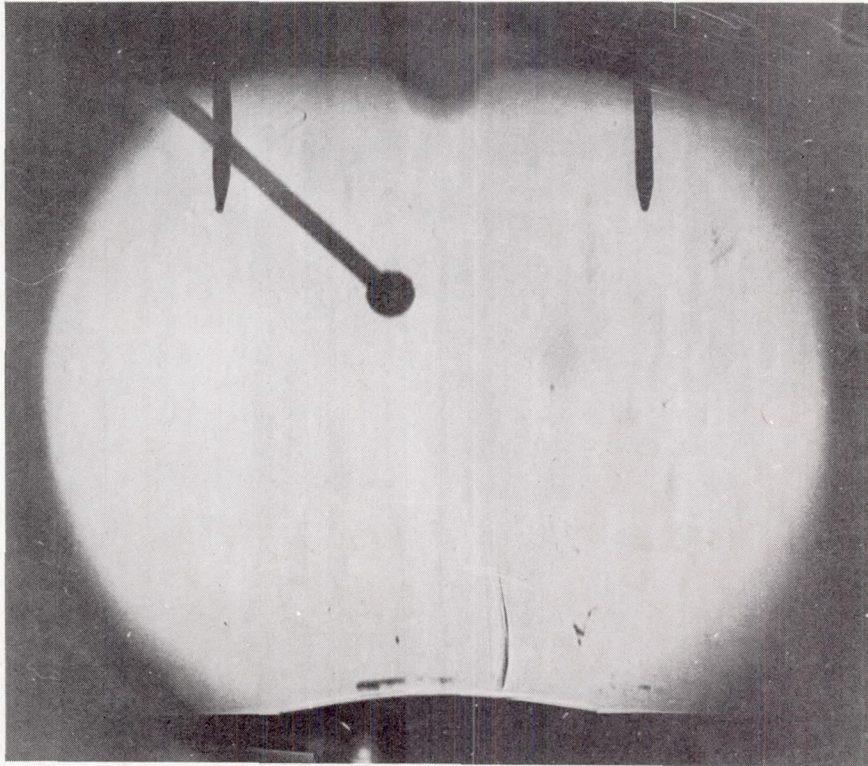
Figure 2.- Models.



(a) $M_0 = 0.78$. Laminar.

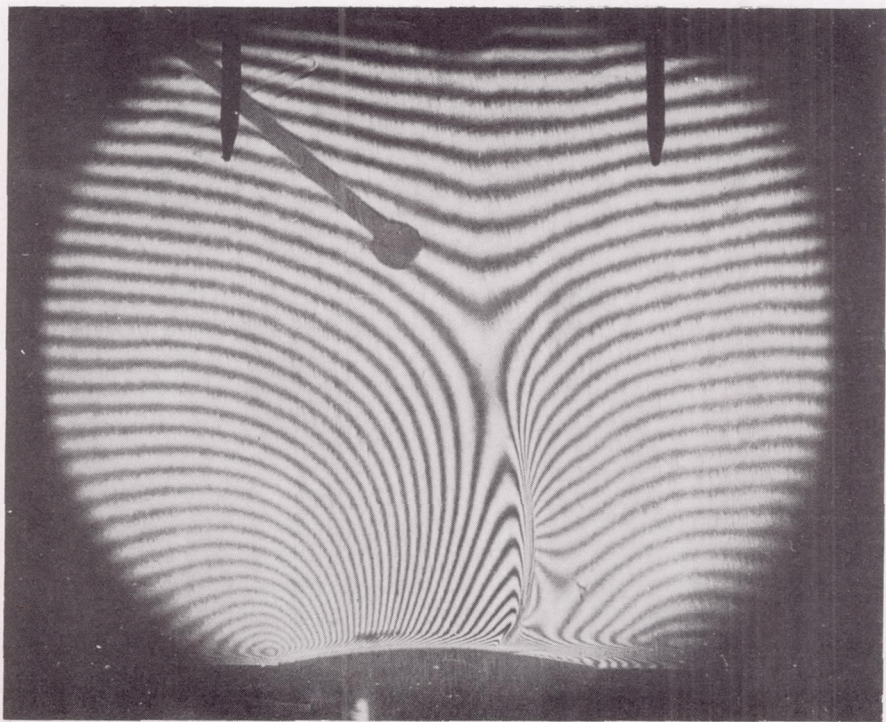
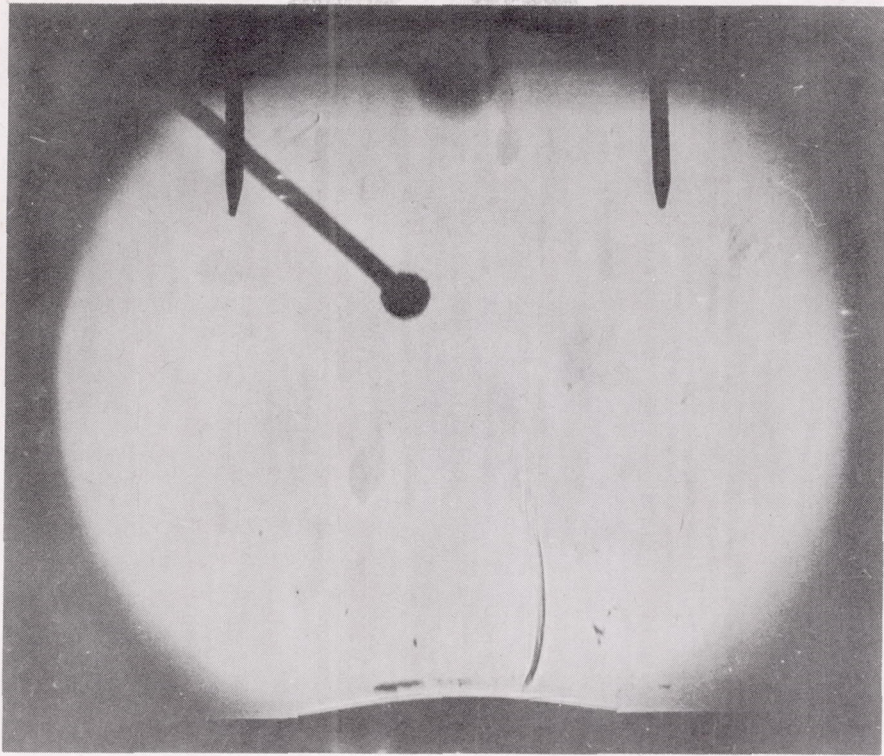
NACA
L-76113

Figure 3.- Interferograms and shadowgraphs of the flow about a 12-percent-thick circular-arc airfoil. $\alpha \approx 0^\circ$.



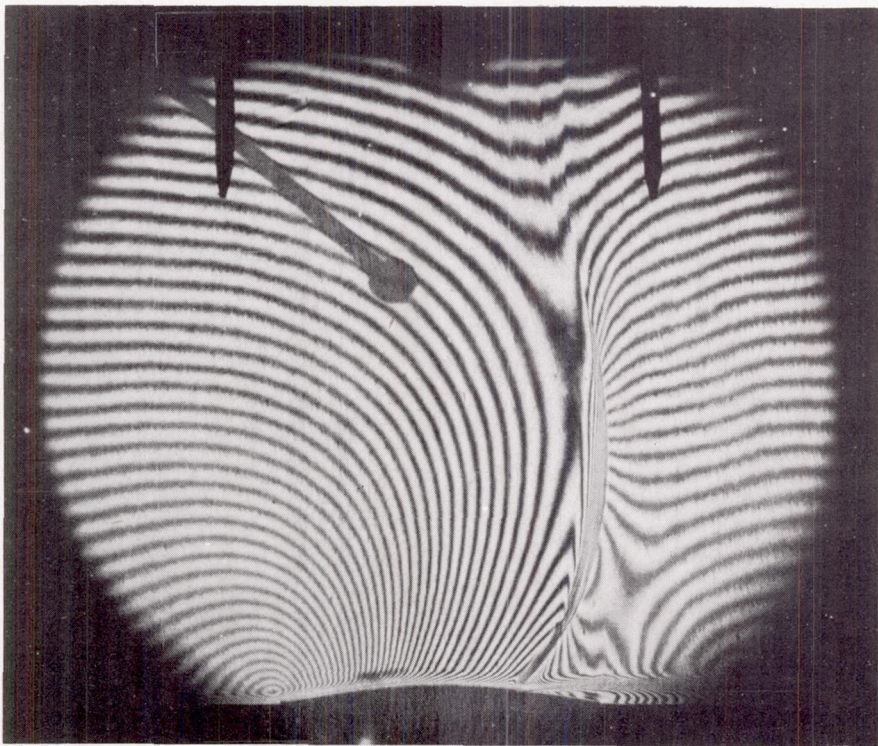
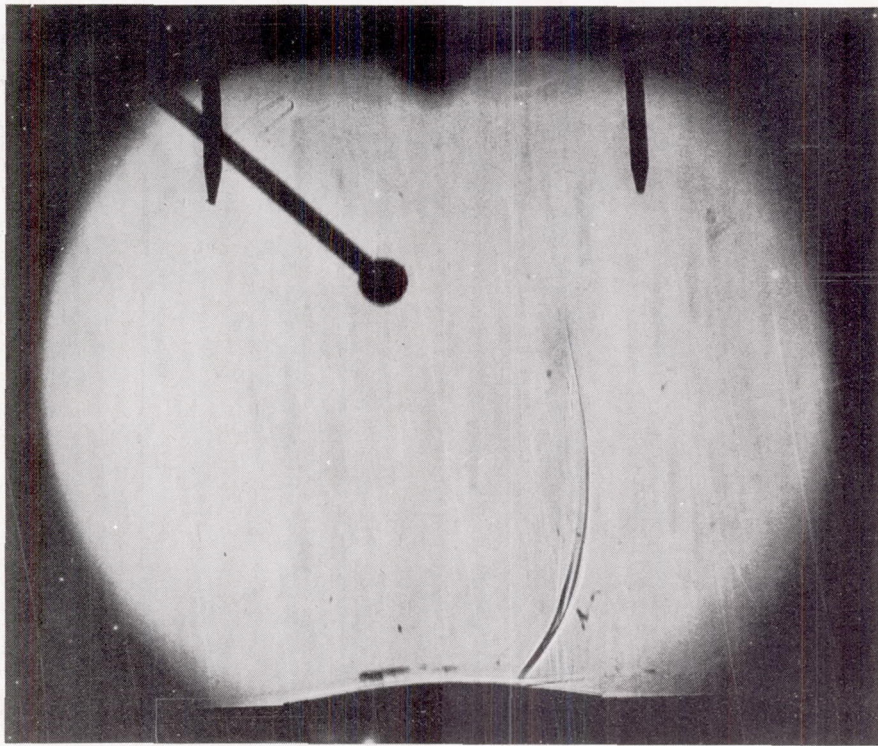
(b) $M_0 = 0.84$. Turbulent.

Figure 3.- Continued.



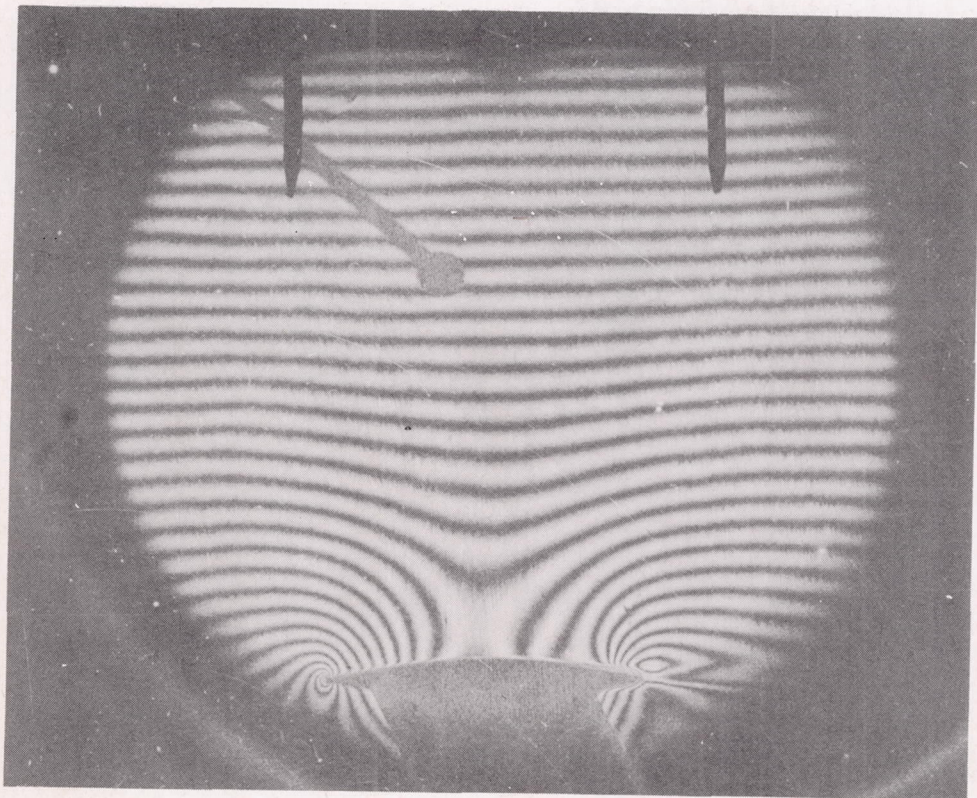
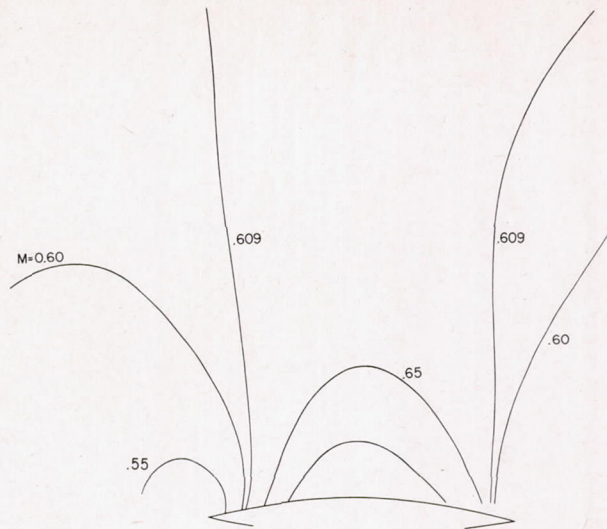
(c) $M_0 = 0.86$. Turbulent.

Figure 3.- Continued.

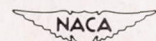


(d) $M_0 = 0.90$. Turbulent.

Figure 3.- Concluded.

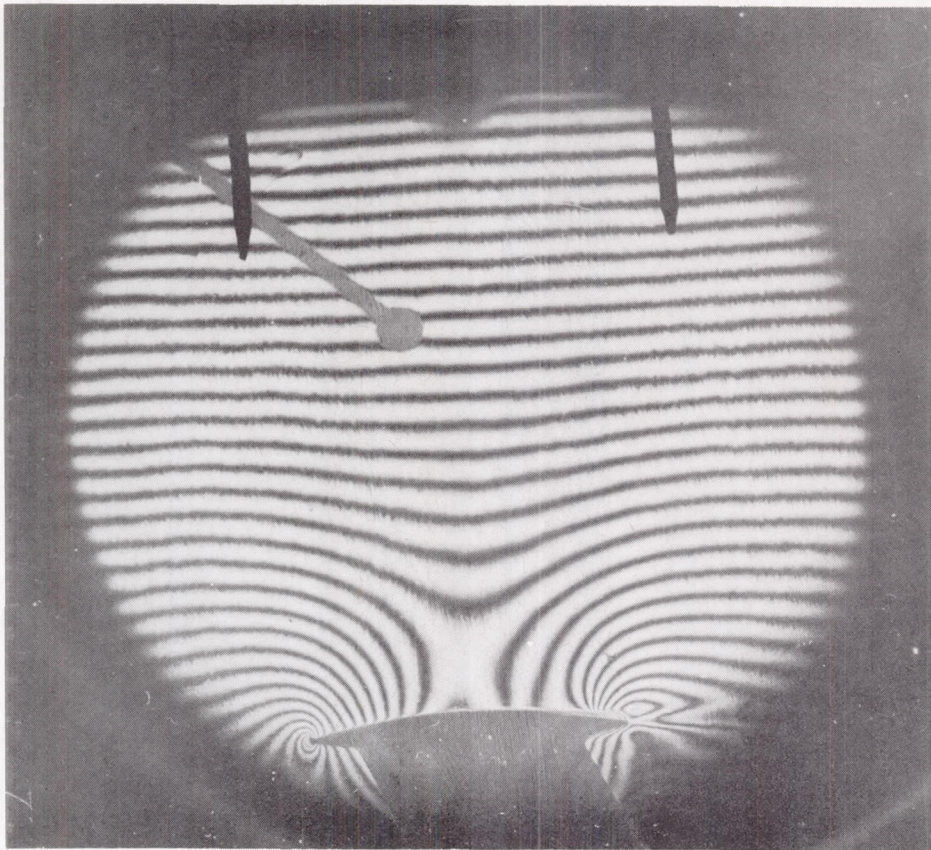
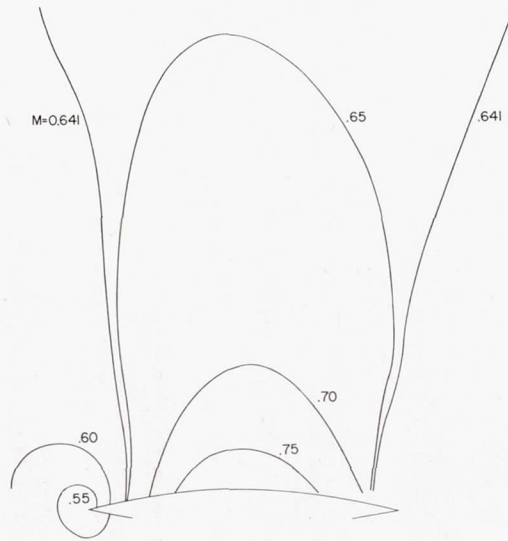


(a) $M_0 = 0.609$. Laminar.



L-76121

Figure 4.- Interferograms and Mach number distributions of the flow about a 12-percent-thick circular-arc airfoil. $\alpha \approx 0^\circ$.

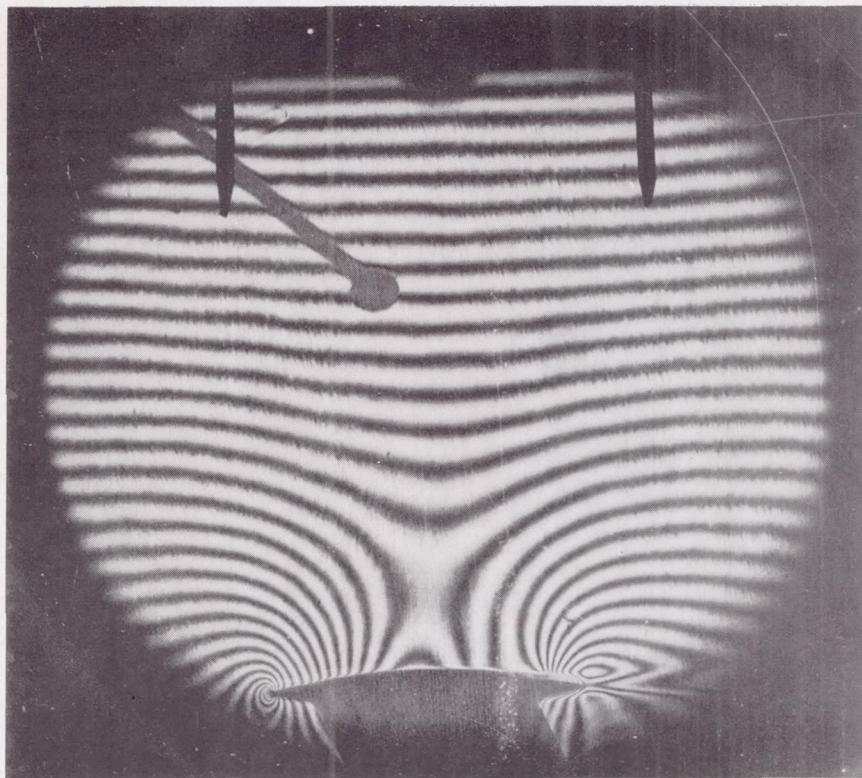
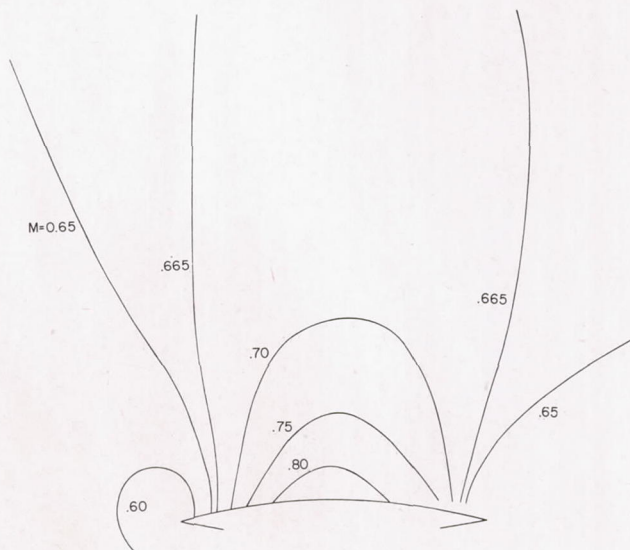


(b) $M_0 = 0.641$. Laminar.

Figure 4.- Continued.

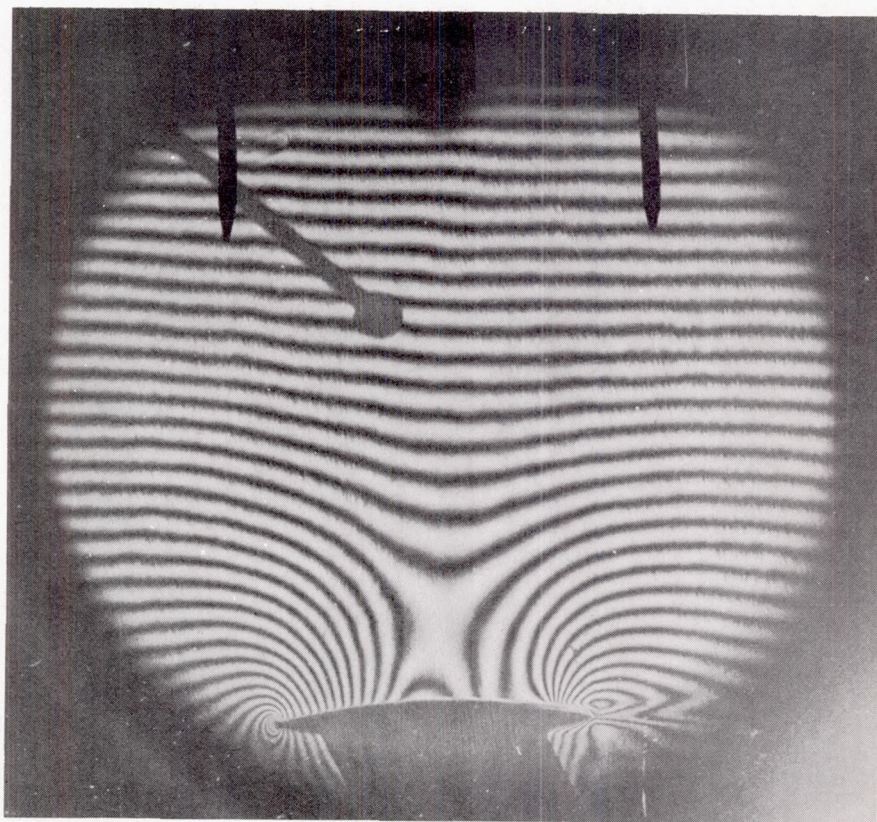
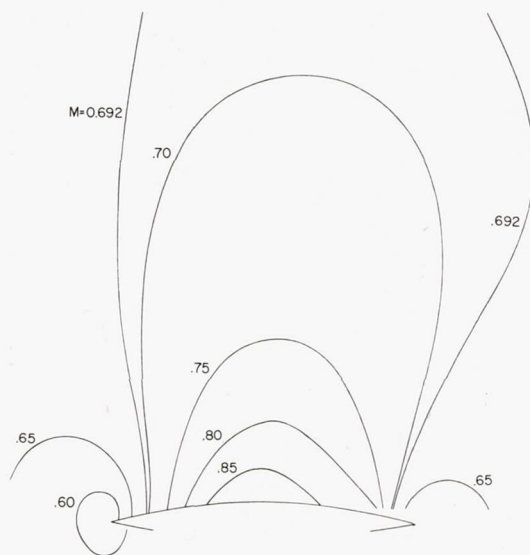


L-76122



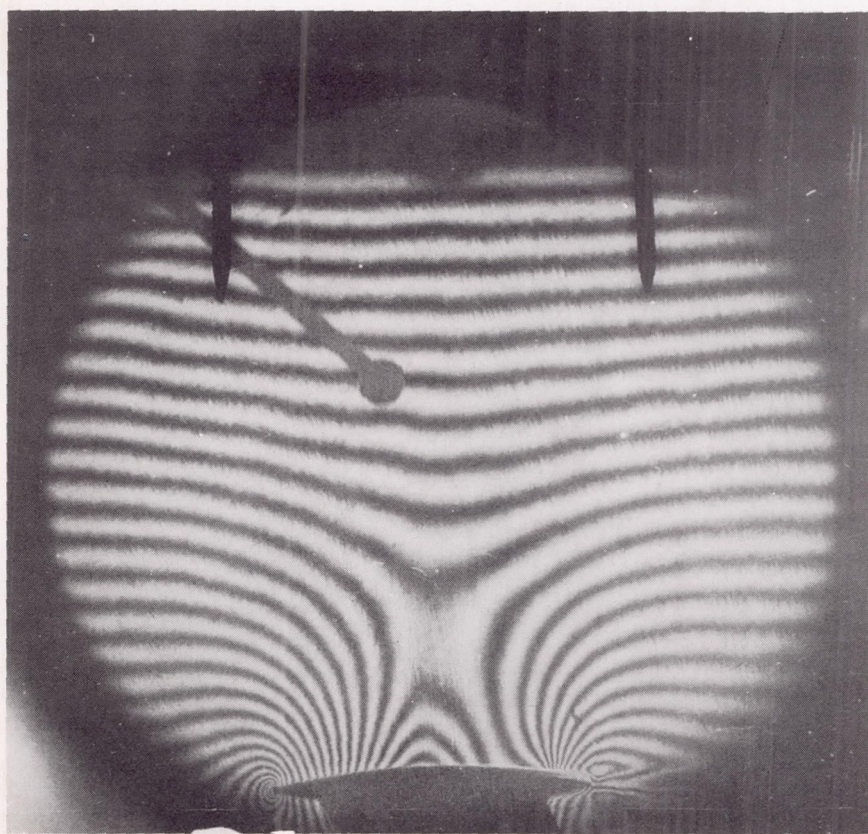
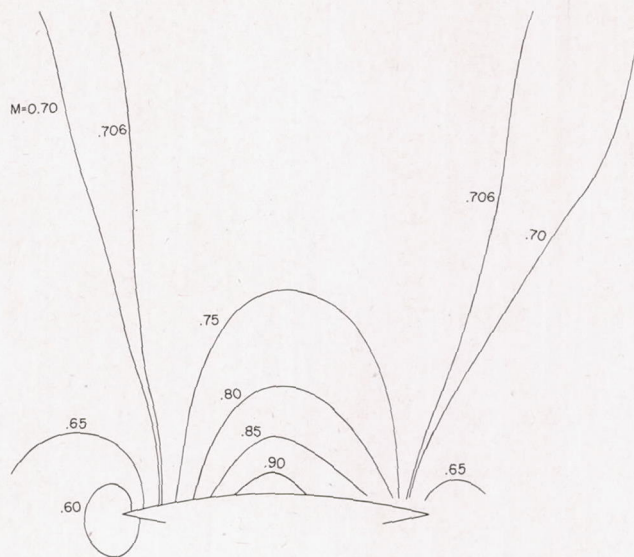
(c) $M_0 = 0.665$. Laminar.

Figure 4.- Continued.



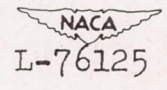
(d) $M_0 = 0.692$. Laminar.

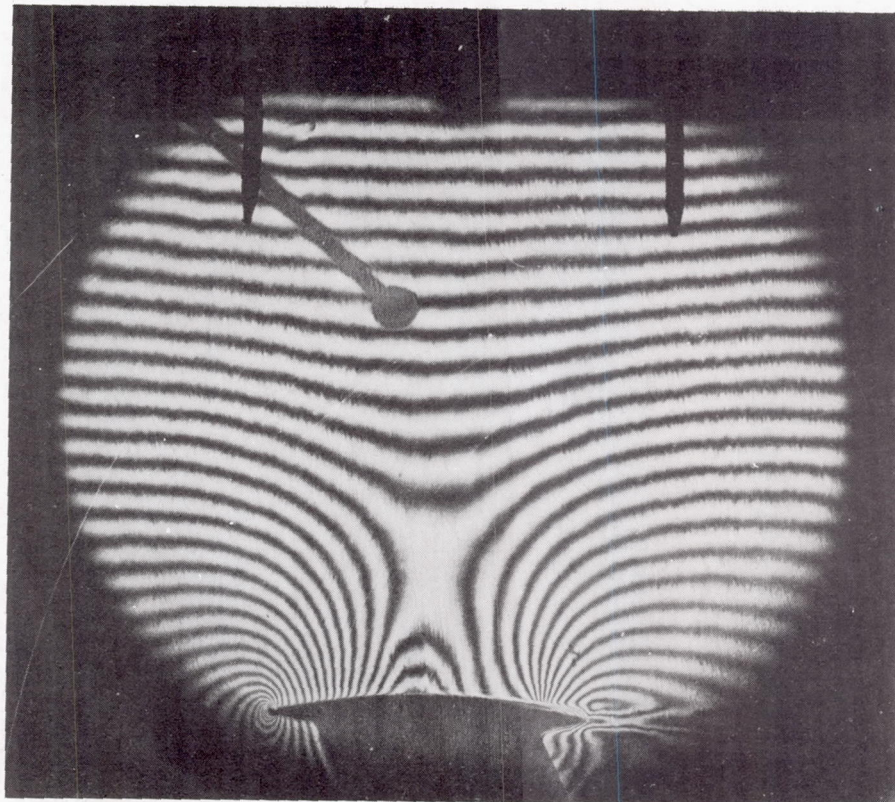
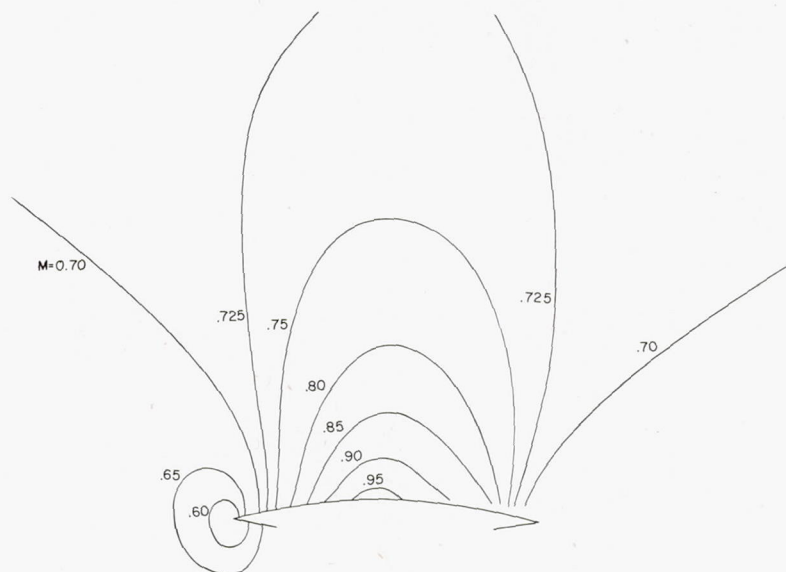
Figure 4.- Continued.



(e) $M_0 = 0.706$. Laminar.

Figure 4.- Continued.

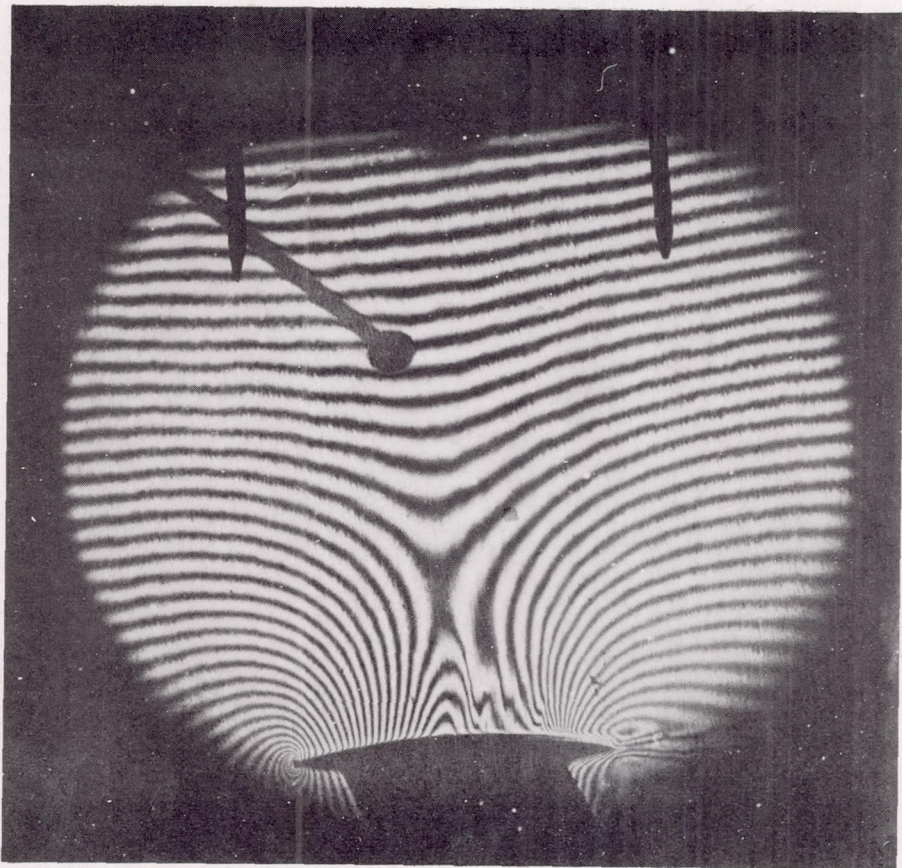
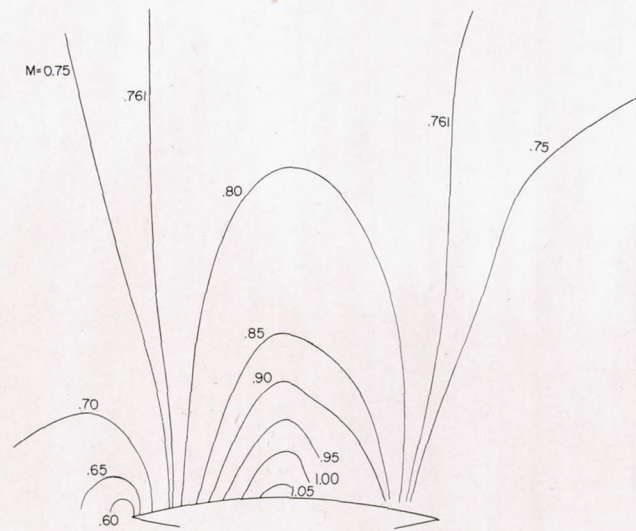




(f) $M_0 = 0.725$. Laminar.

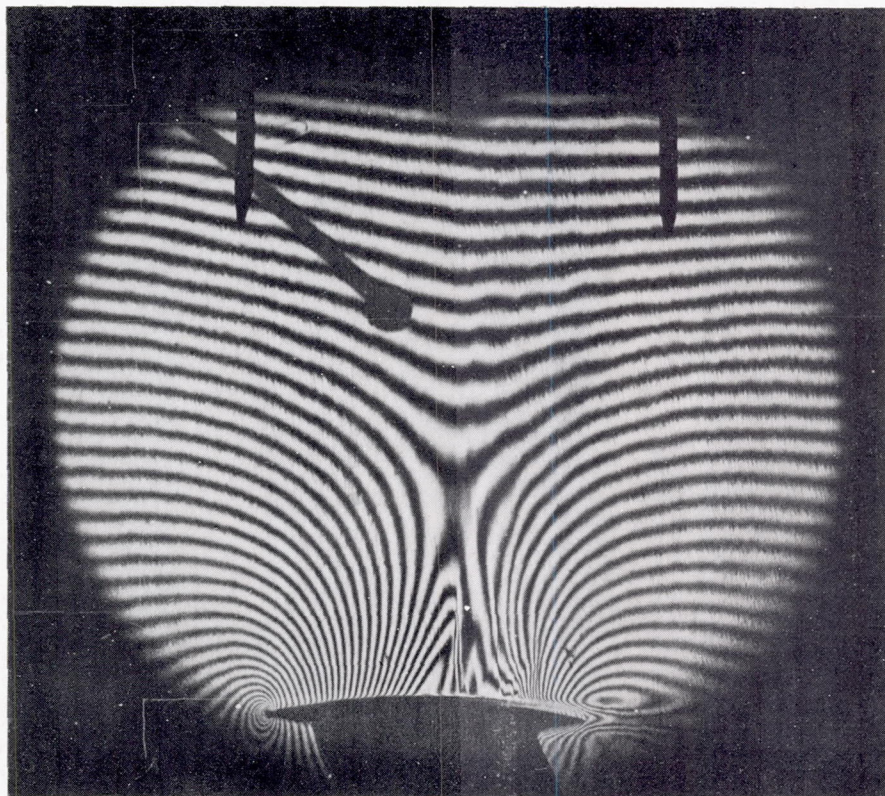
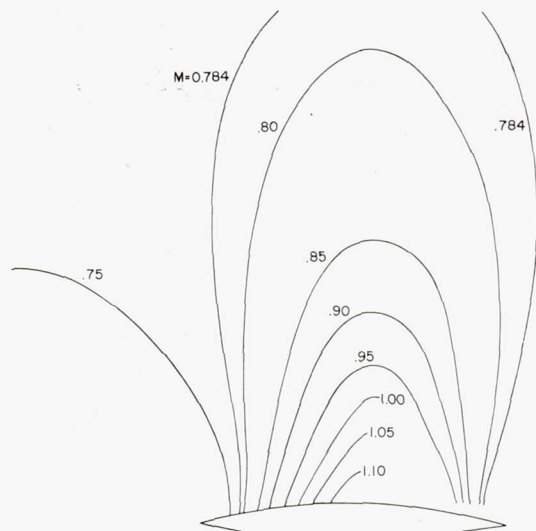
Figure 4.- Continued.

NACA
L-76126



(g) $M_0 = 0.761$. Laminar.

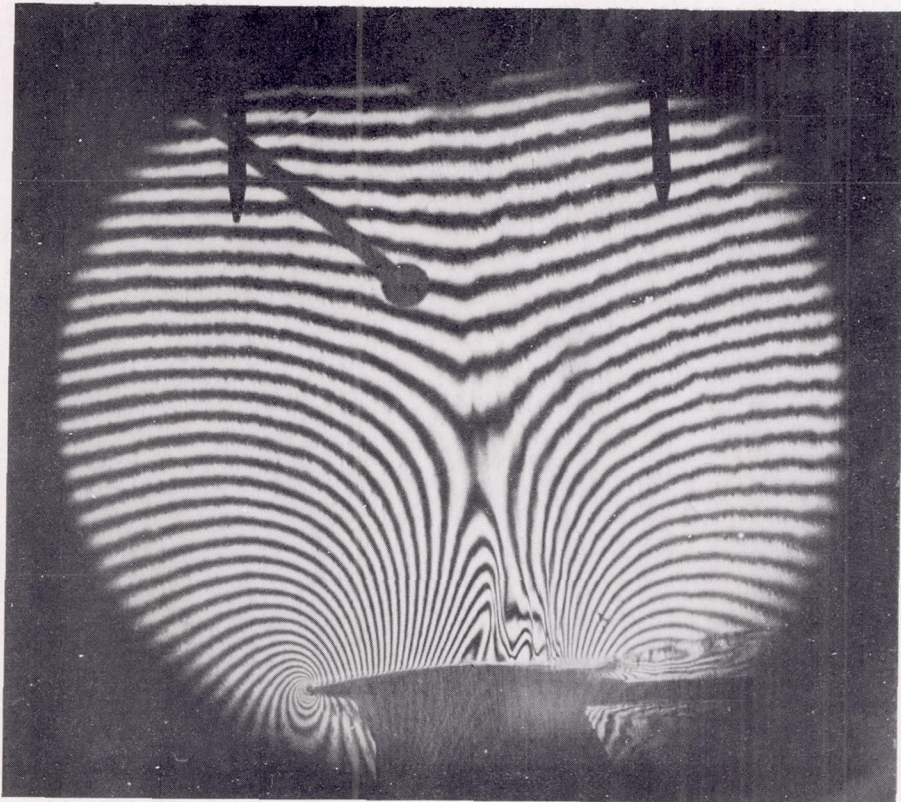
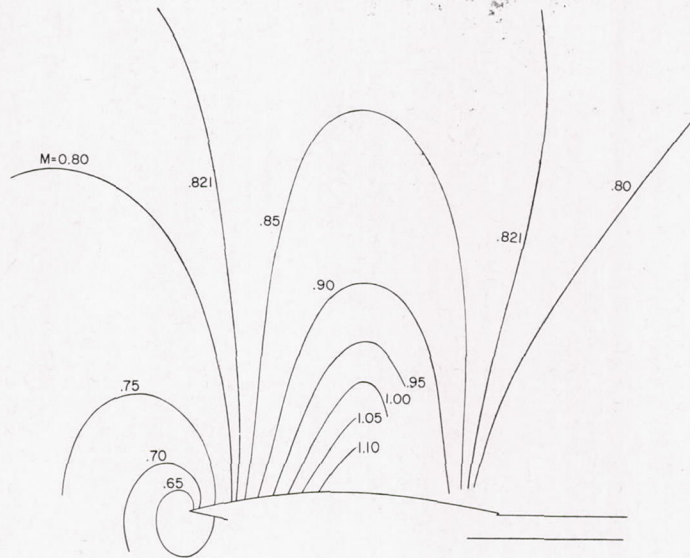
Figure 4.- Continued.



(h) $M_0 = 0.784$. Laminar.

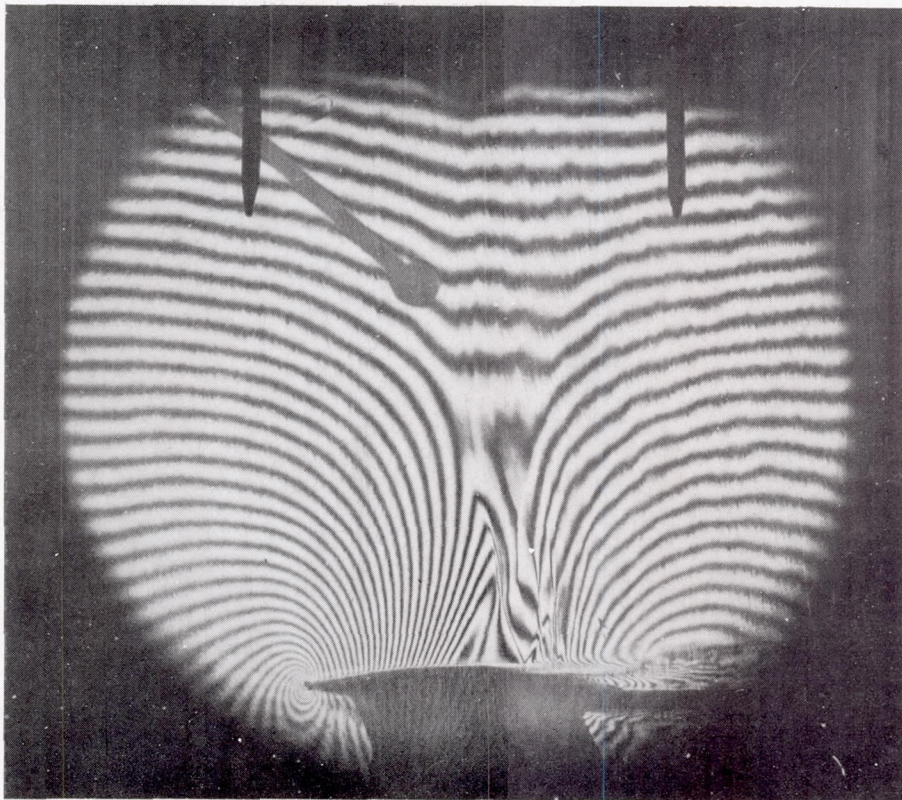
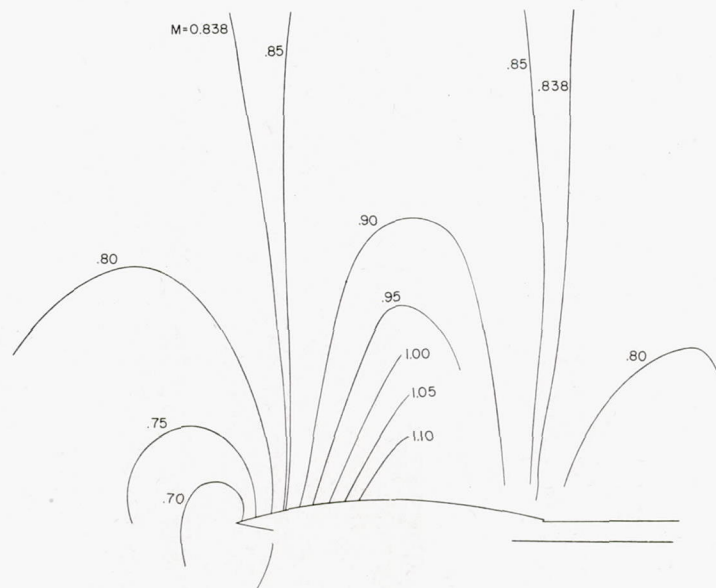
Figure 4.- Continued.

NACA
L-76128



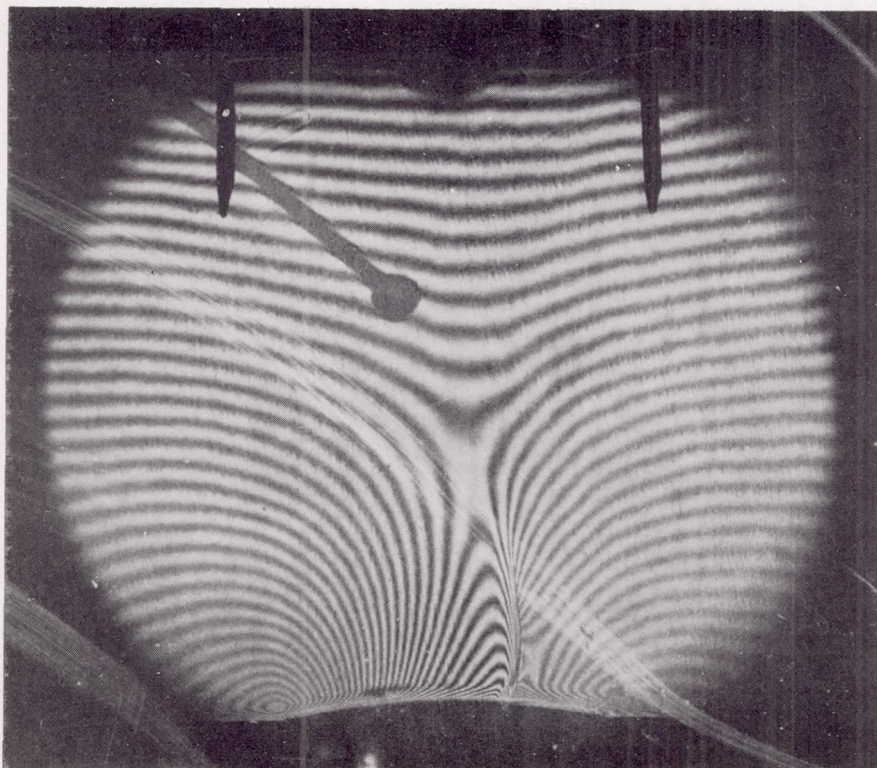
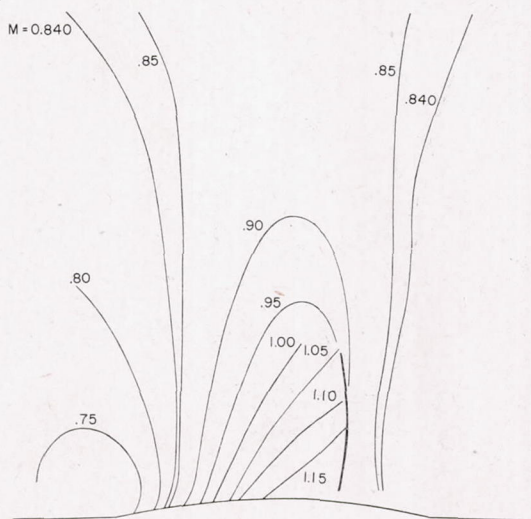
(i) $M_0 = 0.821$. Laminar.

Figure 4.- Continued.



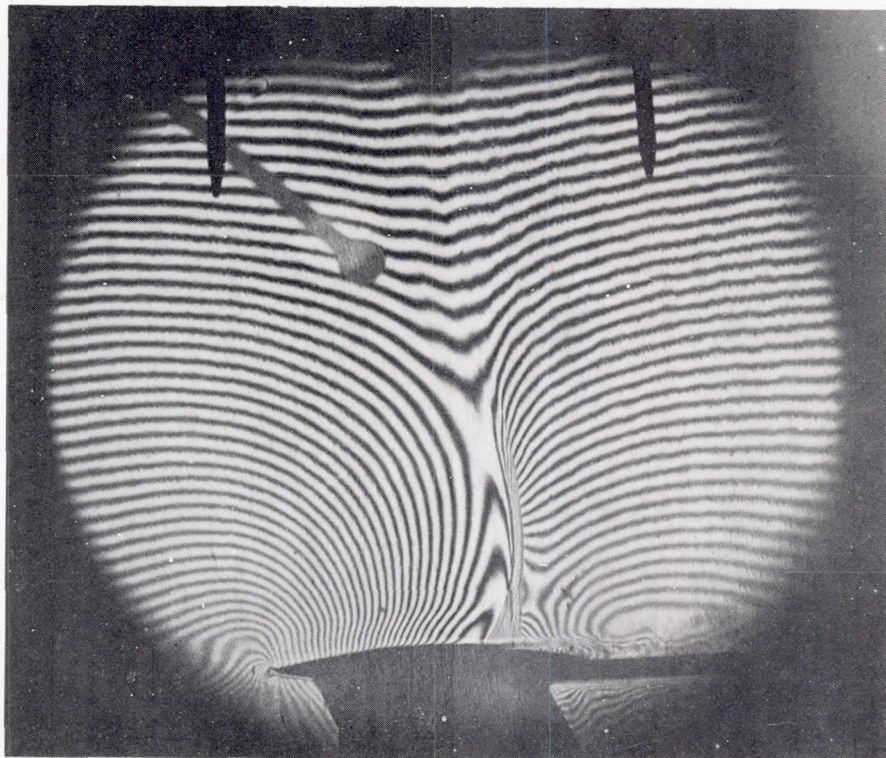
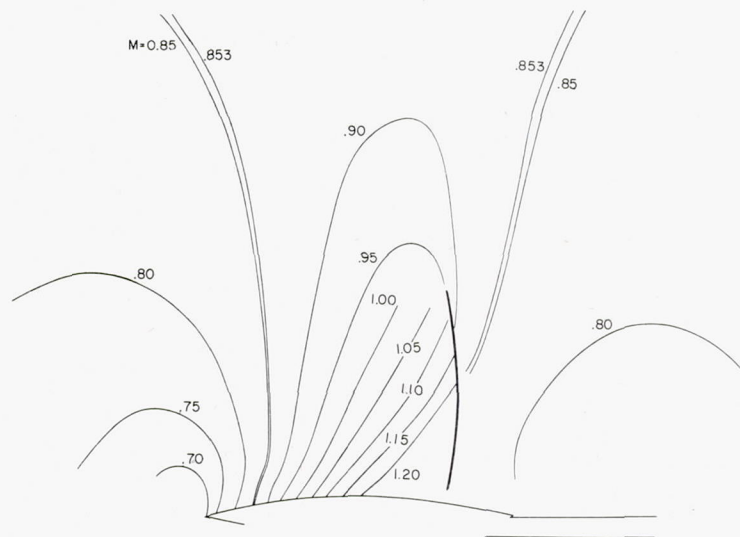
(j) $M_0 = 0.838$. Laminar.

Figure 4.- Continued.



(k) $M_0 = 0.840$. Turbulent.

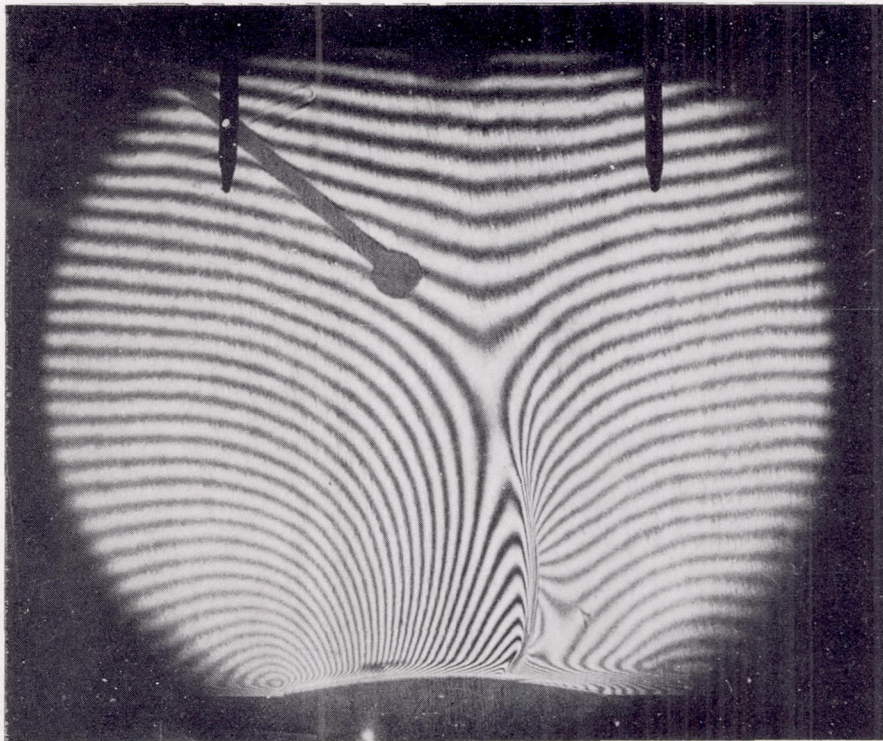
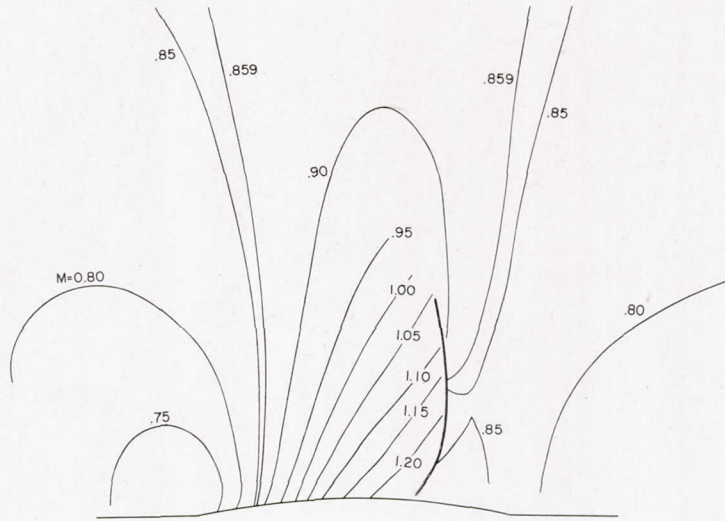
Figure 4.- Continued.



(2) $M_0 = 0.853$. Turbulent.

Figure 4.- Continued.

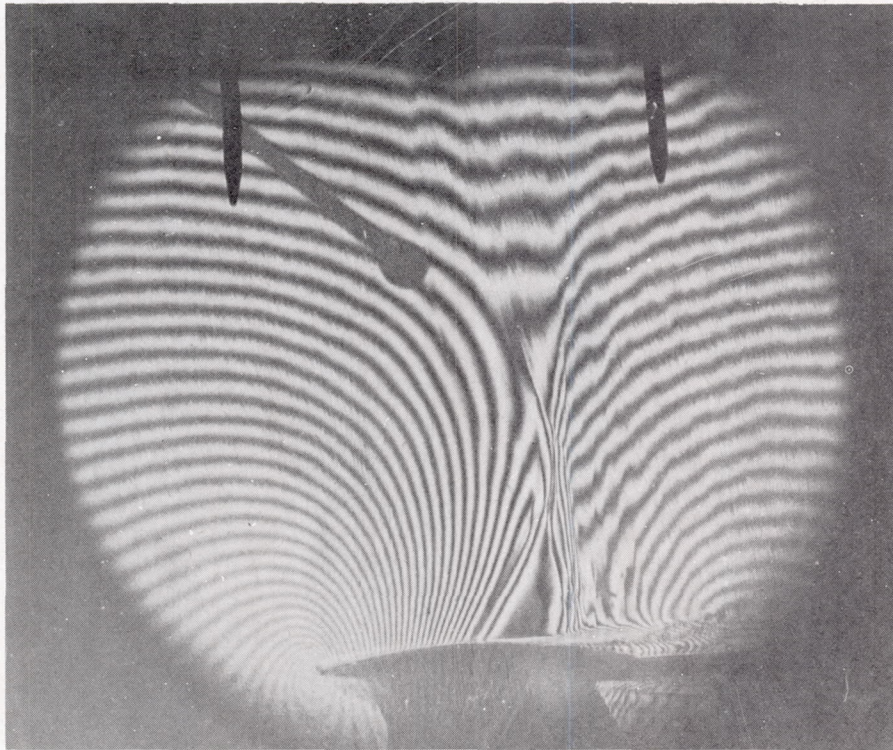
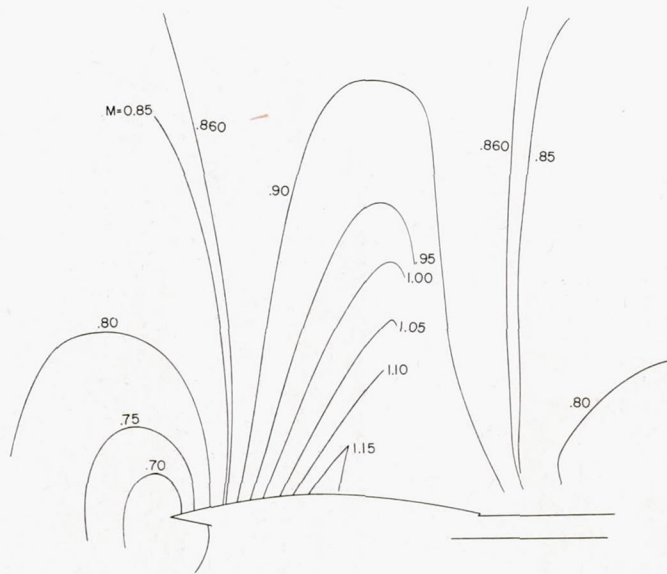
NACA
L-76132



(m) $M_0 = 0.859$. Turbulent.

Figure 4.- Continued.

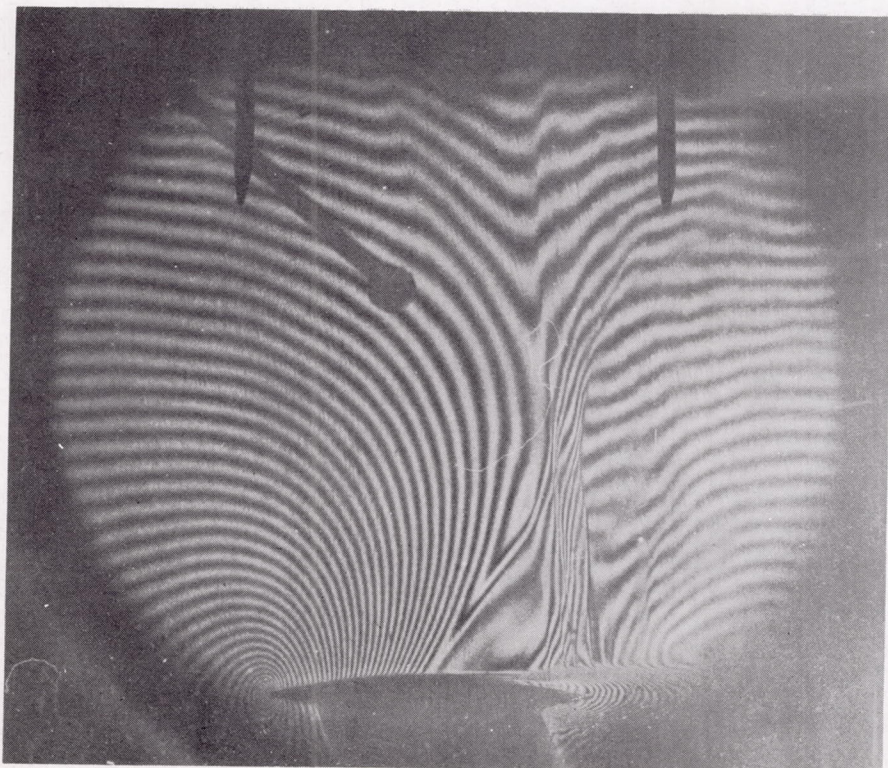
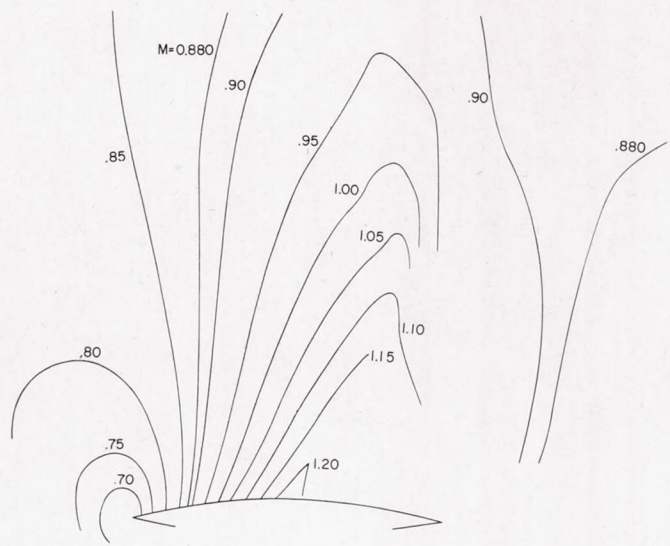
NACA
L-76133



(n) $M_0 = 0.861$. Laminar.

Figure 4.- Continued.

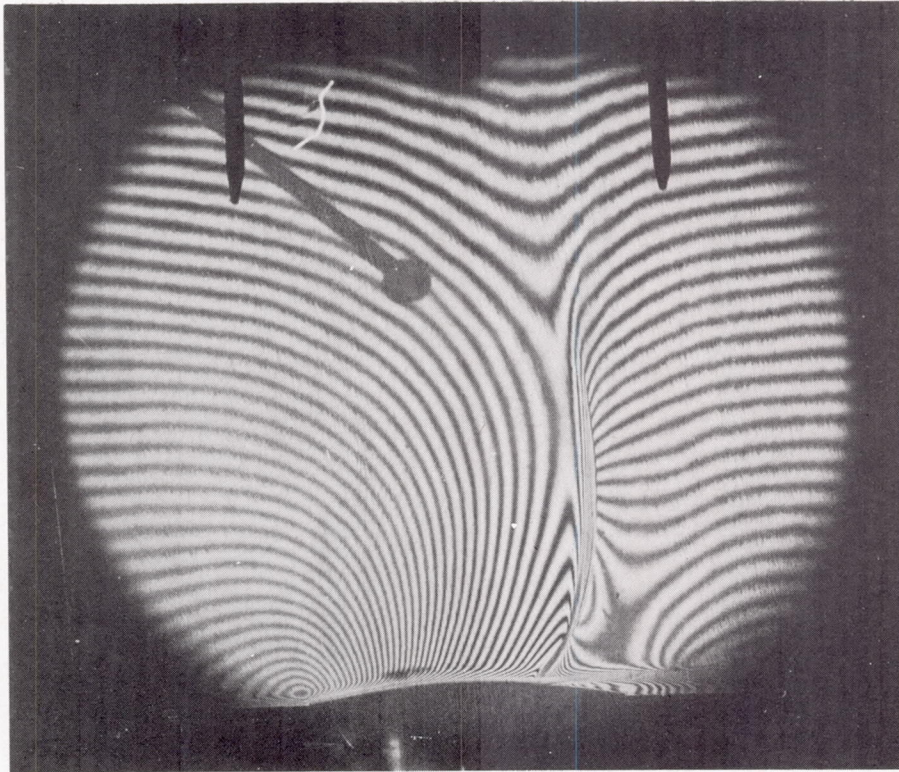
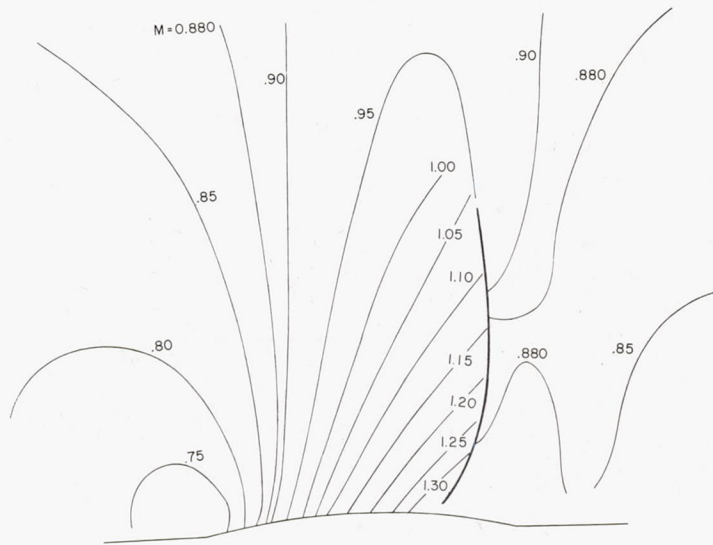
NACA
L-76134



(o) $M_0 = 0.880$. Laminar.

Figure 4.- Continued.

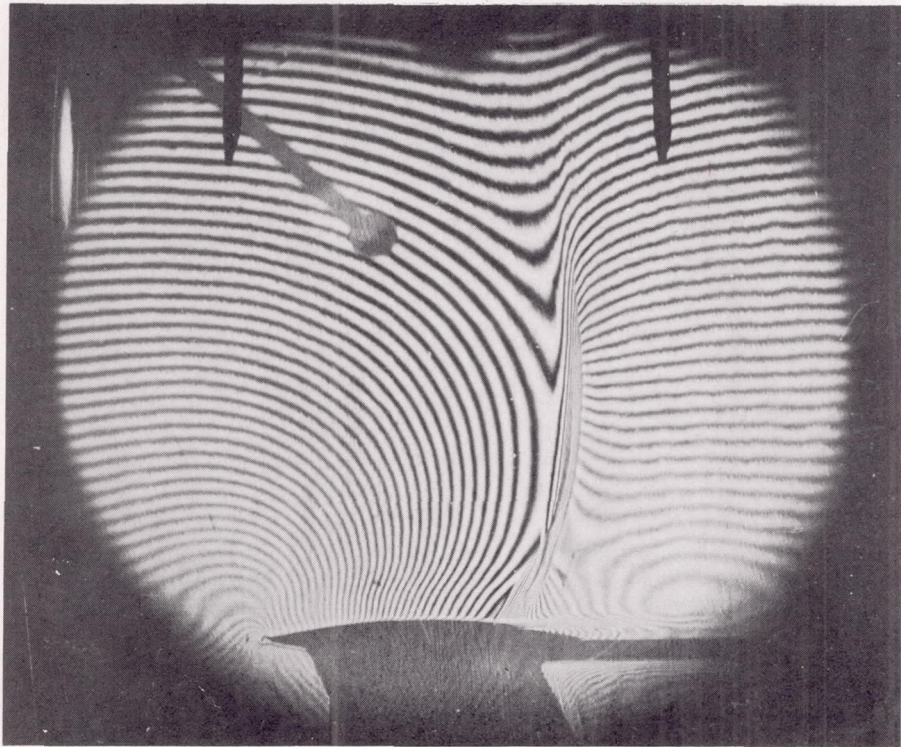
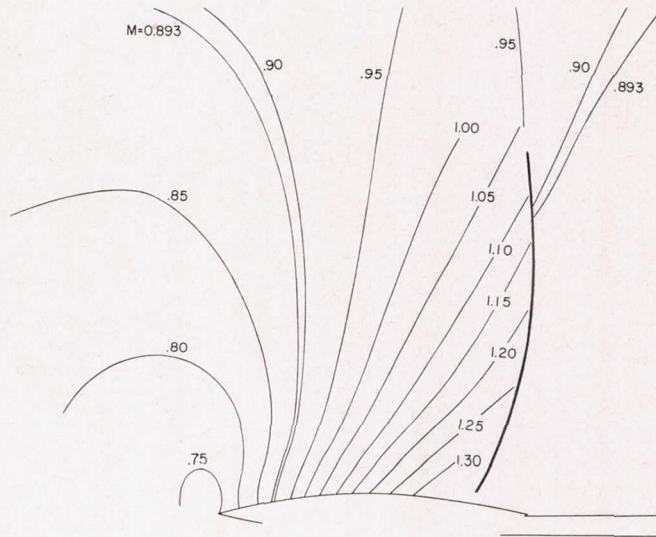
NACA
L-76135



(p) $M_0 = 0.880$. Turbulent.

Figure 4.- Continued.

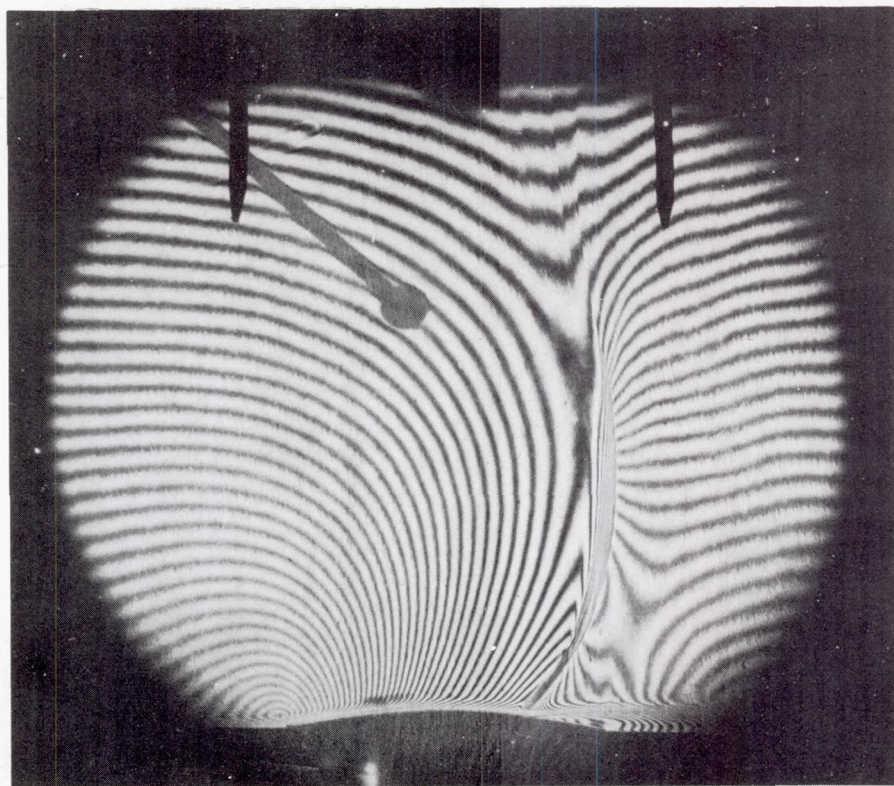
NACA
L-76136



(q). $M_0 = 0.893$. Turbulent.

Figure 4.- Continued.

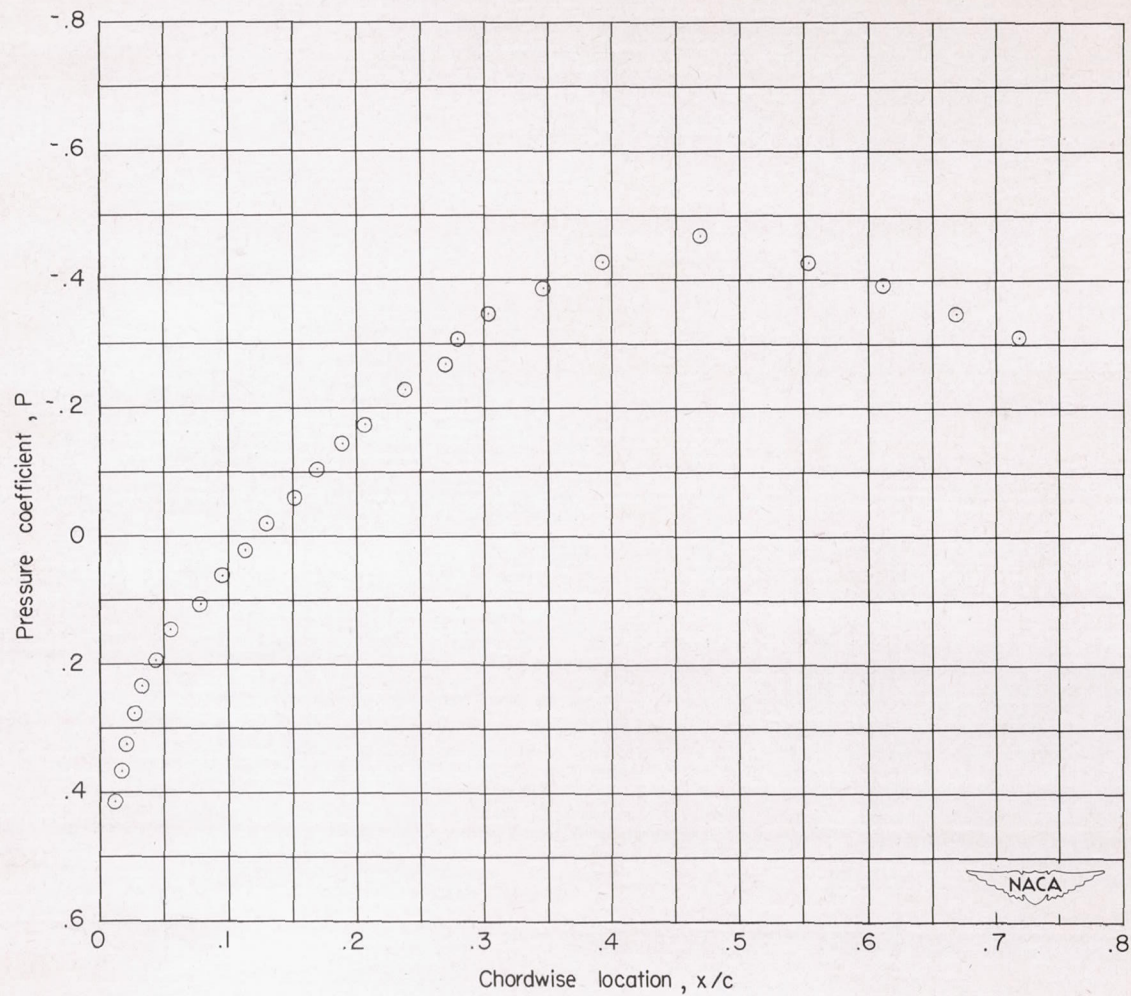
NACA
L-76137



(r) $M_0 = 0.896$. Turbulent.

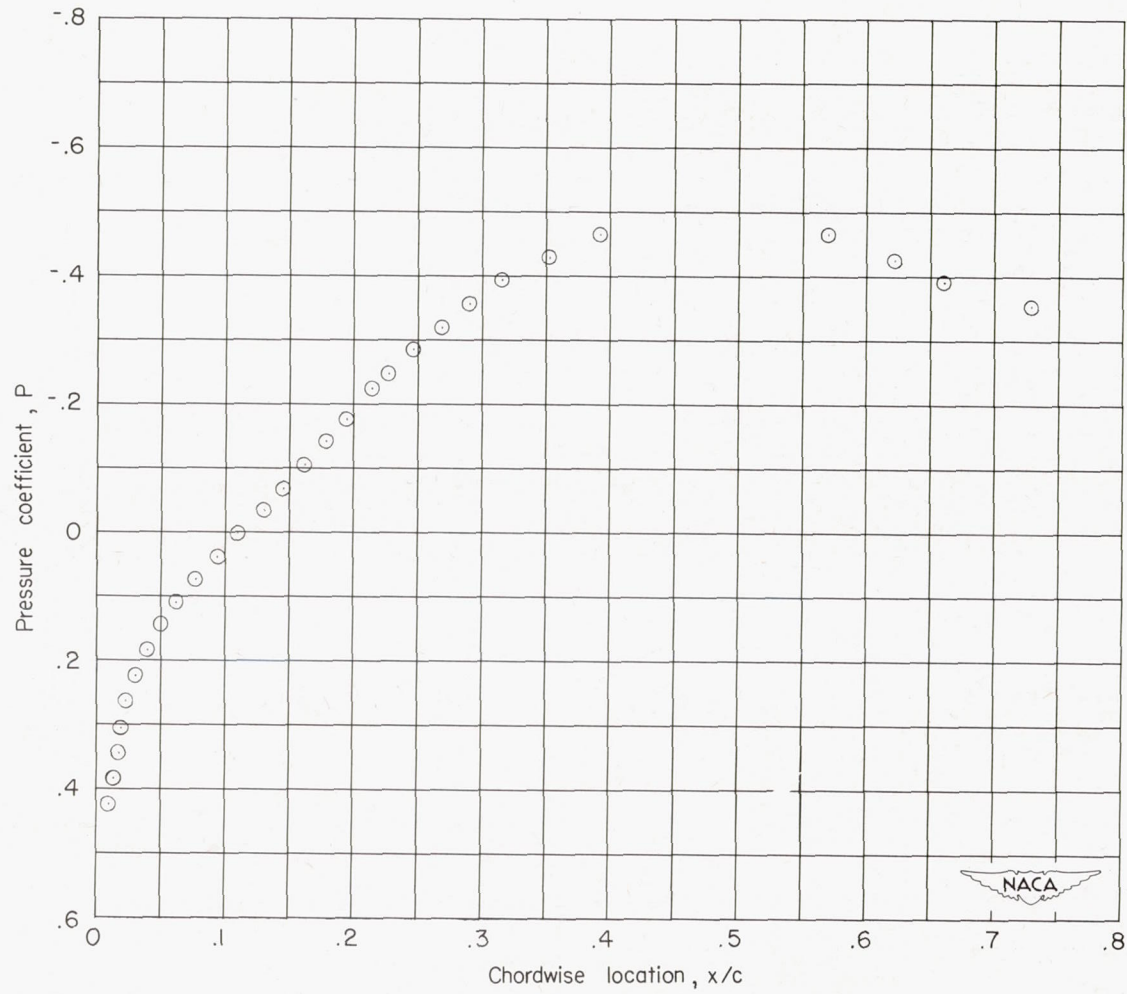
Figure 4.- Concluded.

NACA
L-76138



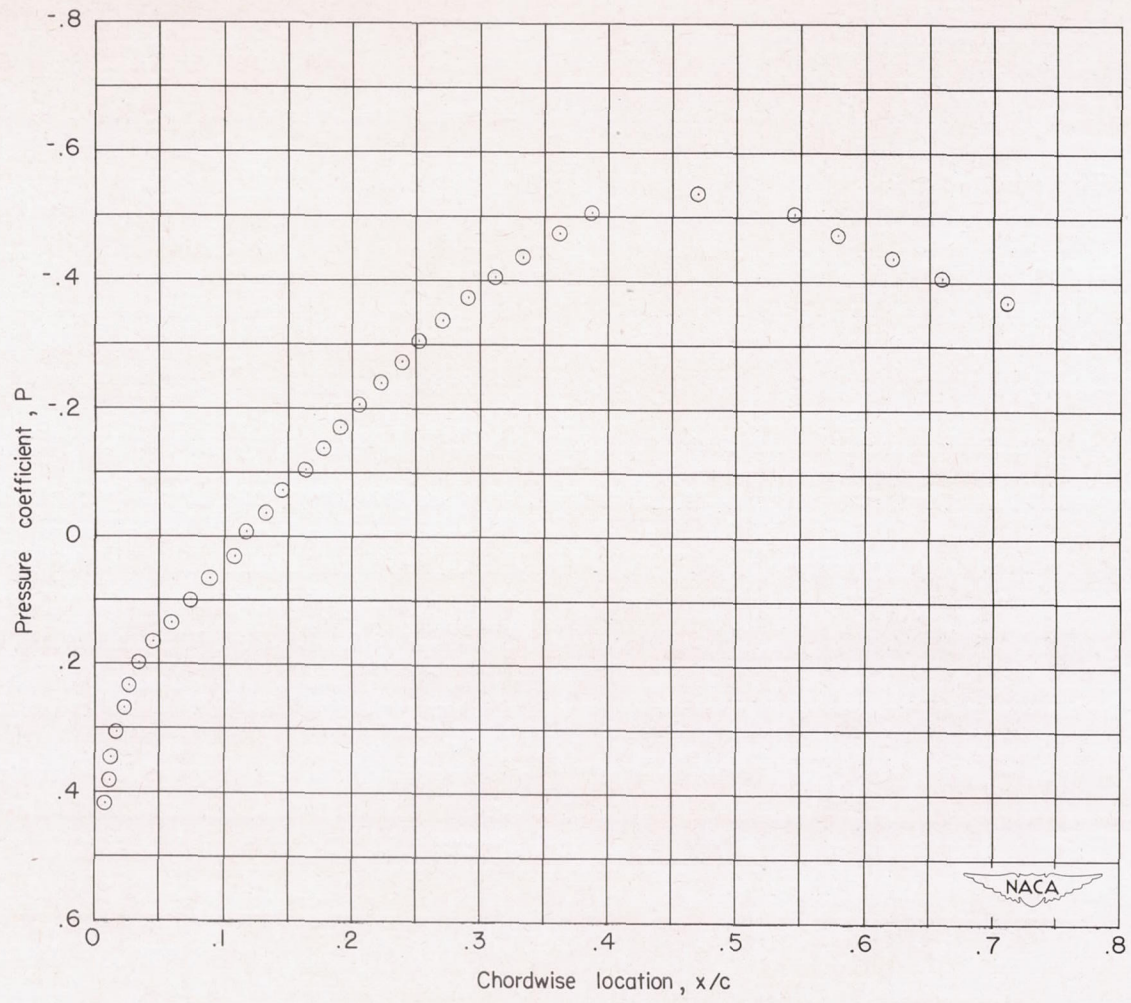
(a) $M_0 = 0.609$.

Figure 5.- Pressure coefficient as a function of chordwise location.



(b) $M_0 = 0.641$.

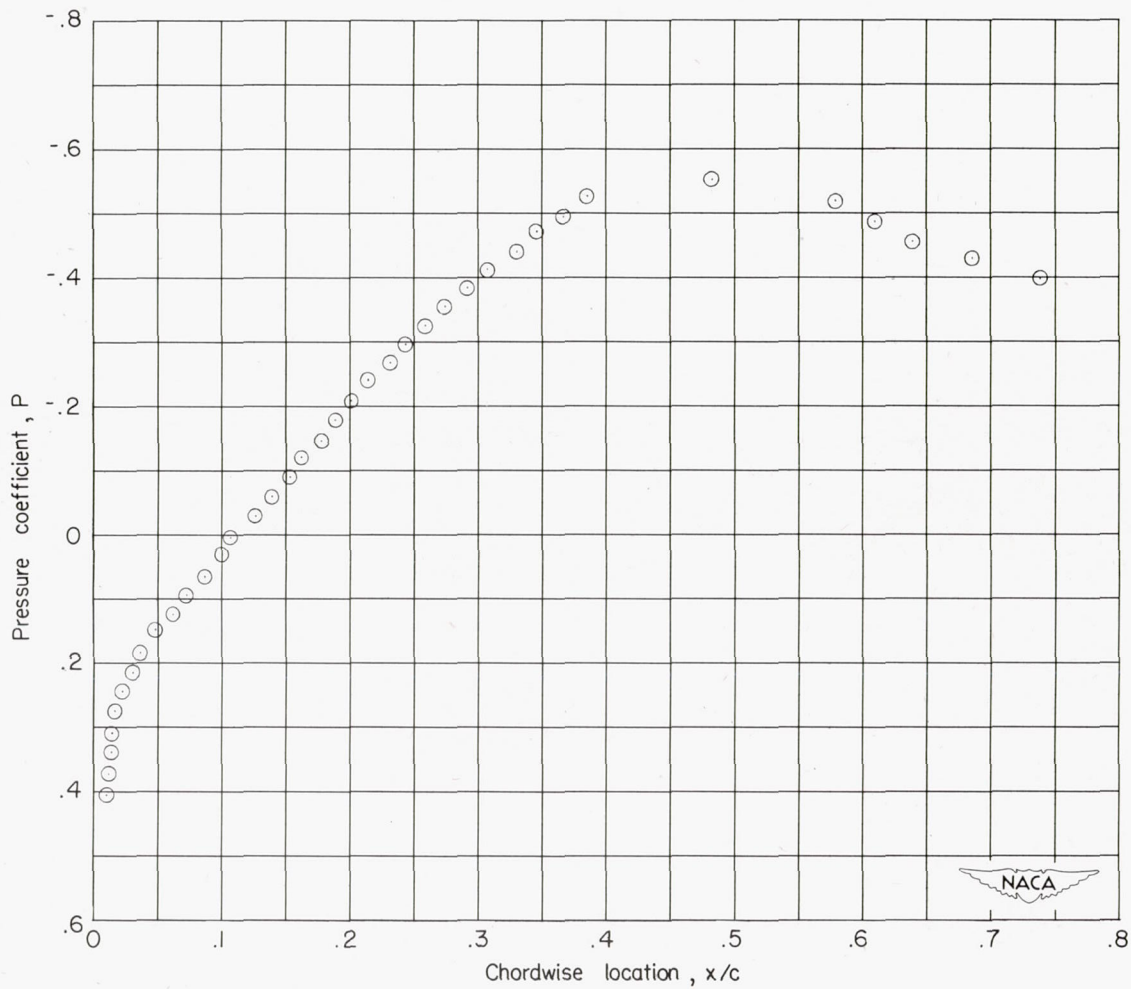
Figure 5.- Continued.



(c) $M_0 = 0.665$.

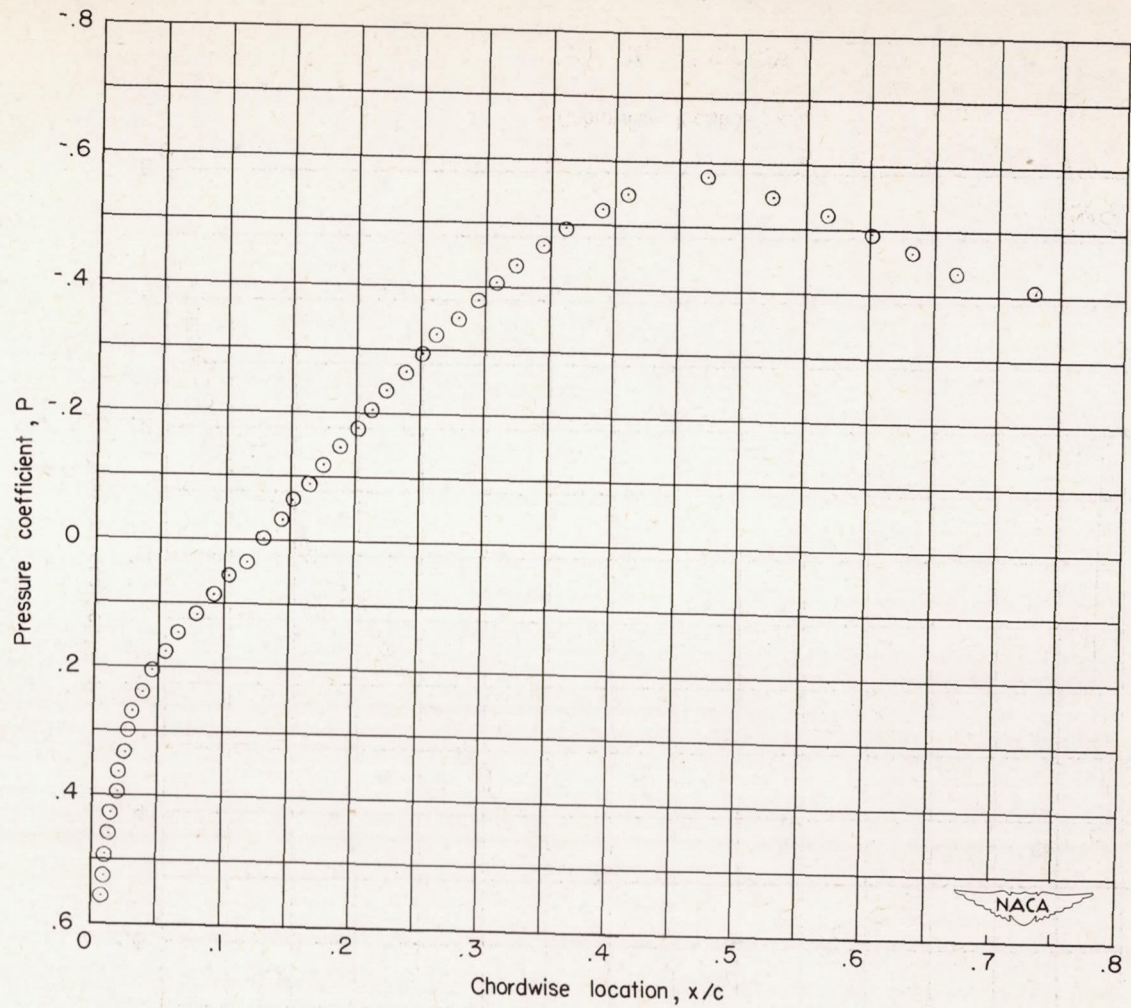
Figure 5.- Continued.





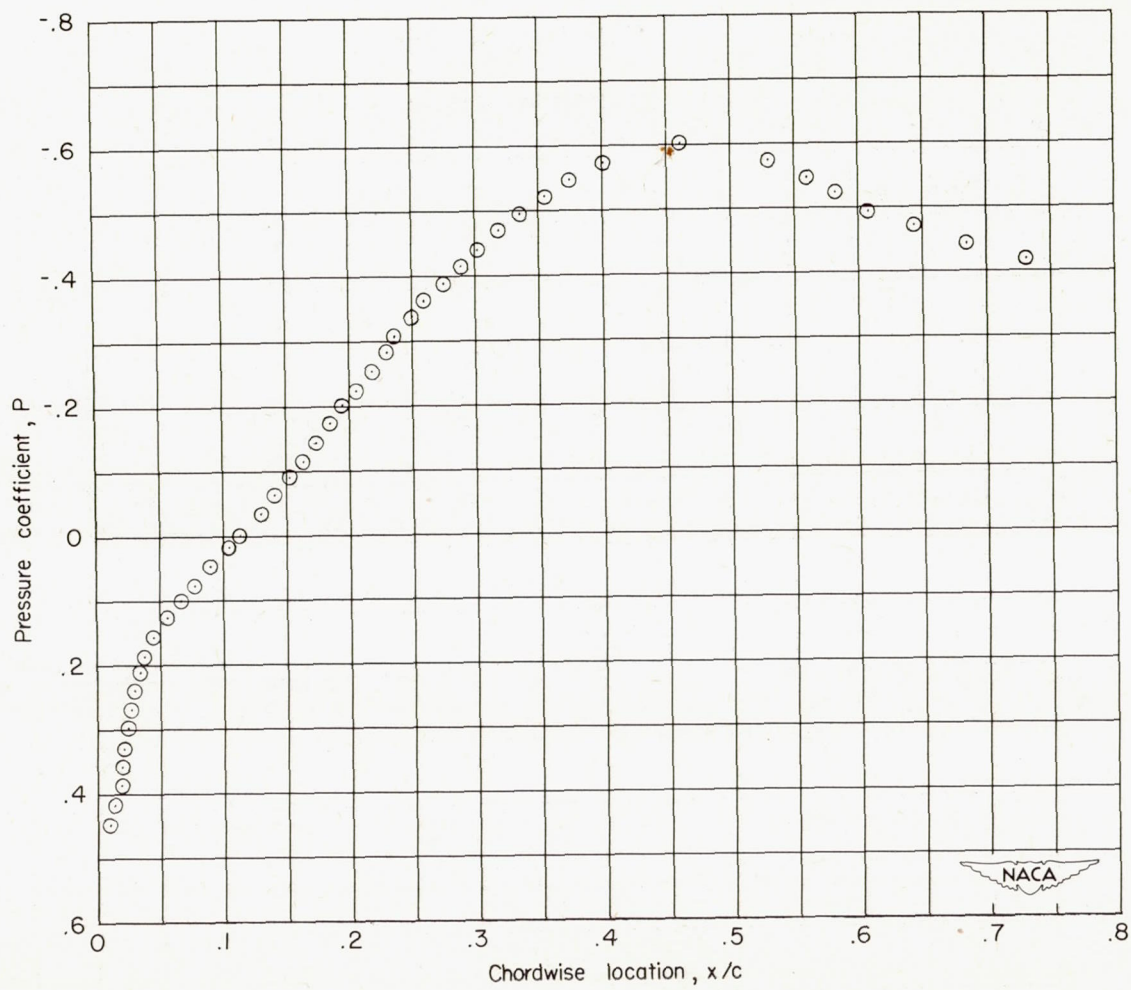
(d) $M_0 = 0.692$.

Figure 5.- Continued.



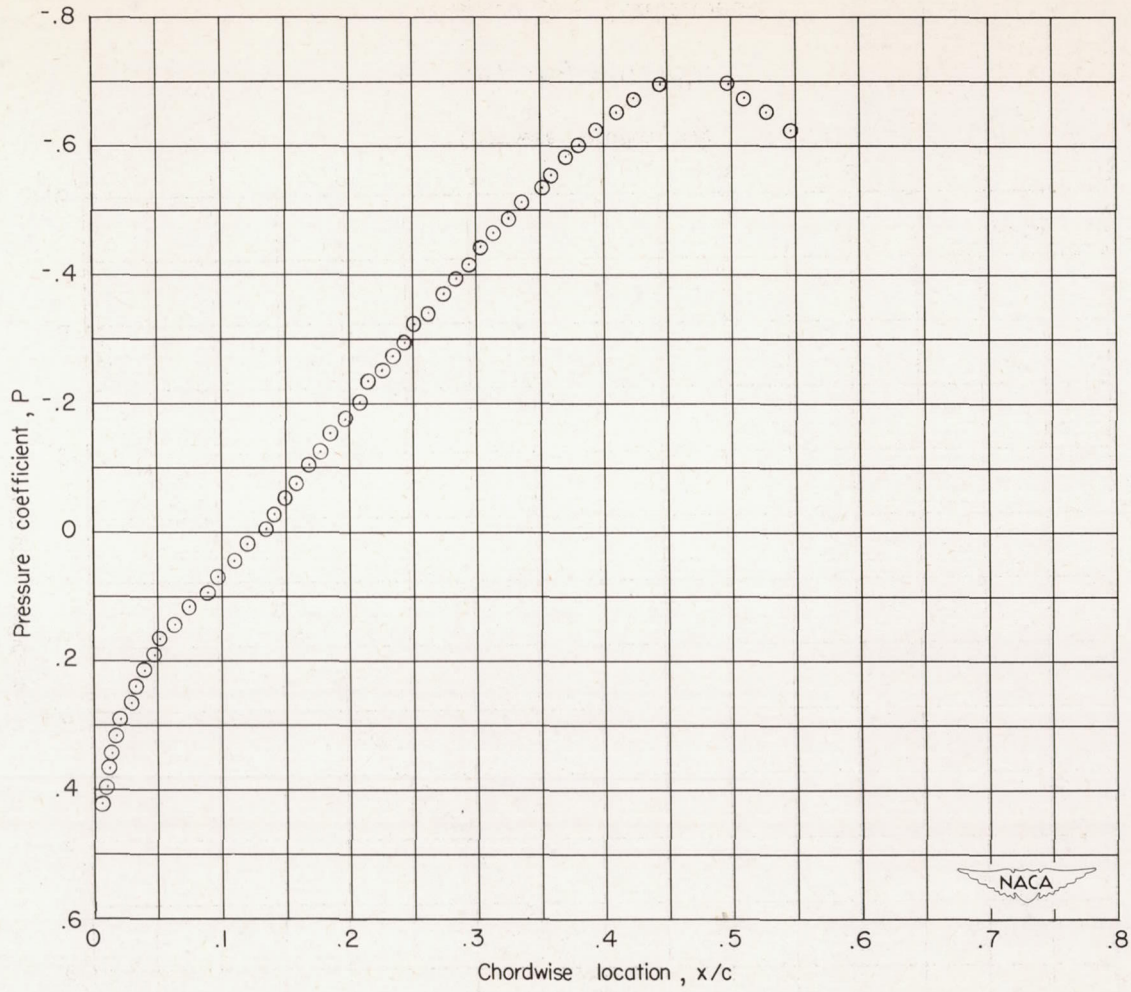
(e) $M_0 = 0.706$.

Figure 5.- Continued.



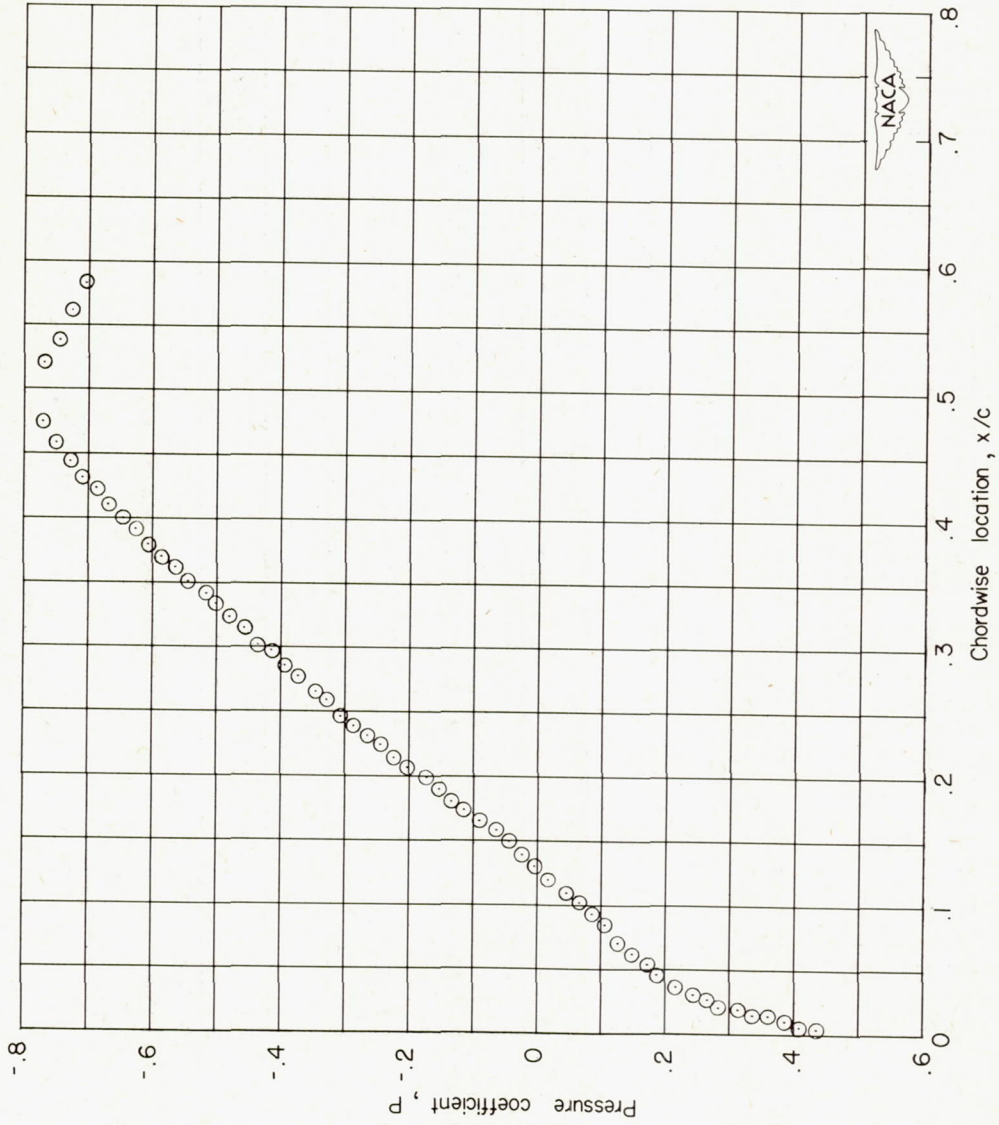
(f) $M_0 = 0.725$.

Figure 5.- Continued.



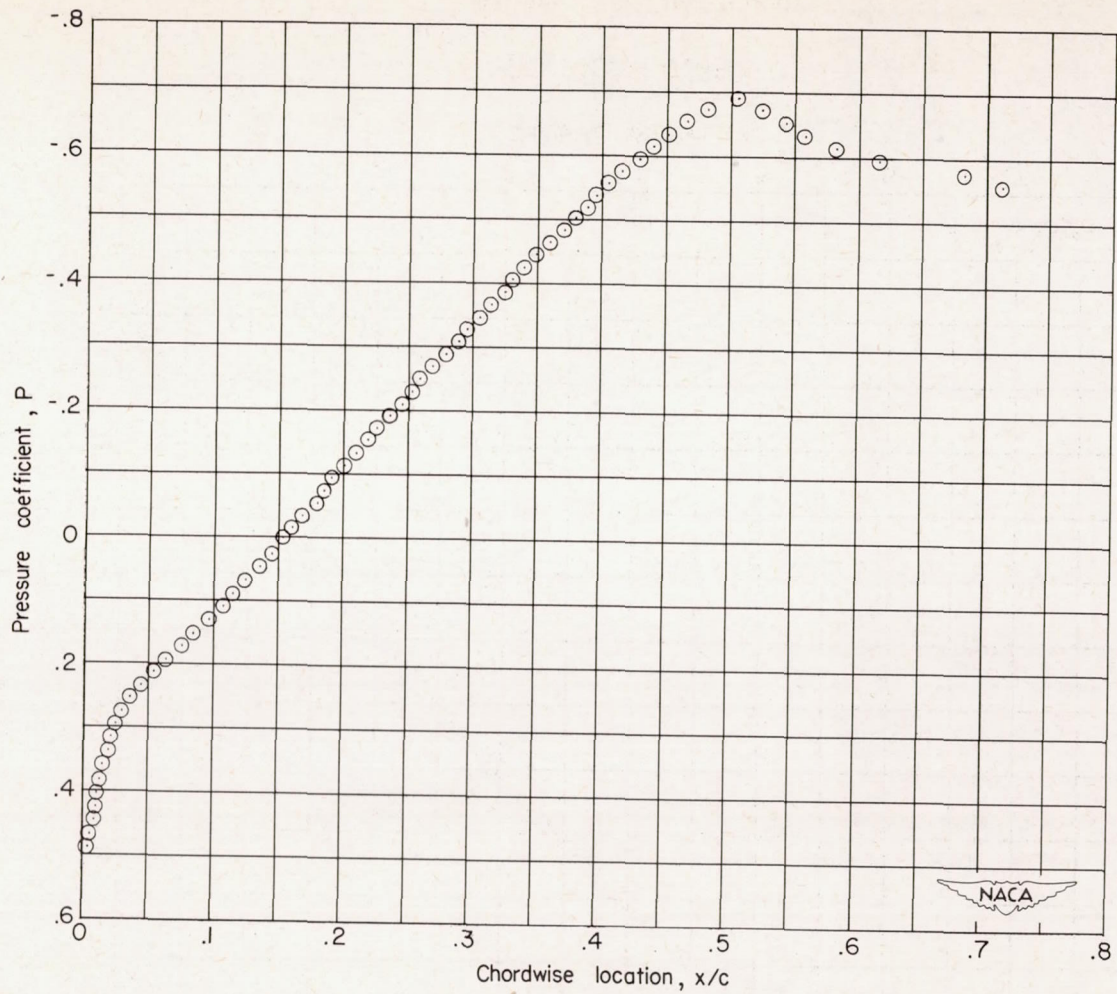
(g) $M_0 = 0.761$.

Figure 5.- Continued.



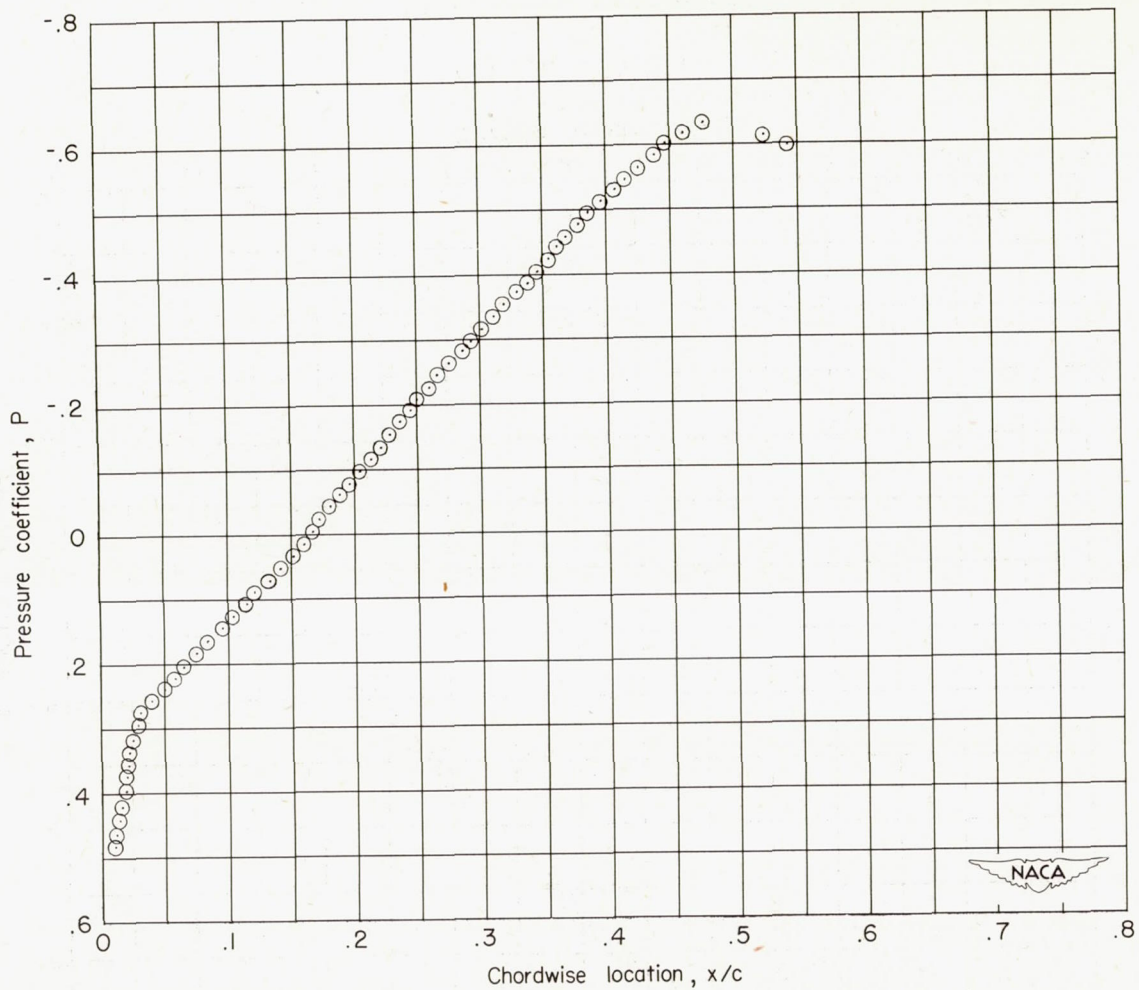
(h) $M_0 = 0.784$.

Figure 5.- Continued.



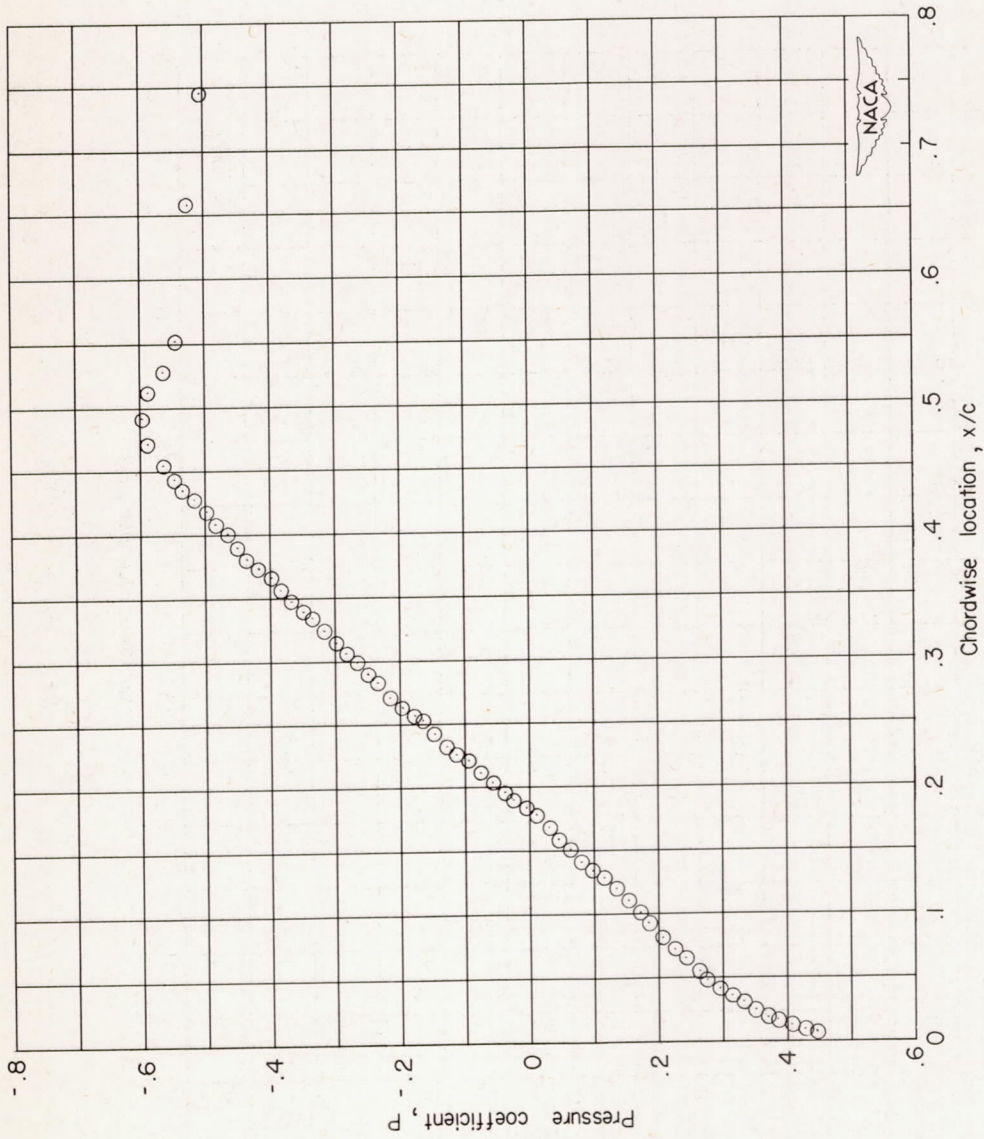
(i) $M_0 = 0.821$.

Figure 5.- Continued.



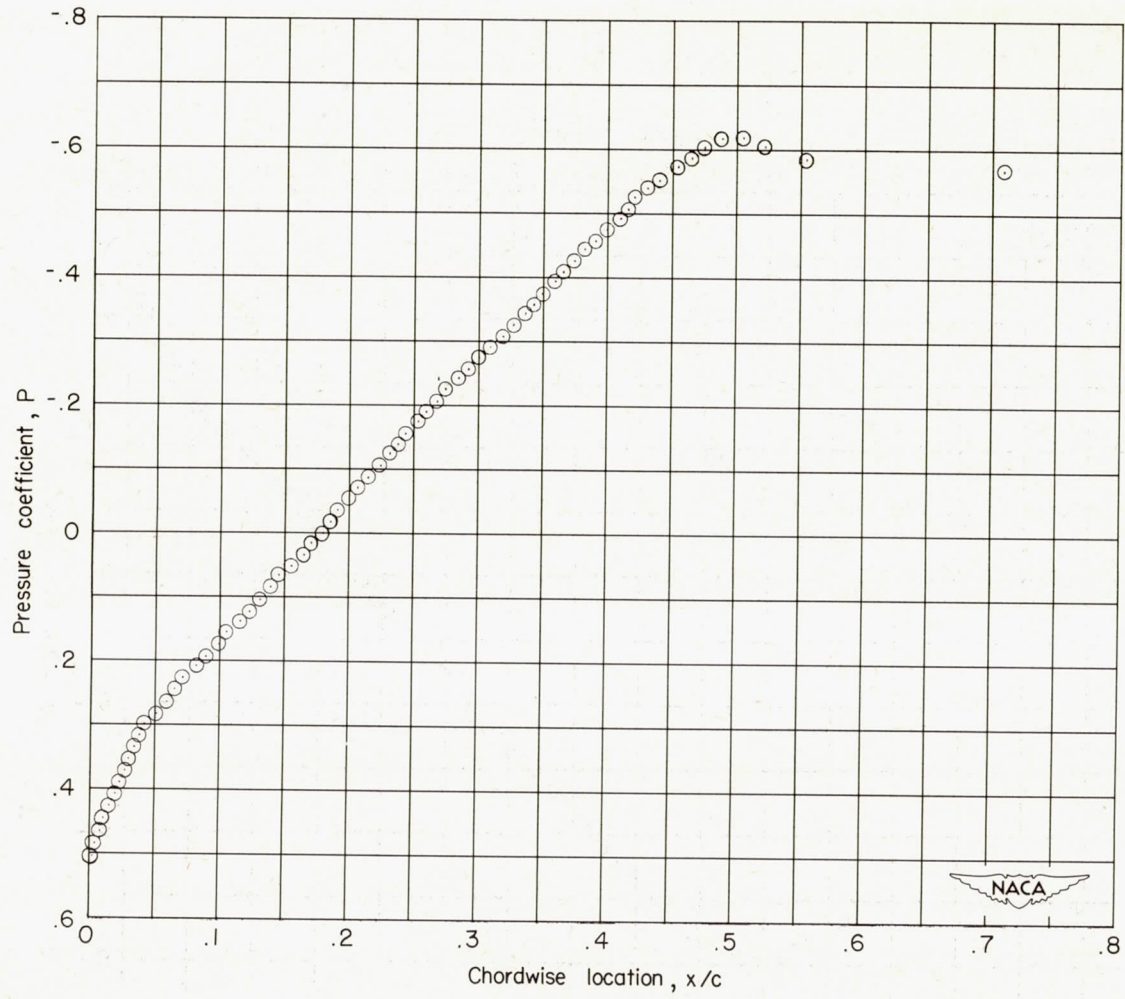
(j) $M_0 = 0.838$.

Figure 5.- Continued.



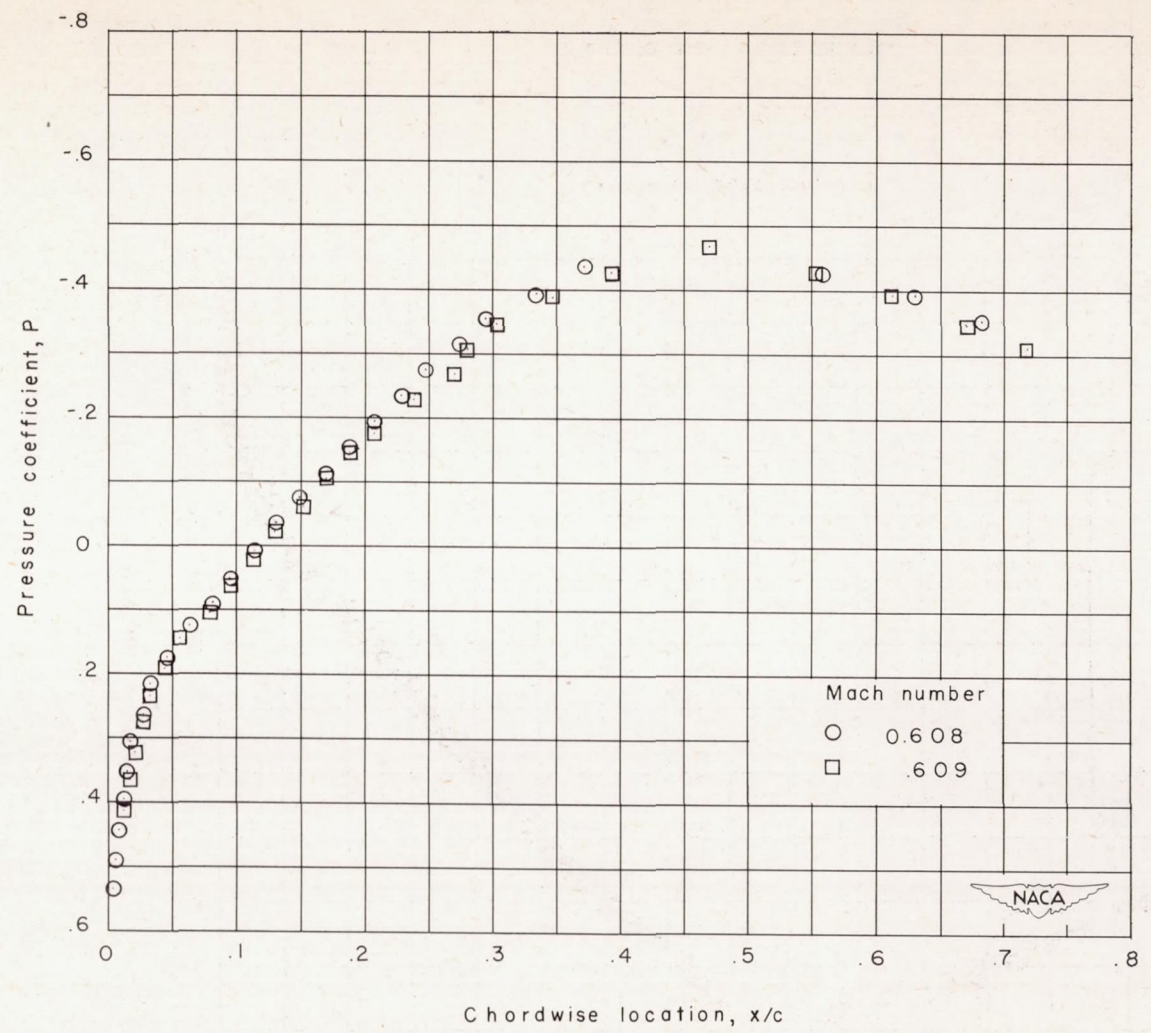
(k) $M_0 = 0.861$.

Figure 5.- Continued.



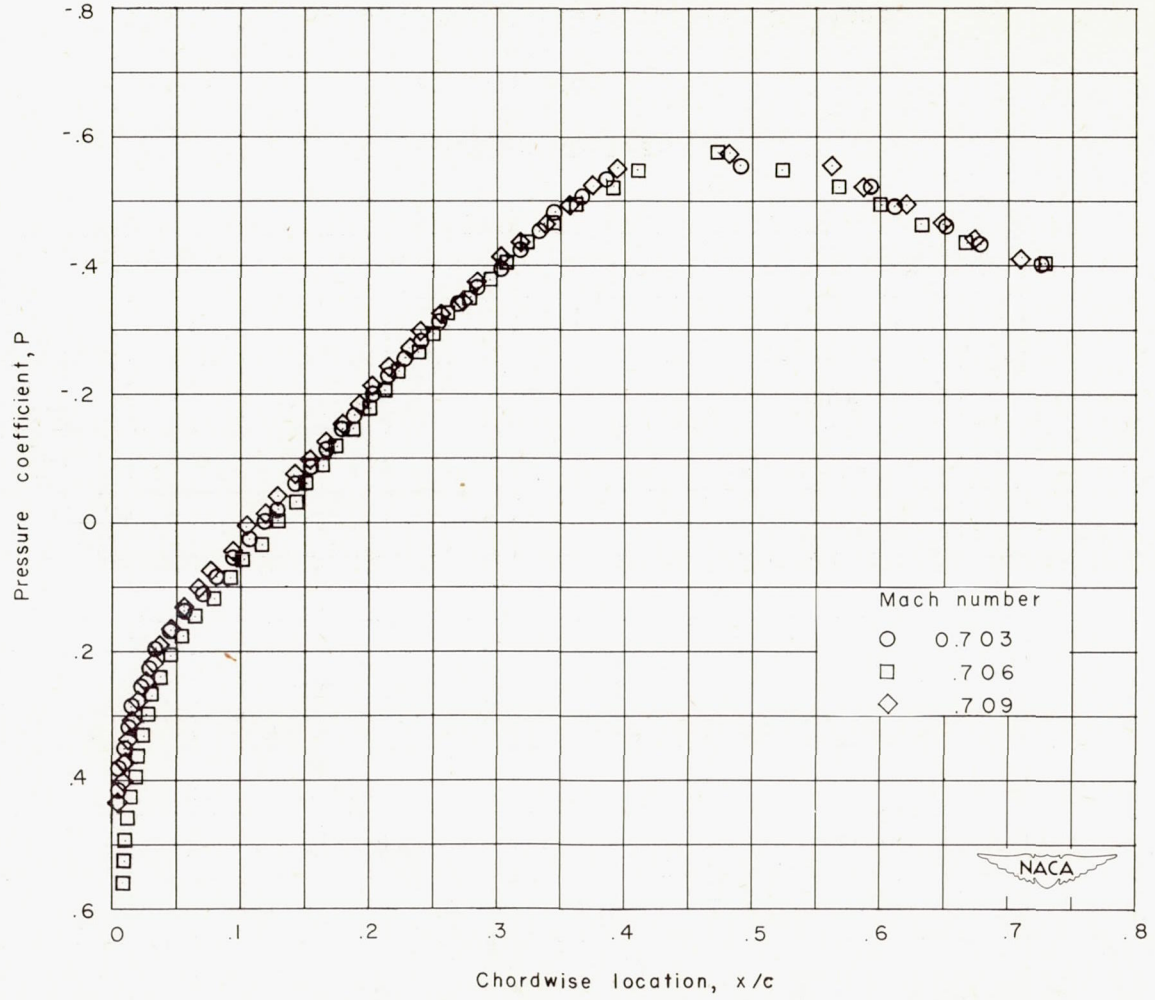
(2) $M_0 = 0.880$.

Figure 5.- Concluded.



(a) $M \approx 0.61$.

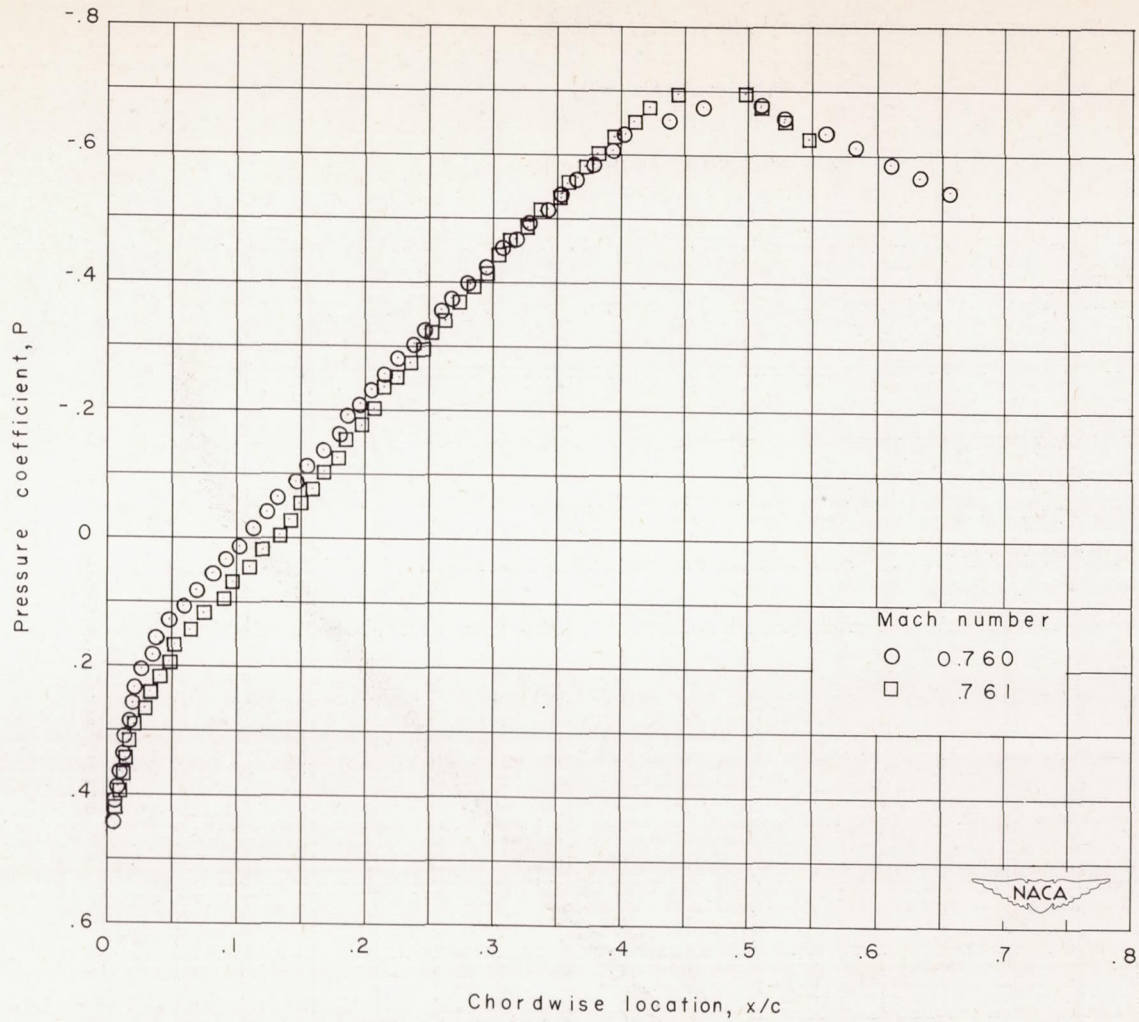
Figure 6.- Comparisons of pressure distributions.



(b) $M \approx 0.70$.

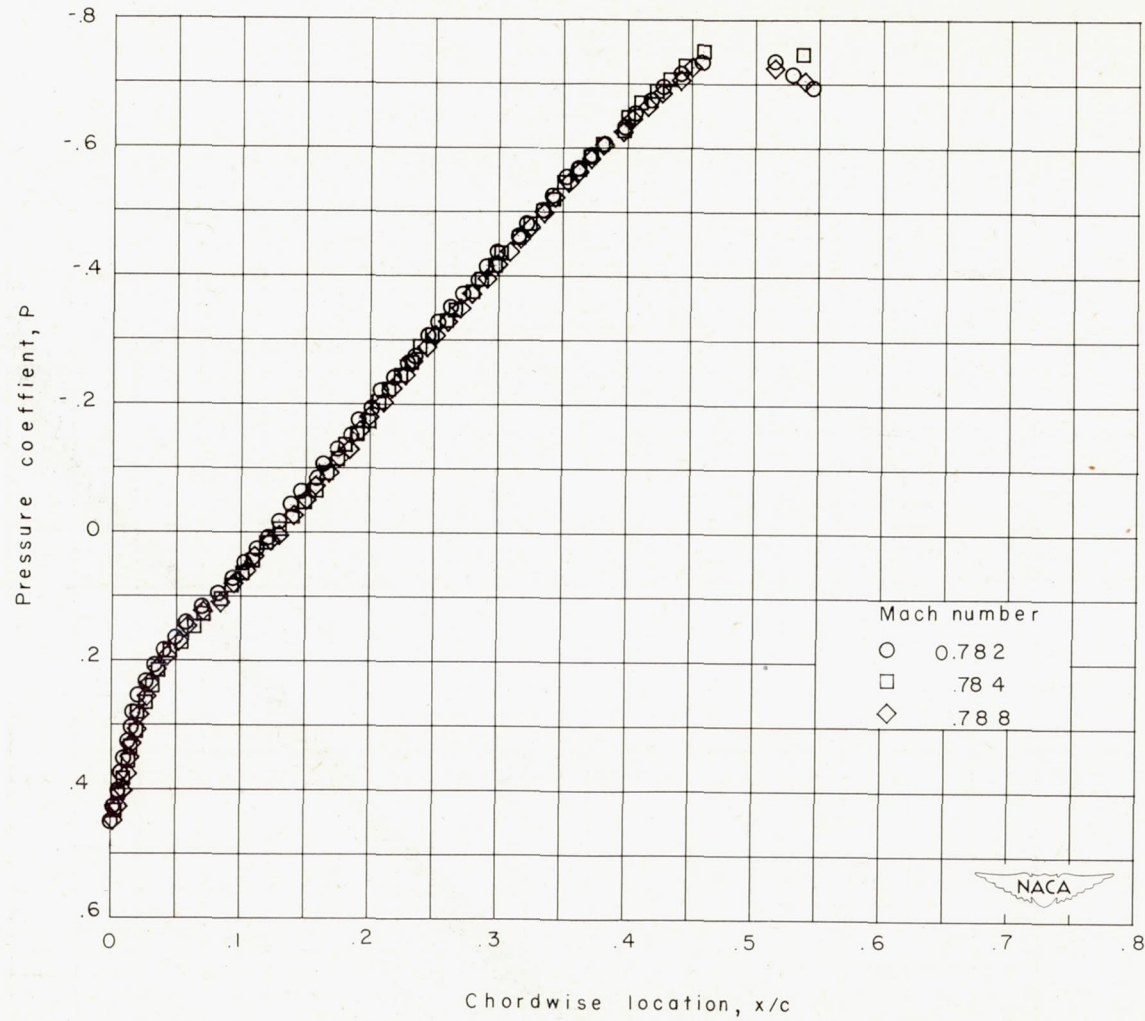
Figure 6.- Continued.





(c) $M \approx 0.76$.

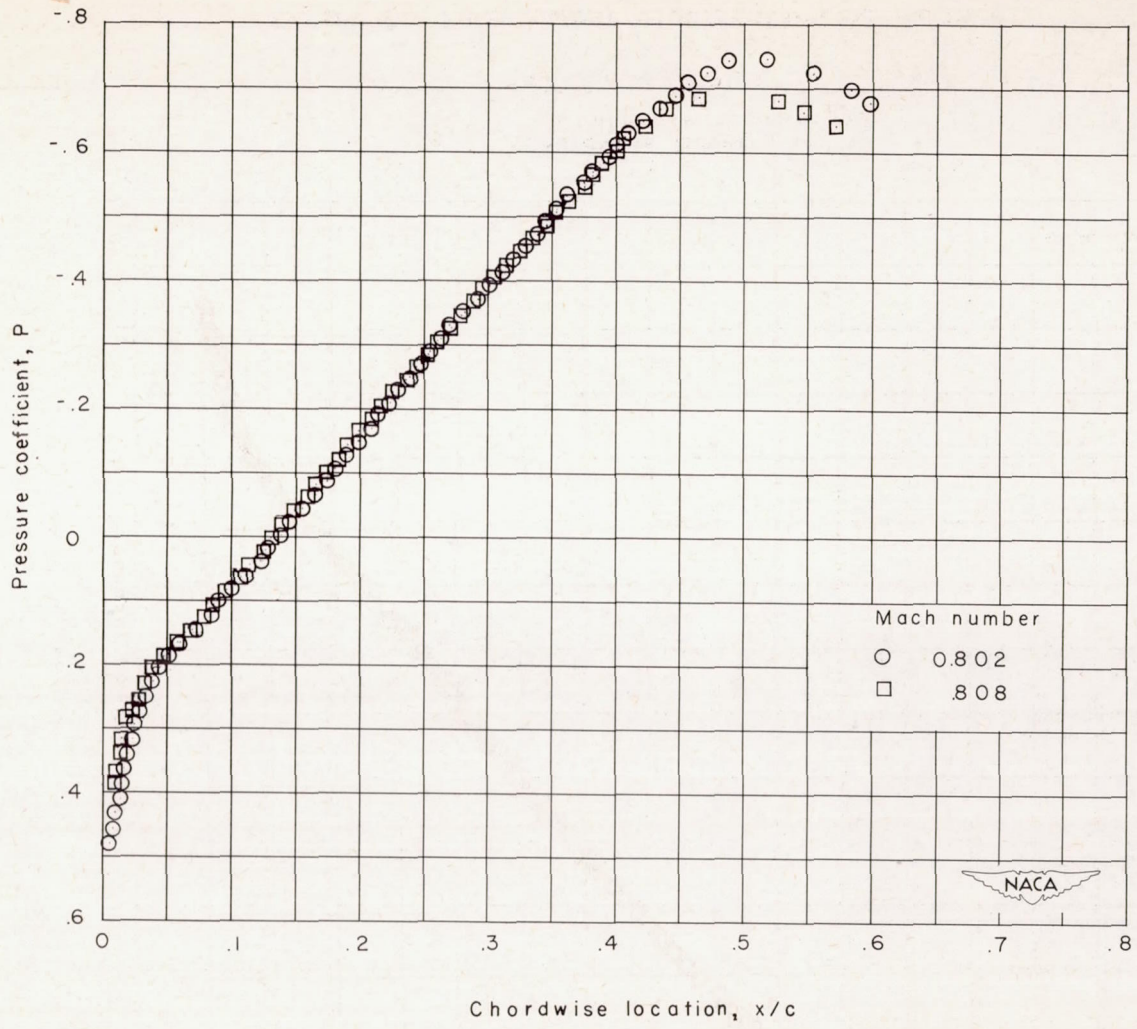
Figure 6.- Continued.



(d) $M \approx 0.78$.

Figure 6.- Continued.

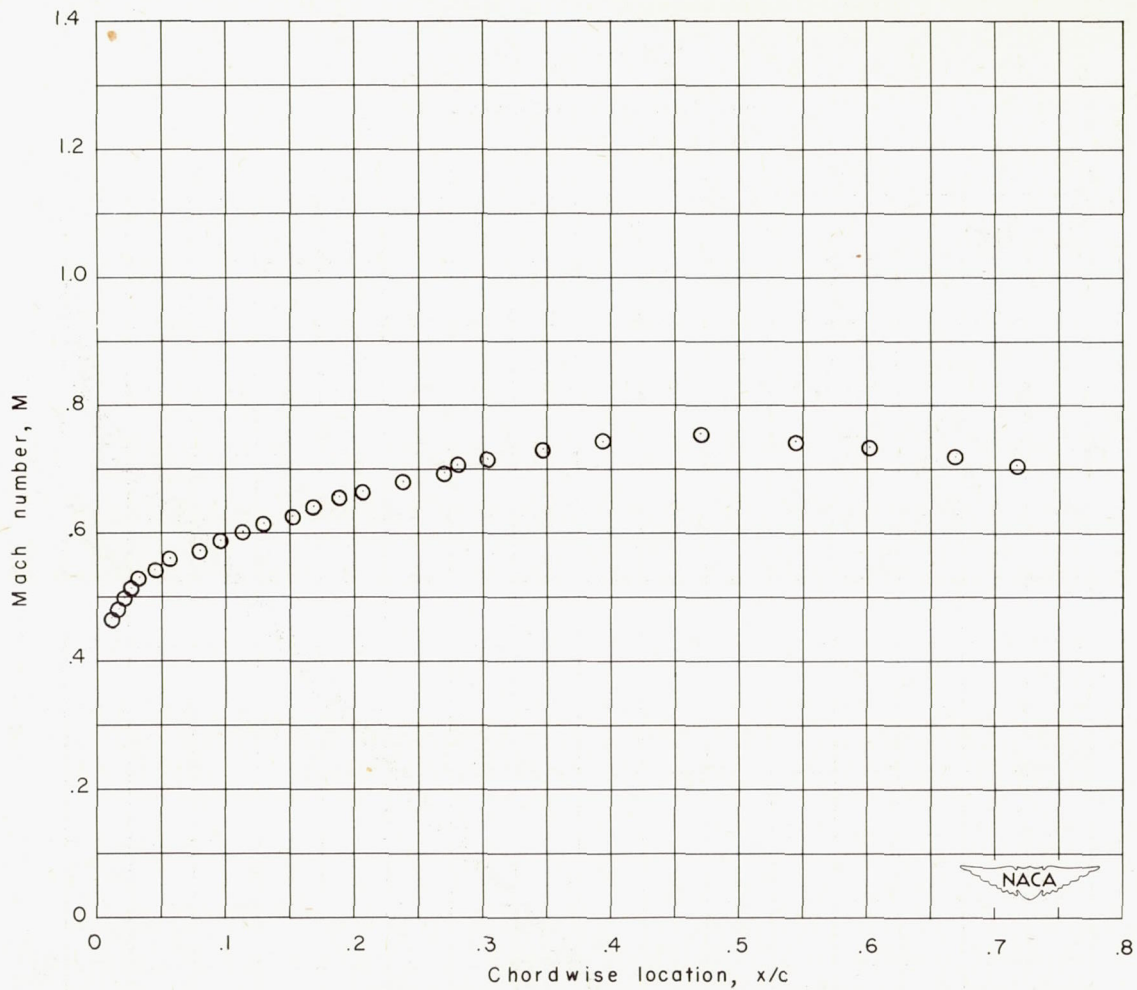




Chordwise location, x/c

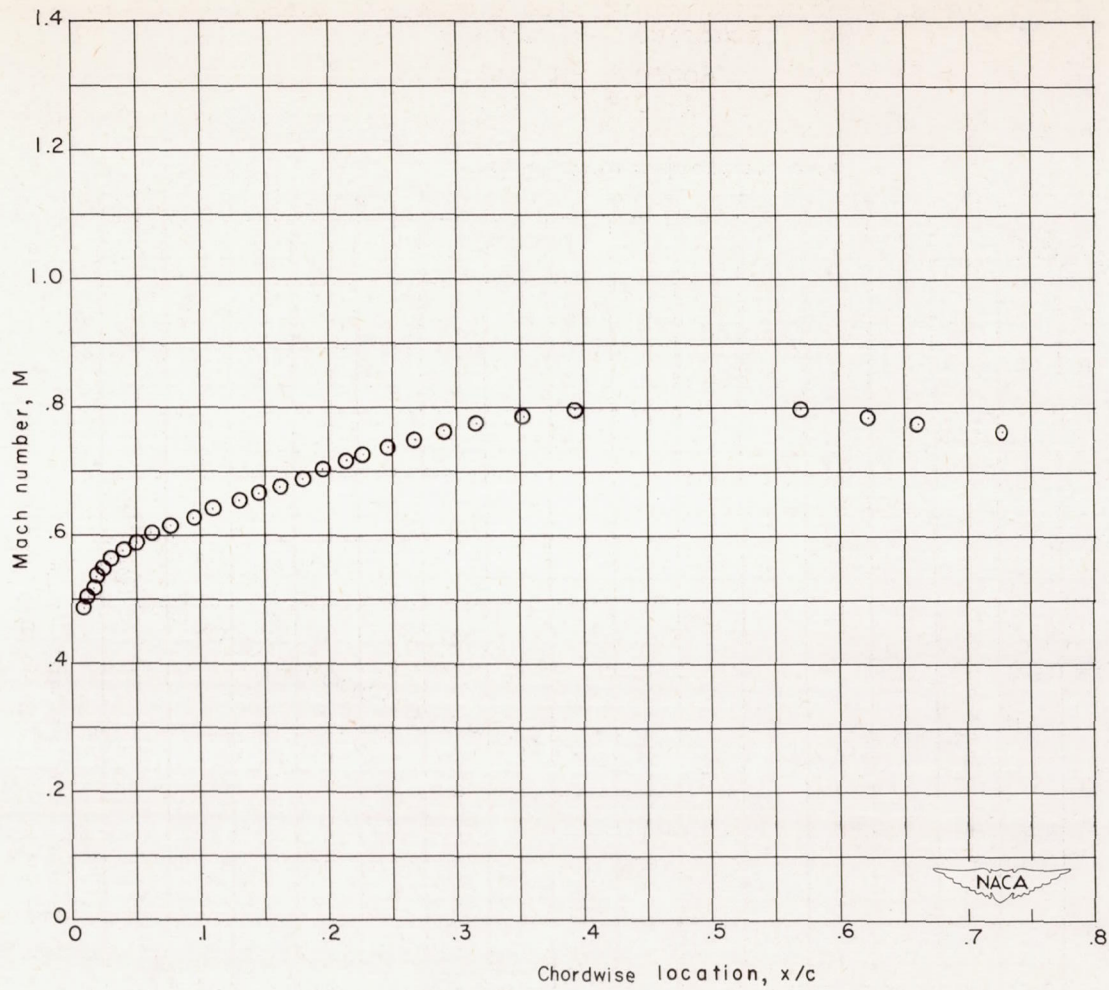
(e) $M \approx 0.80$.

Figure 6.- Concluded.



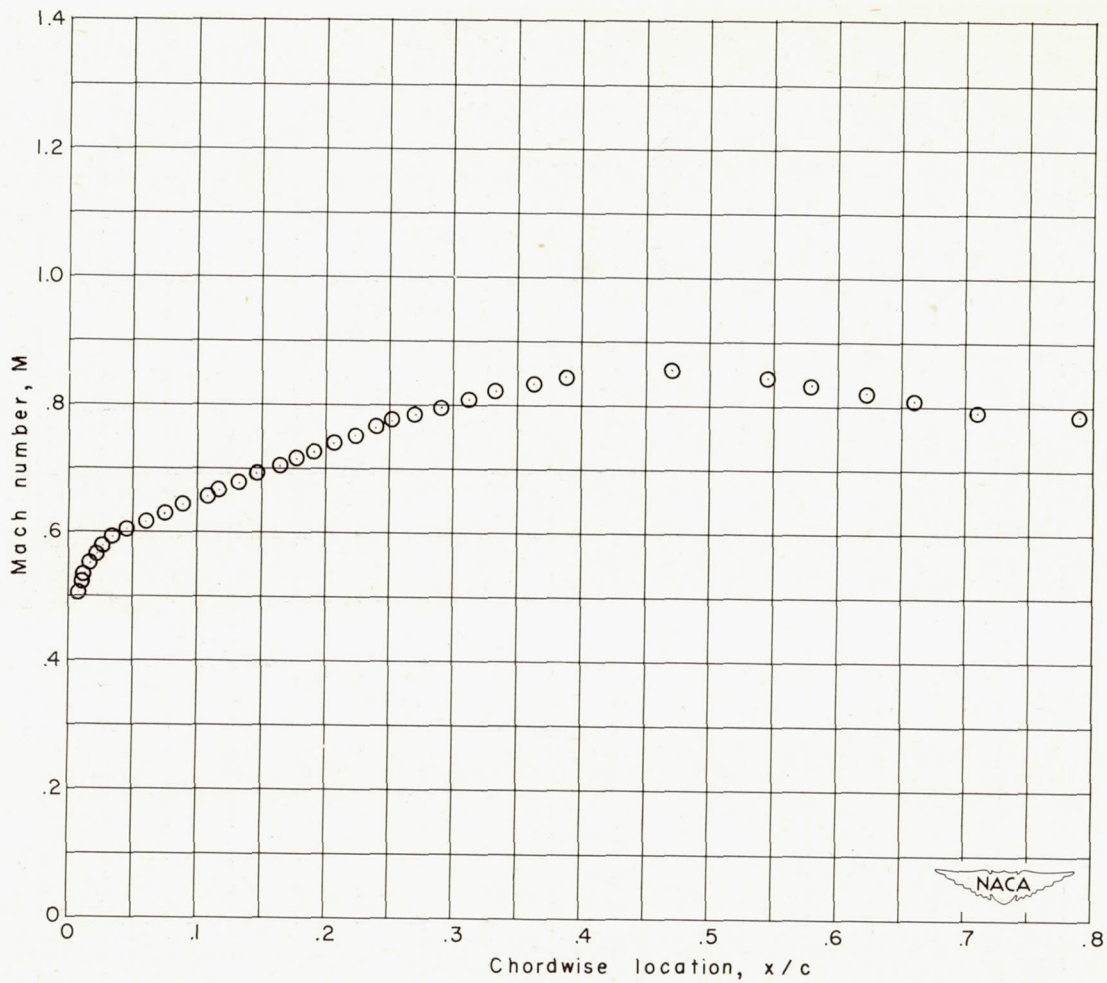
(a) $M_0 = 0.609$.

Figure 7.- Mach number distribution on surface.



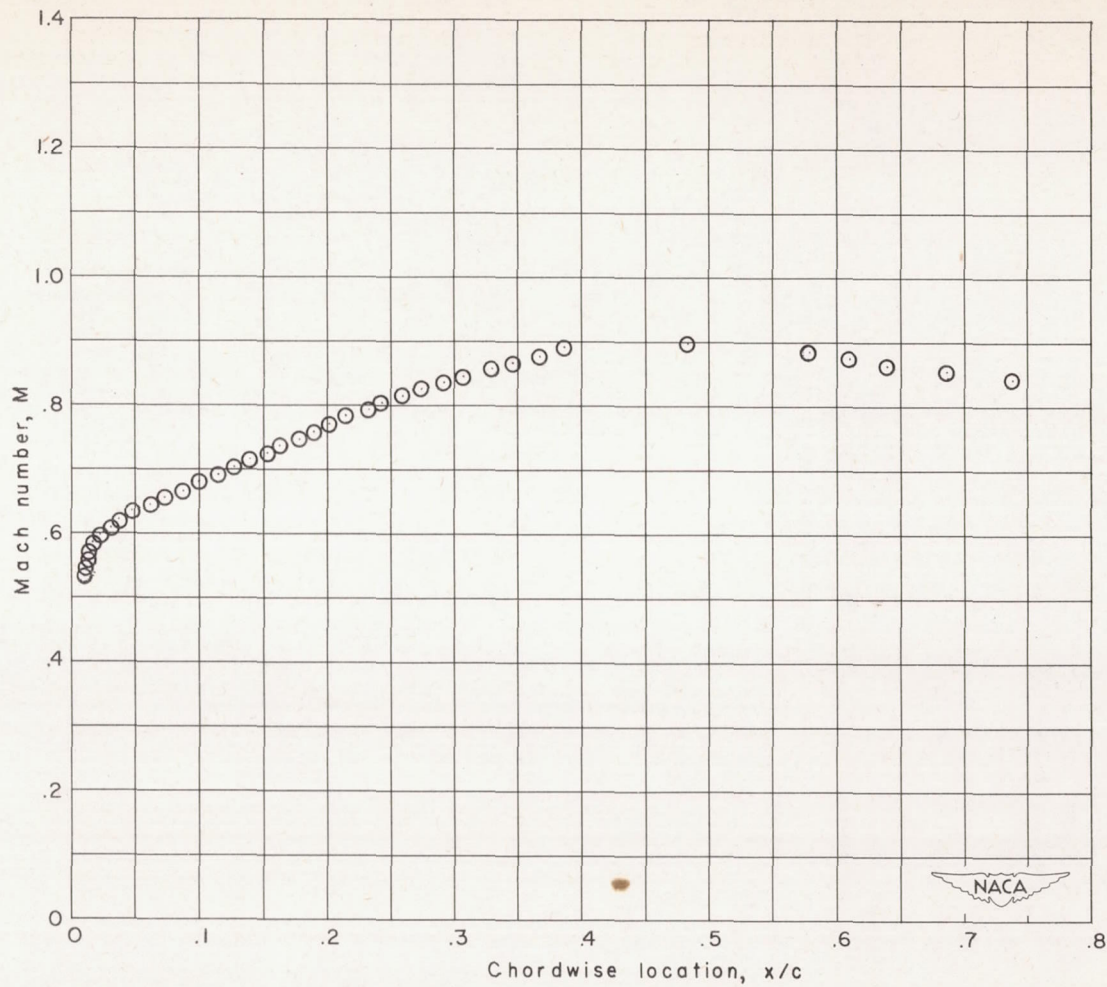
(b) $M_0 = 0.641$.

Figure 7.- Continued.



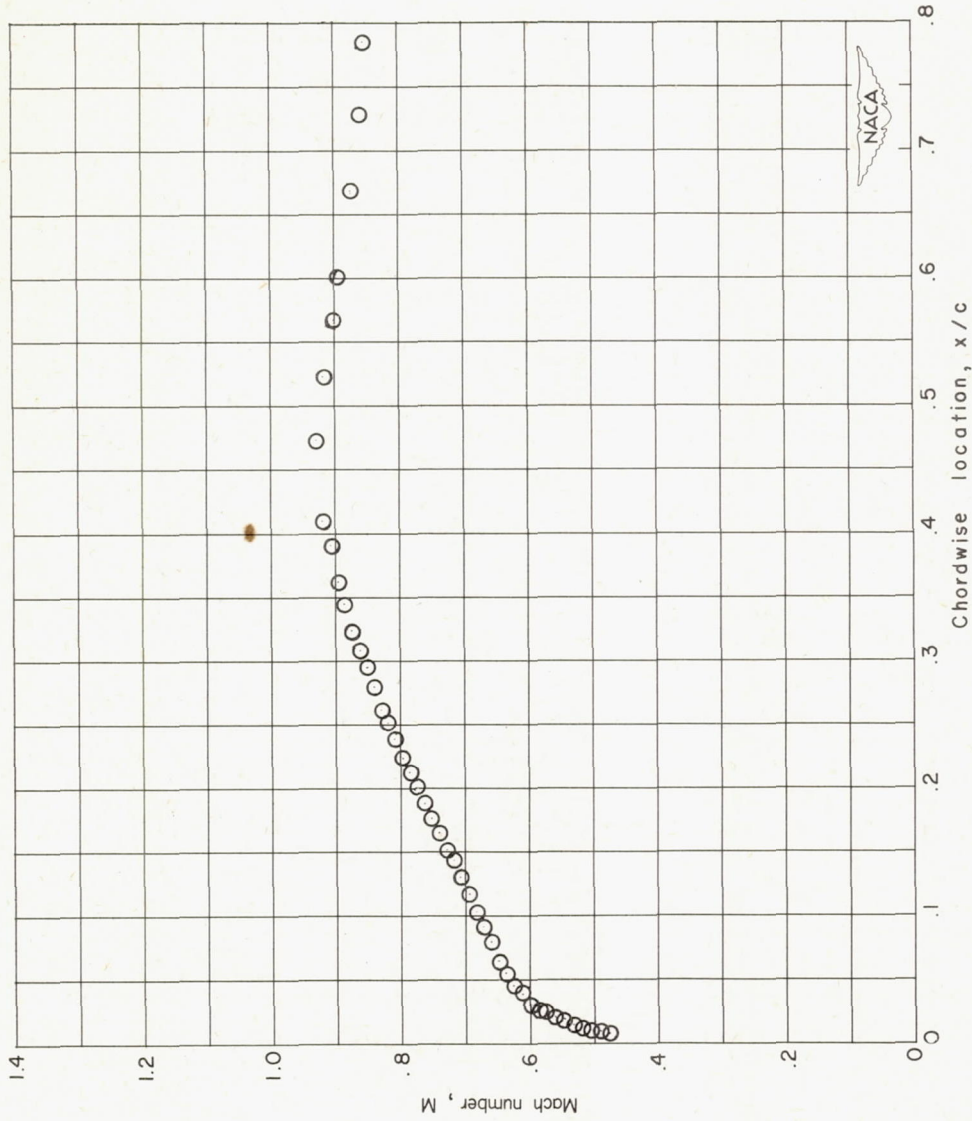
(c) $M_0 = 0.665$.

Figure 7.- Continued.



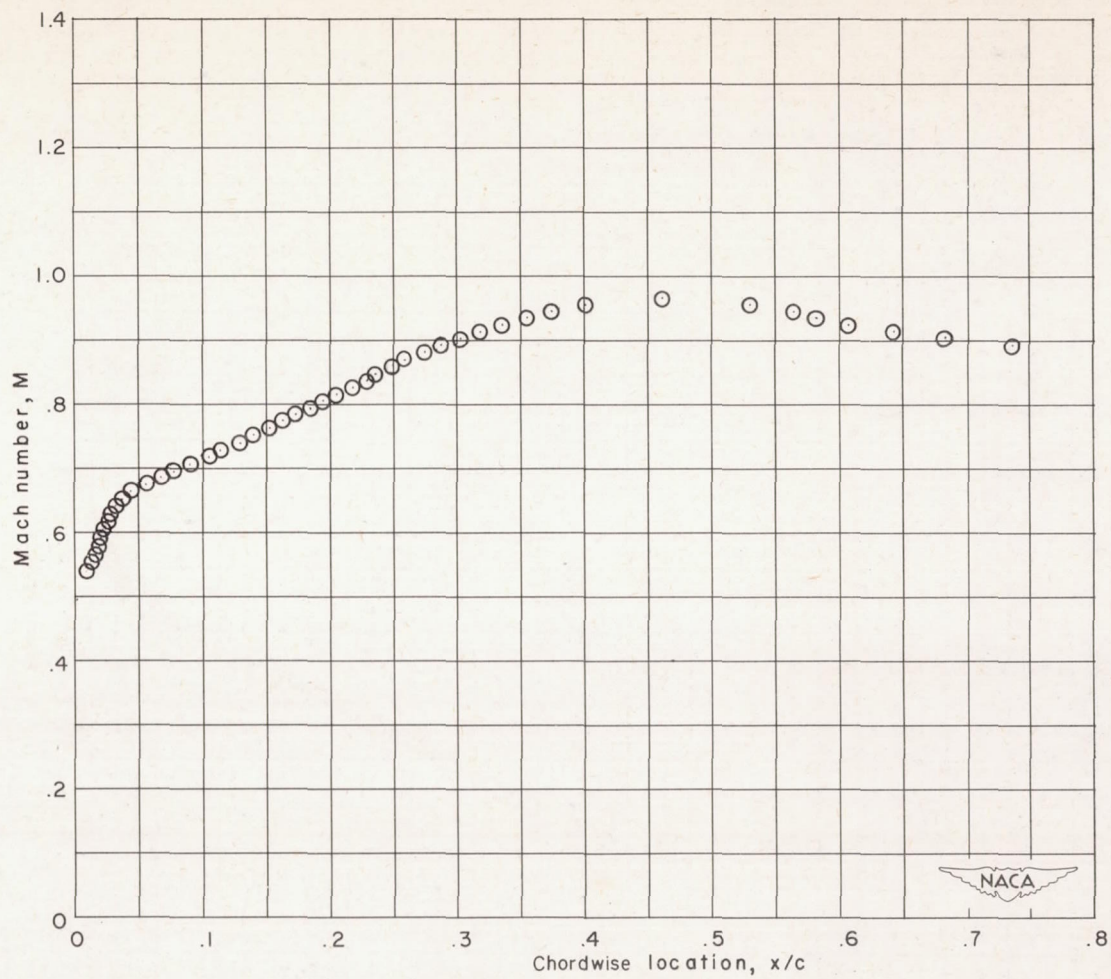
(d) $M_0 = 0.692$.

Figure 7.- Continued.



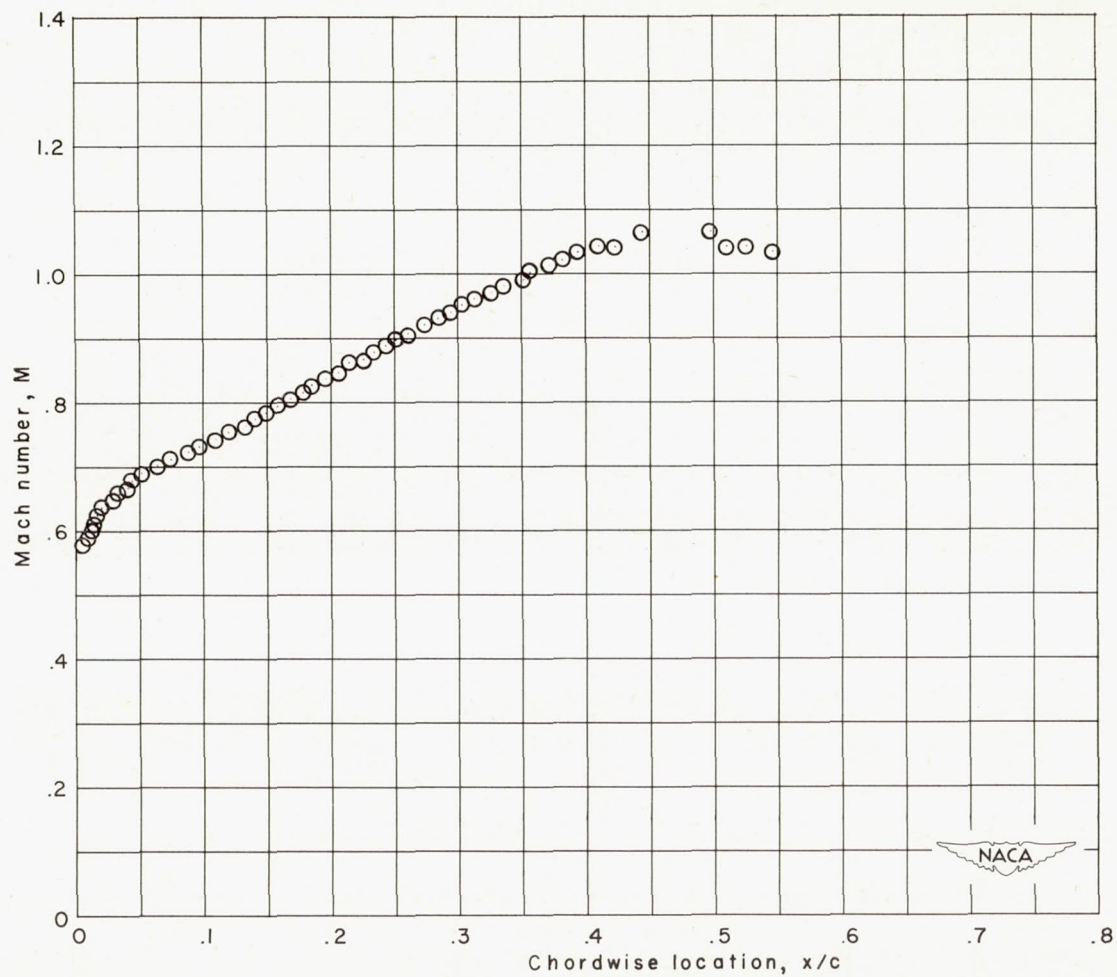
(e) $M_0 = 0.706$.

Figure 7.- Continued.



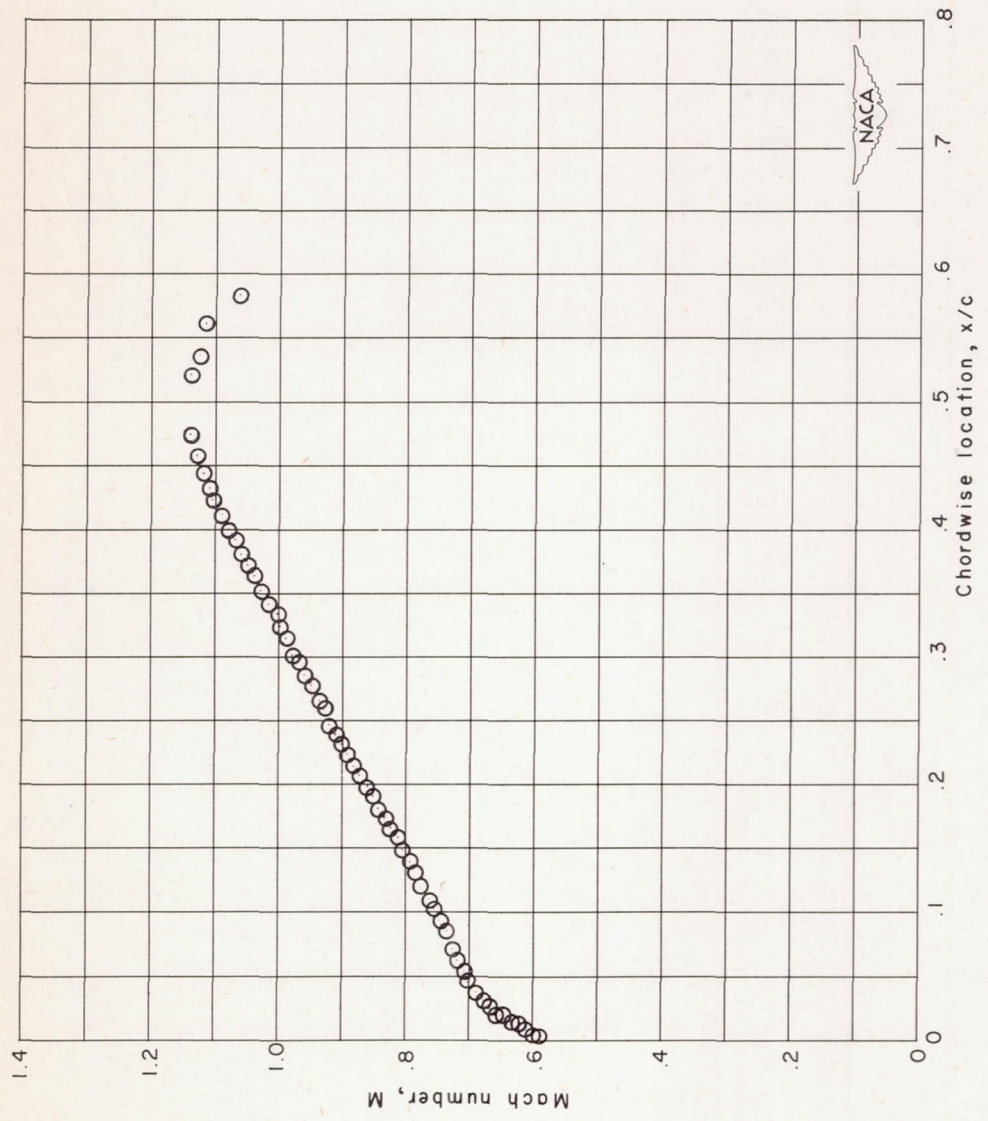
(f) $M_0 = 0.725$.

Figure 7.- Continued.



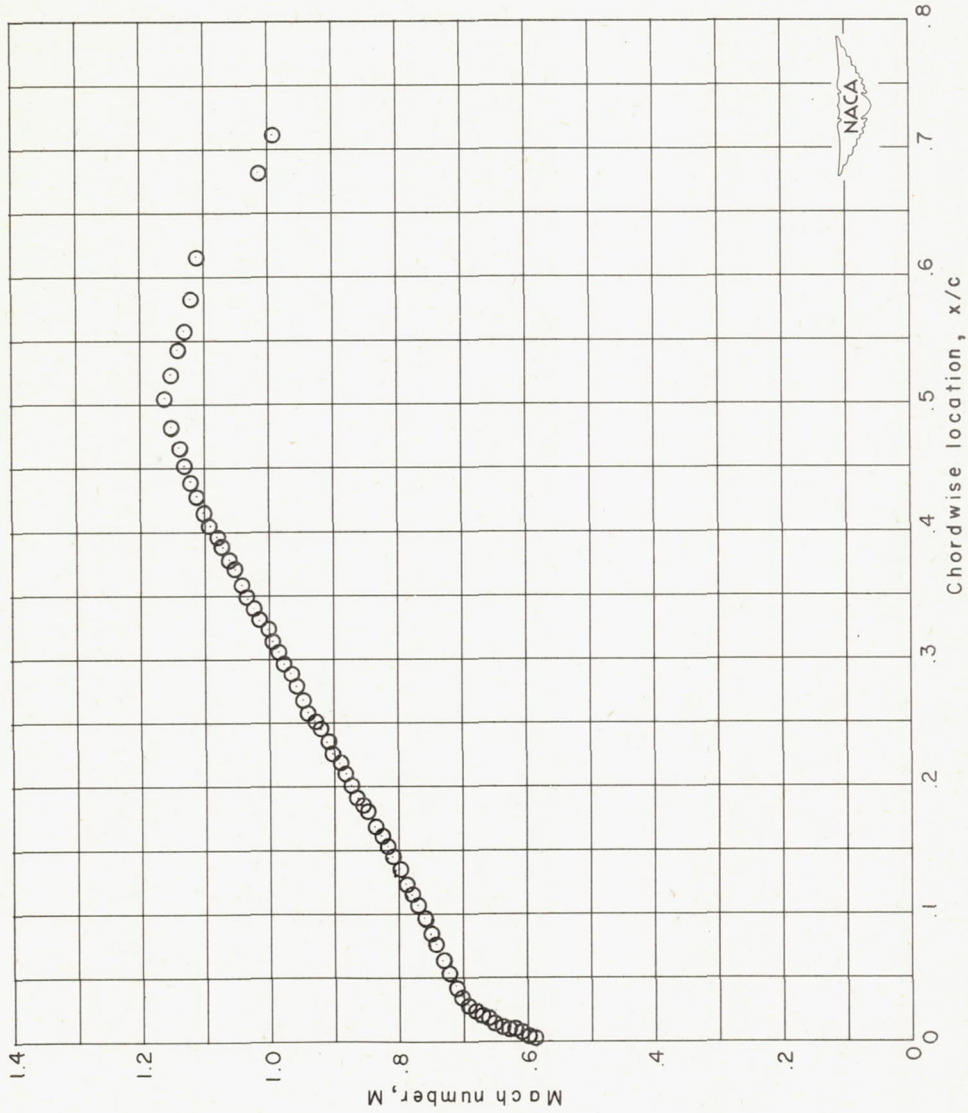
(g) $M_0 = 0.761$.

Figure 7.- Continued.



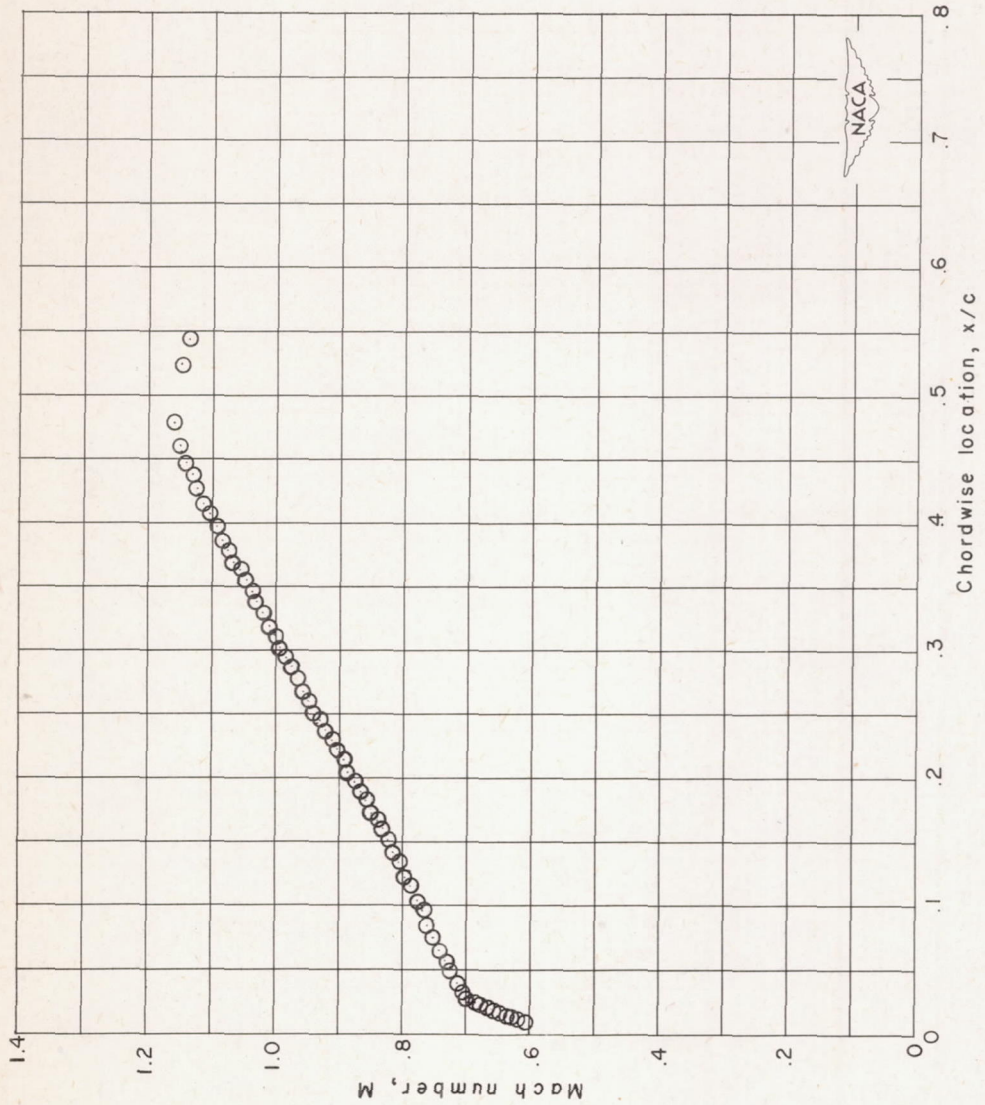
(h) $M_0 = 0.784$.

Figure 7.- Continued.



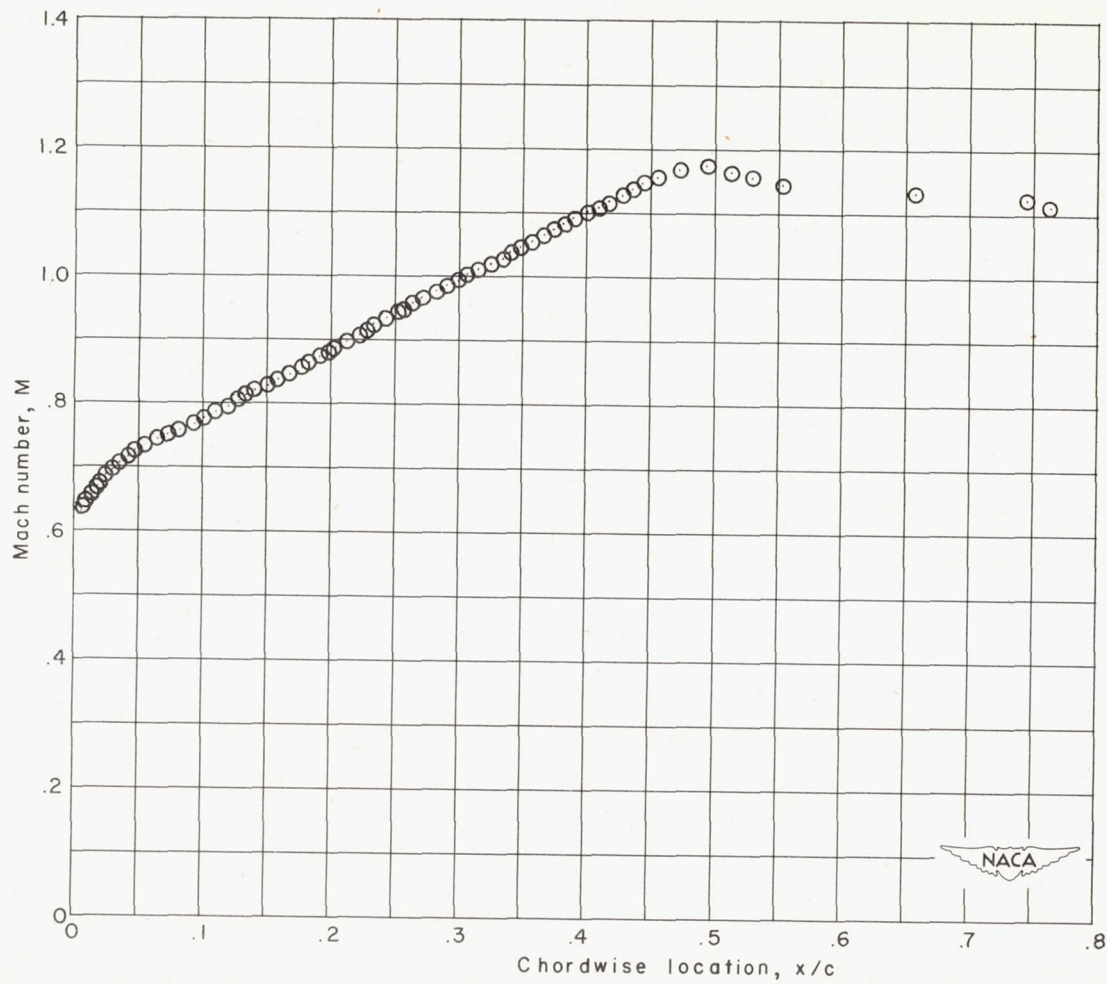
(i) $M_0 = 0.821$.

Figure 7.- Continued.



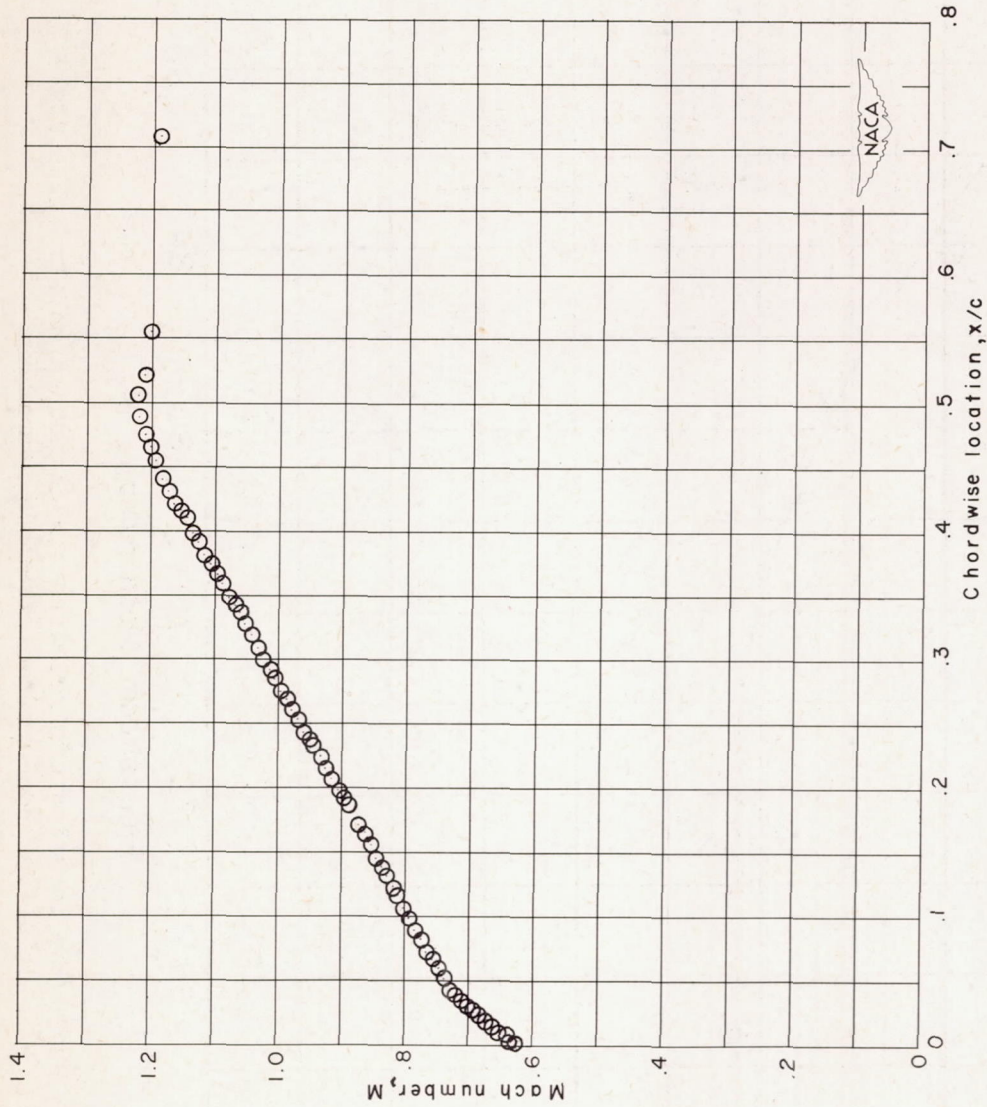
(j) $M_0 = 0.838$.

Figure 7.- Continued.



(k) $M_0 = 0.861$.

Figure 7.- Continued.



(7) $M_0 = 0.880$.

Figure 7.- Concluded.

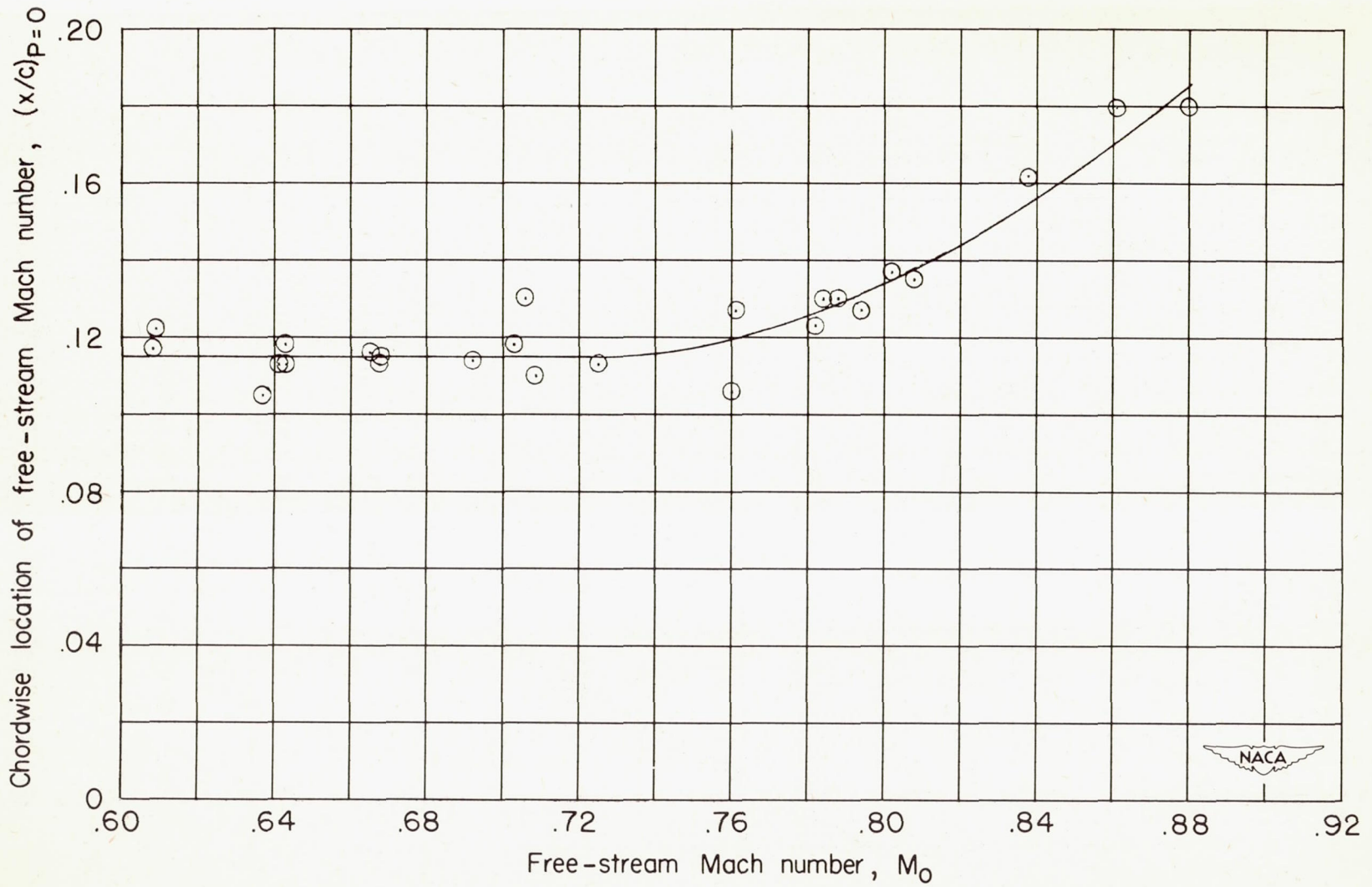


Figure 8.- Chordwise location of free-stream Mach number on airfoil surface as a function of free-stream Mach number.

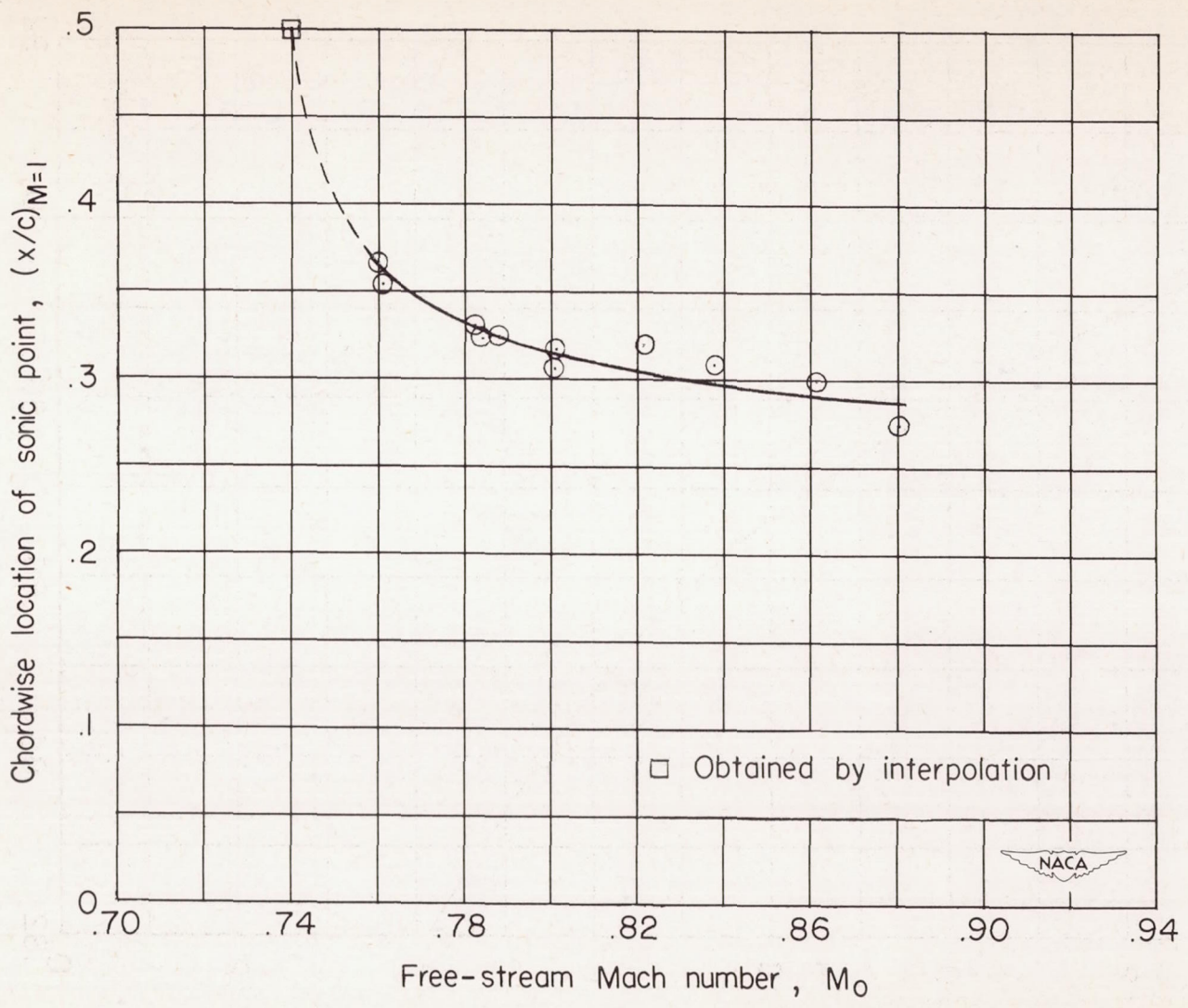


Figure 9.- Chordwise location of sonic point on airfoil surface as a function of free-stream Mach number.

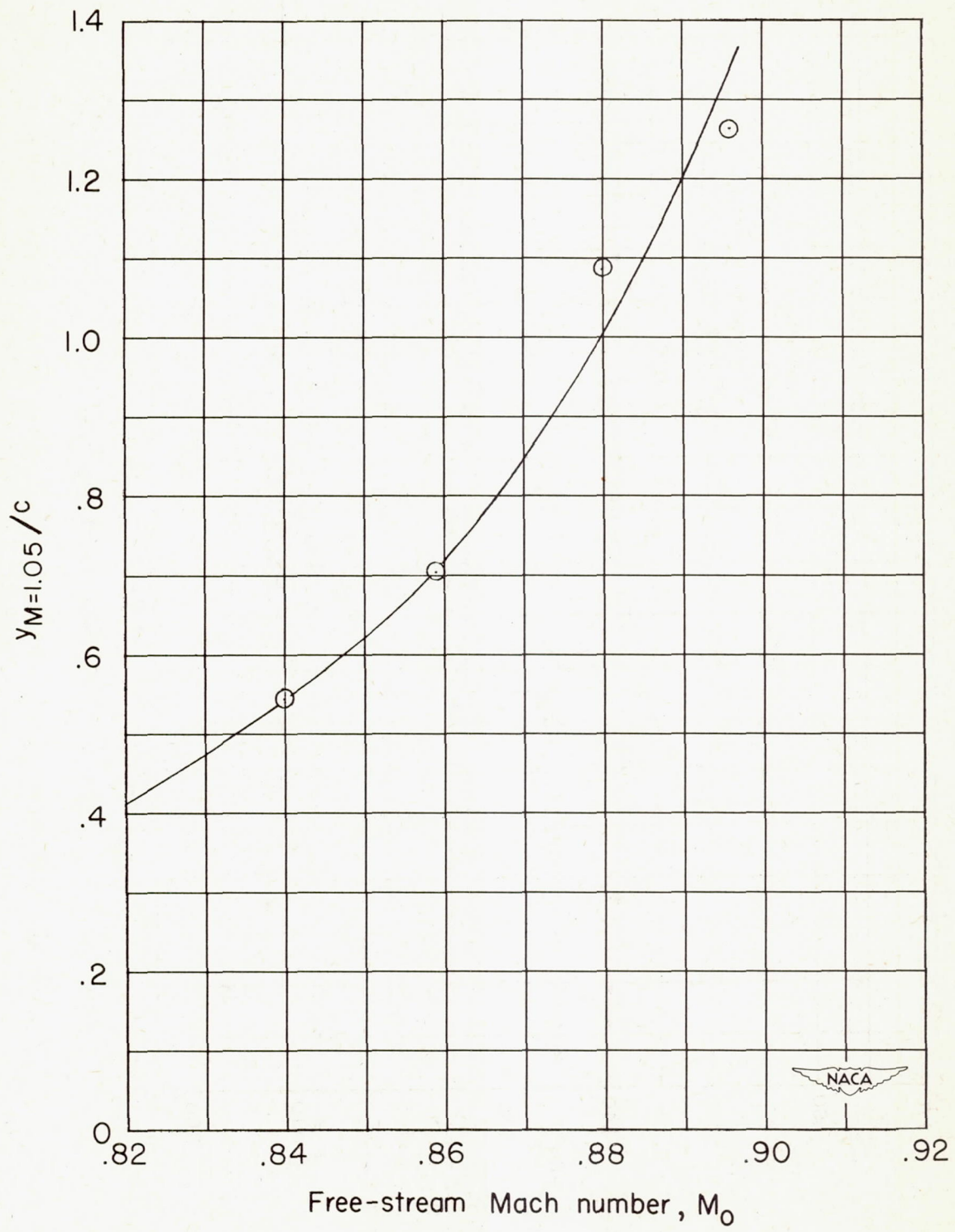
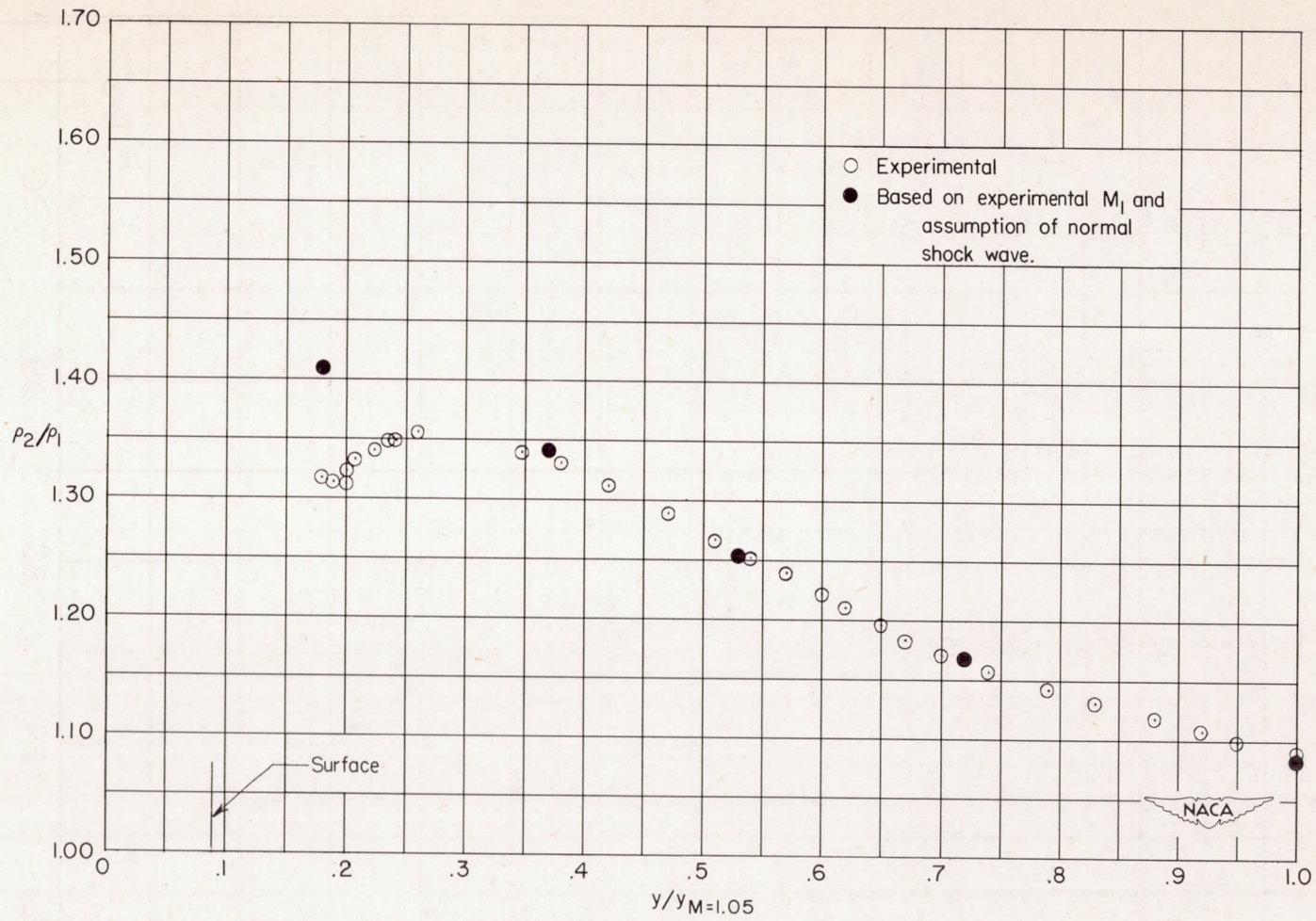
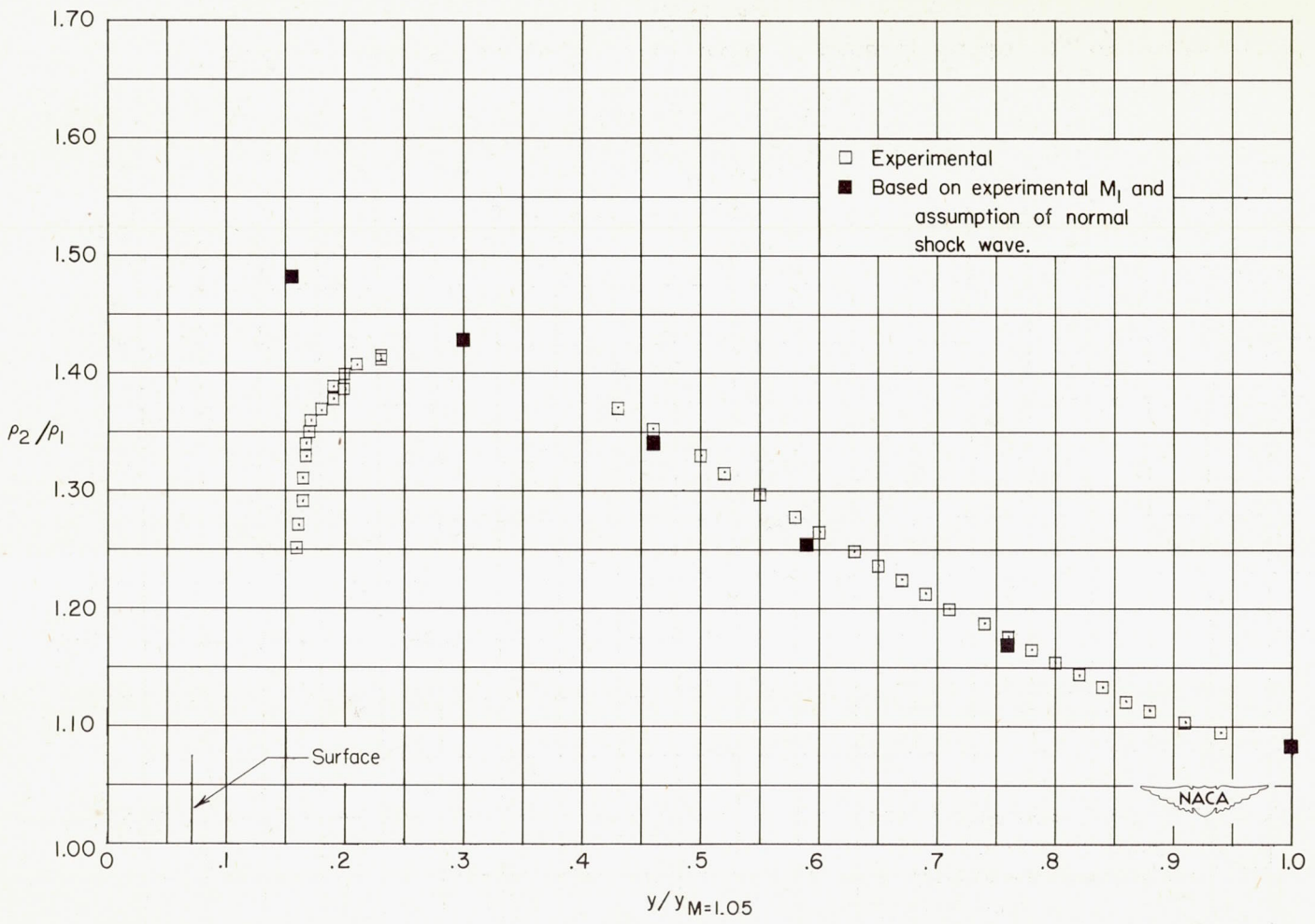


Figure 10.- Vertical distance of intersection of Mach number 1.05 contour and shock wave, measured from chord line, as a function of free-stream Mach number.



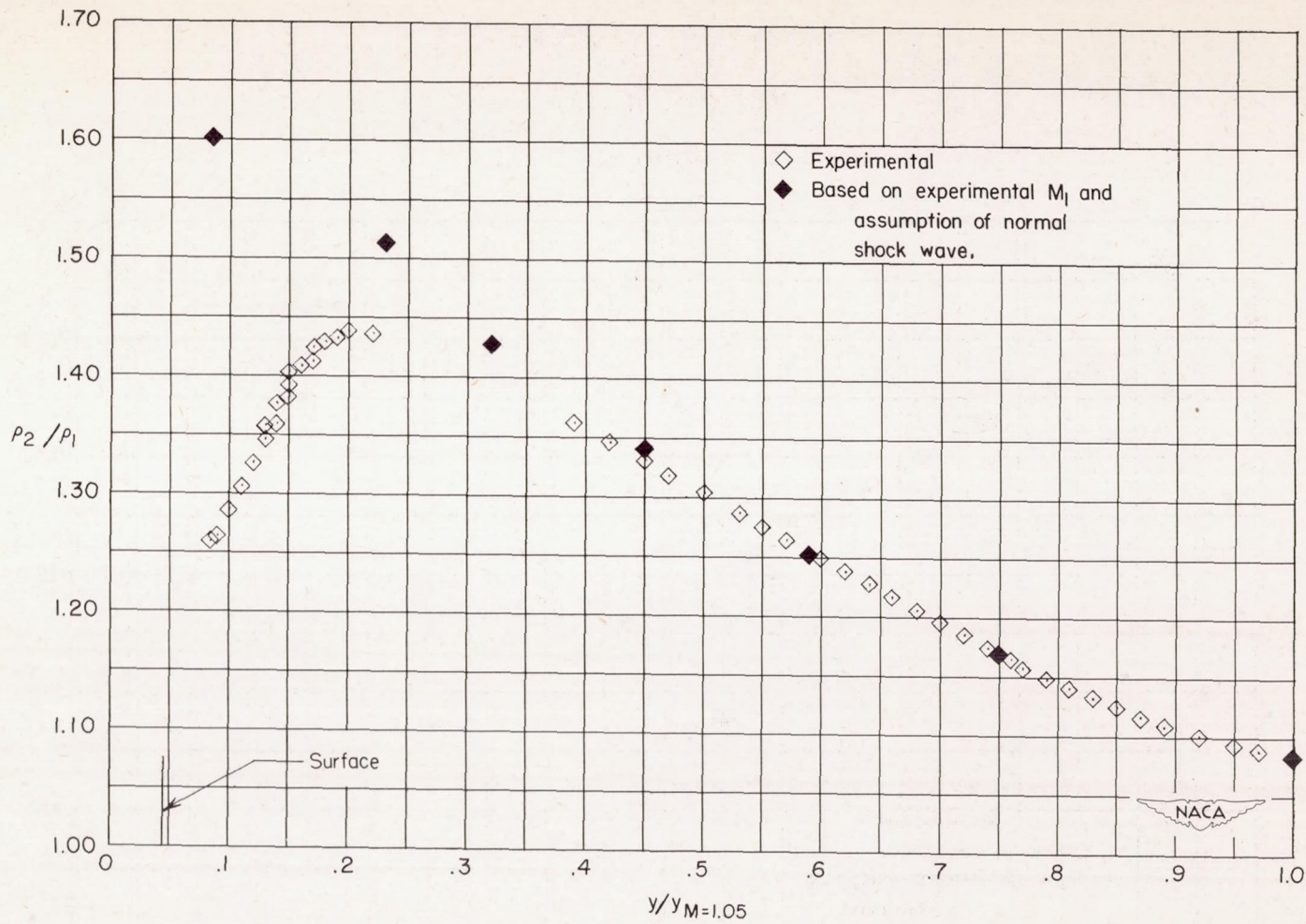
(a) $M_0 = 0.840$.

Figure 11.- Variation along shock wave of density ratio ρ_2/ρ_1 across shock wave.



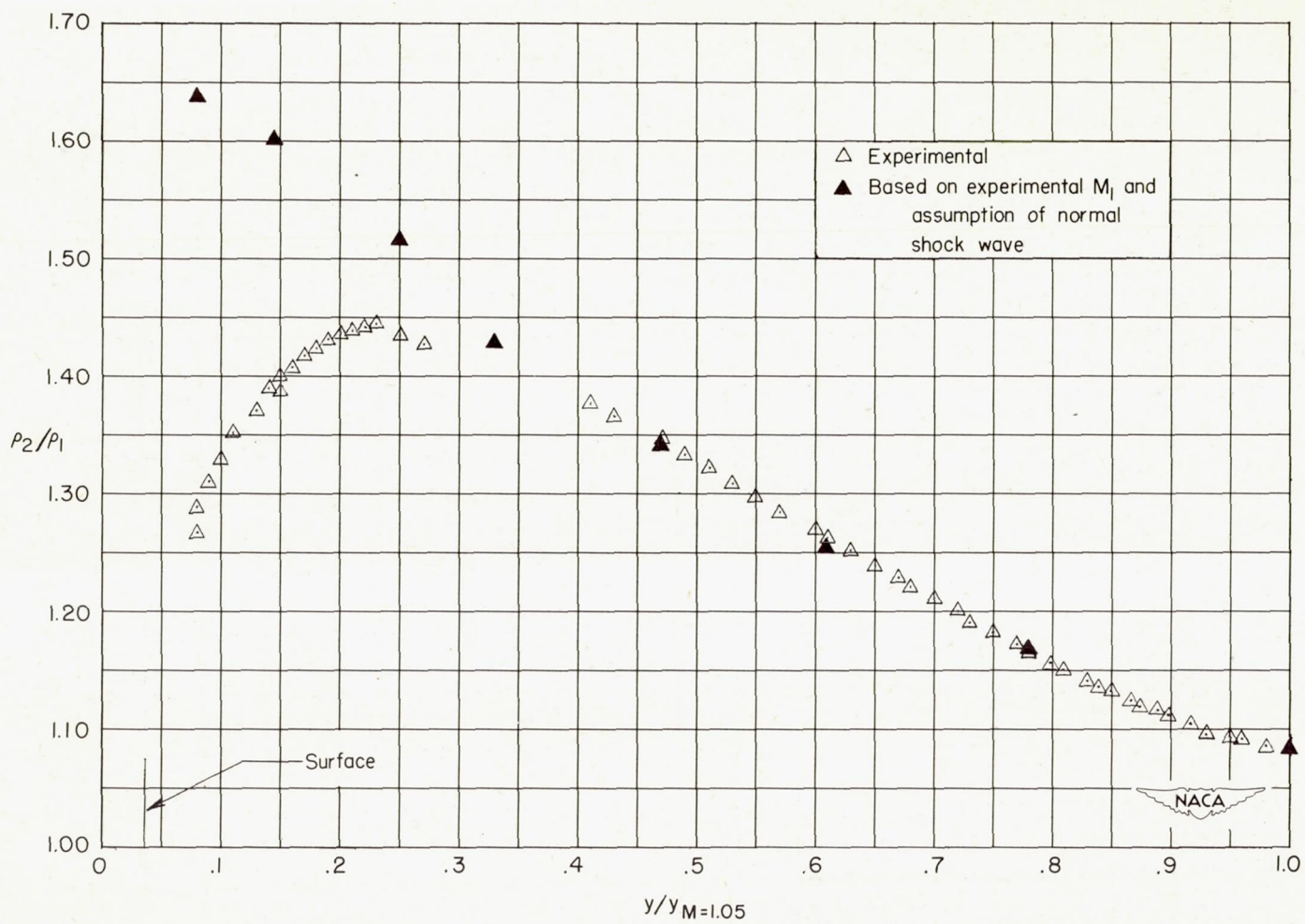
(b) $M_0 = 0.859$.

Figure 11.- Continued.



(c) $M_0 = 0.880$.

Figure 11.- Continued.



(d) $M_0 = 0.896$.

Figure 11.- Concluded.

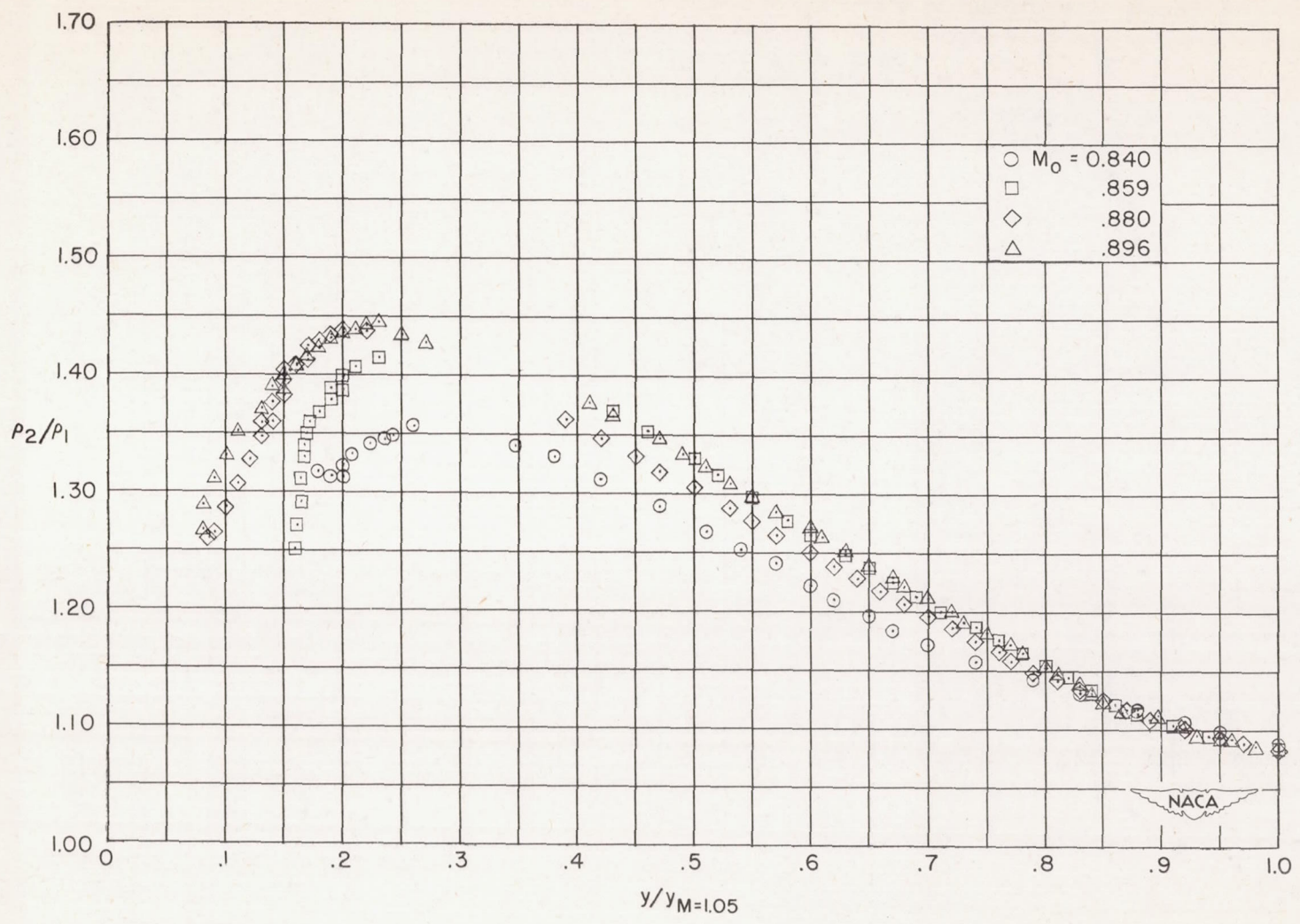


Figure 12.- Variation along shock wave of density ratio ρ_2/ρ_1 across shock wave for various free-stream Mach numbers.

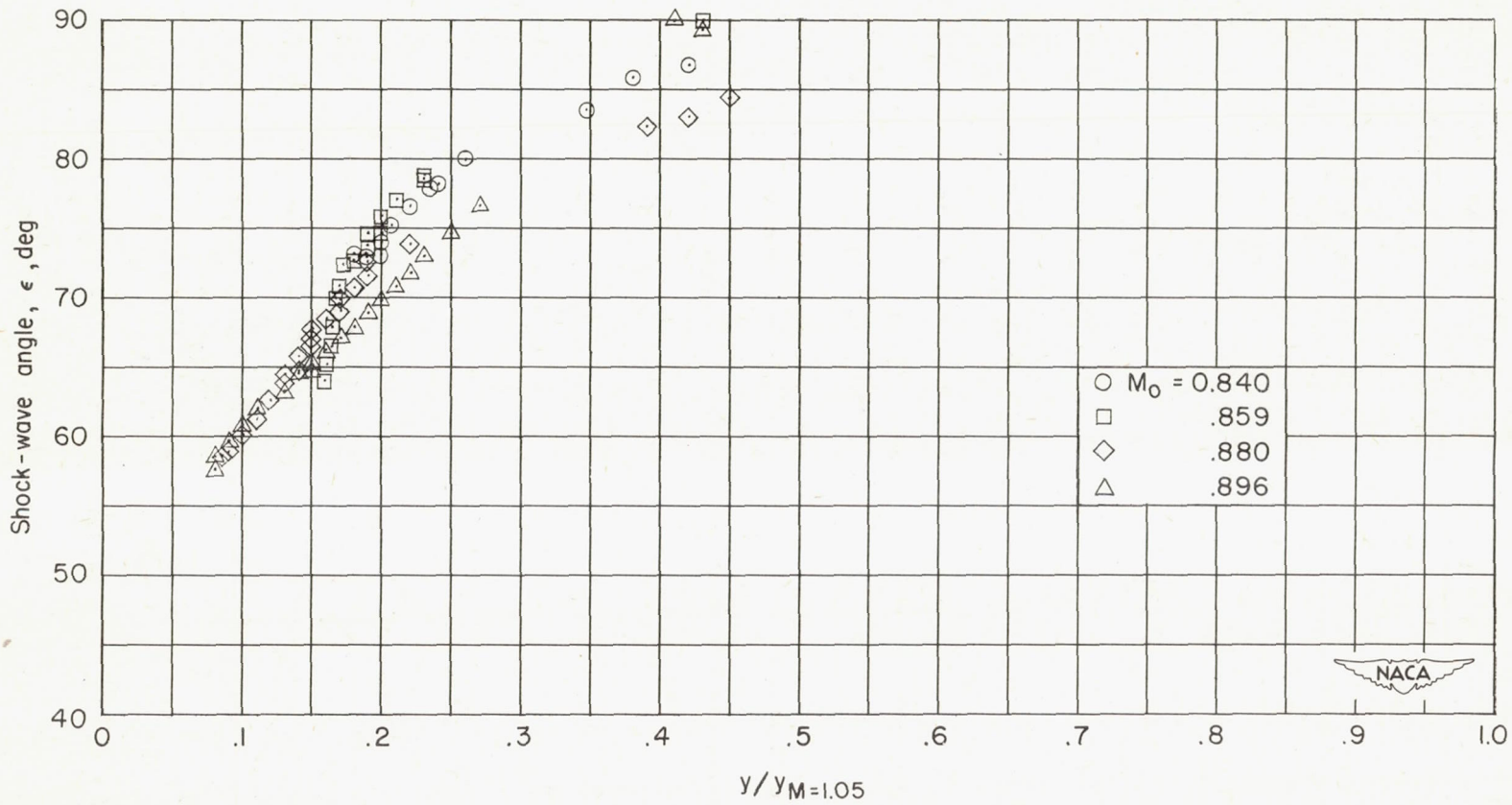
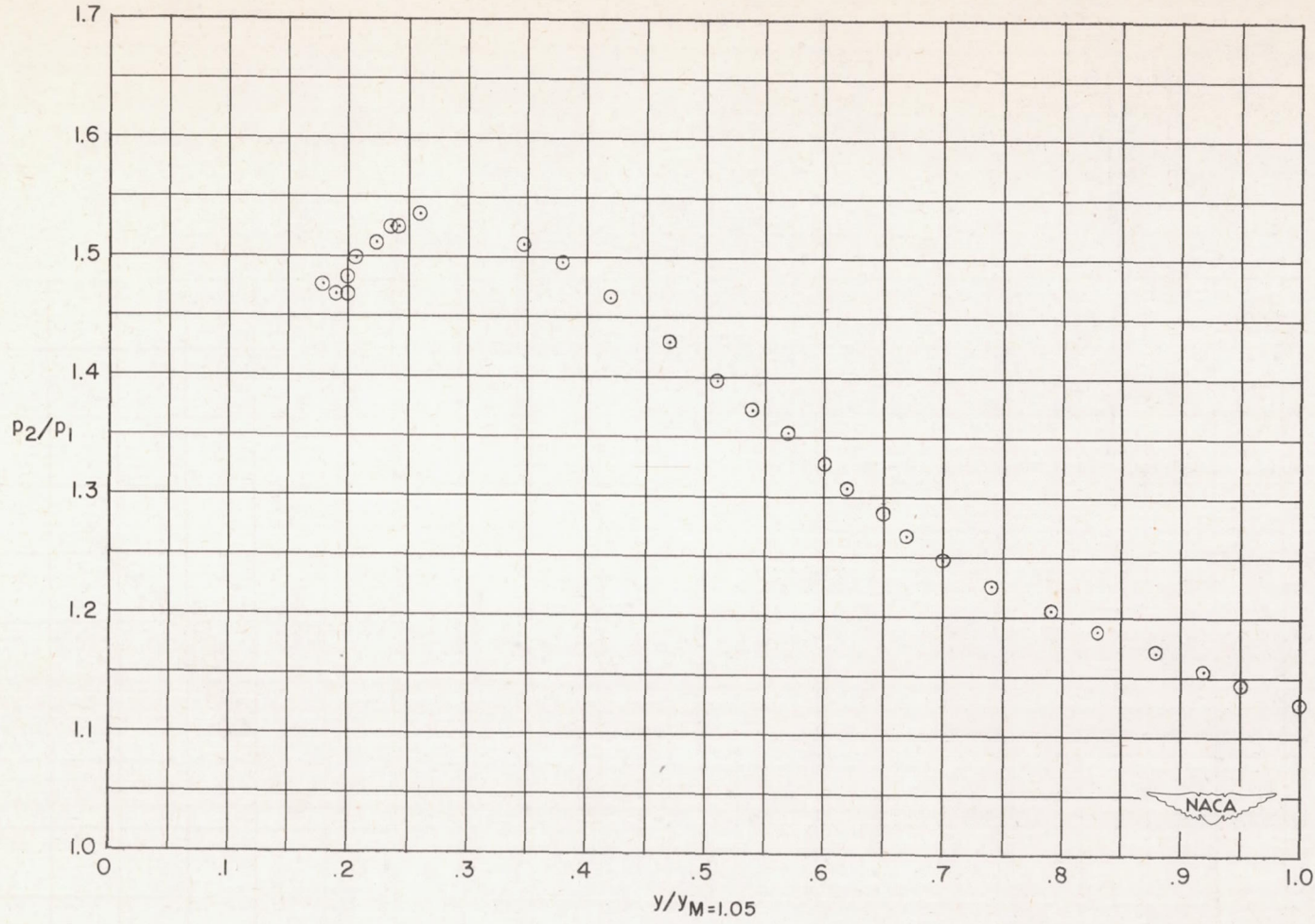
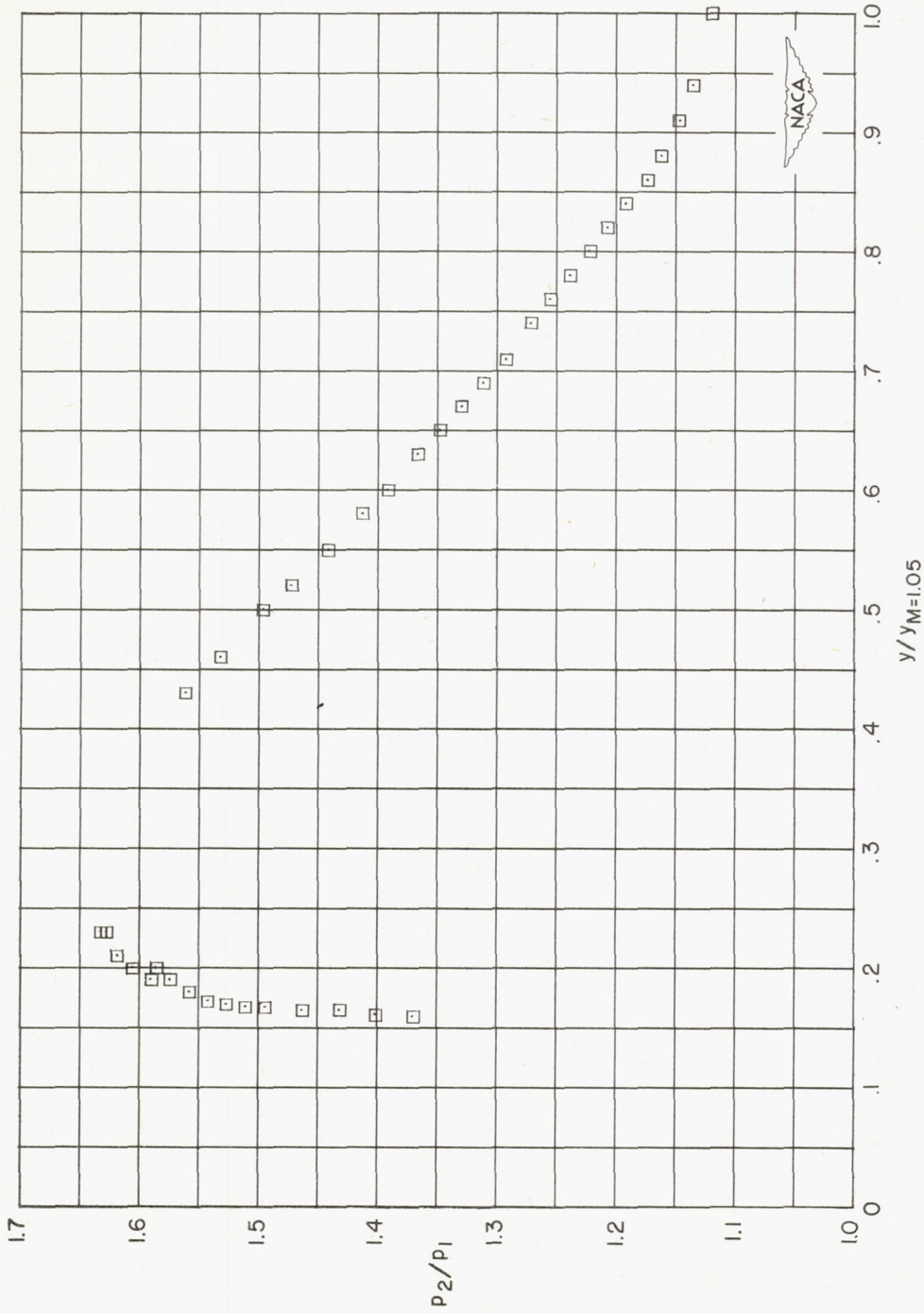


Figure 13.- Variation of calculated shock-wave angle along shock wave.



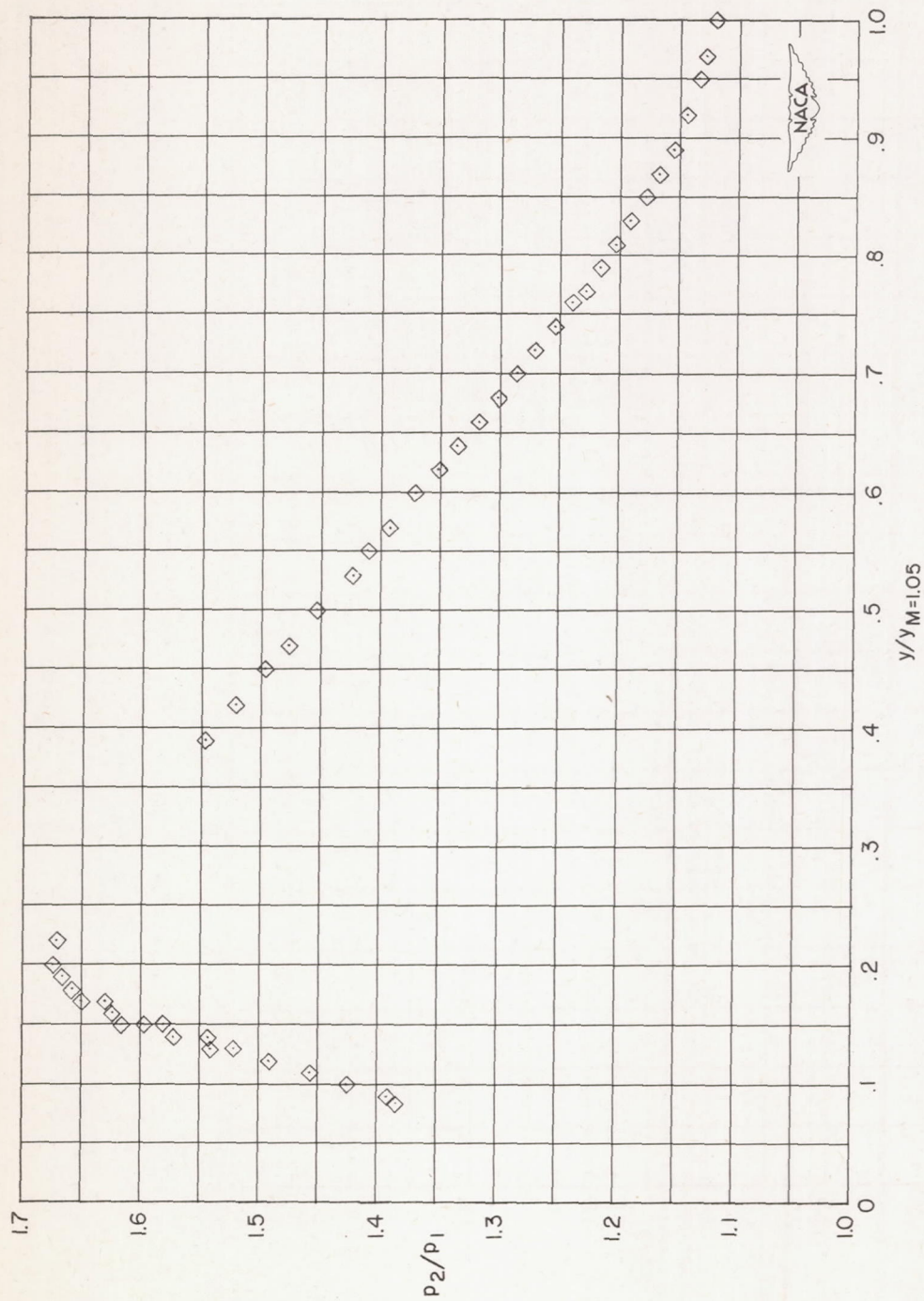
(a) $M_0 = 0.840$.

Figure 14.- Variation along shock wave of pressure ratio p_2/p_1 across shock wave.



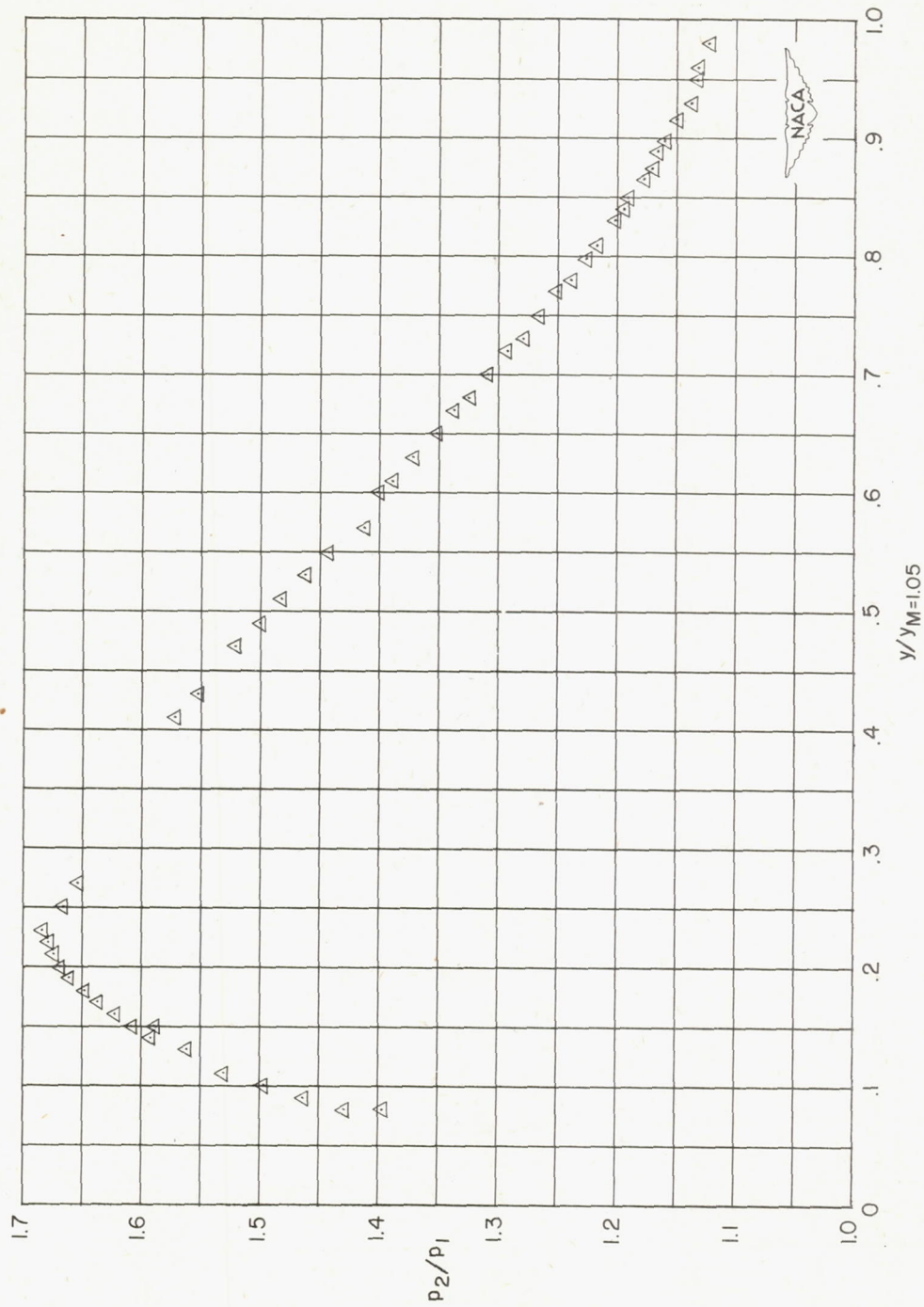
(b) $M_0 = 0.859$.

Figure 14.- Continued.



(c) $M_0 = 0.880$.

Figure 14.- Continued.



(d) $M_0 = 0.896$.

Figure 14.- Concluded.

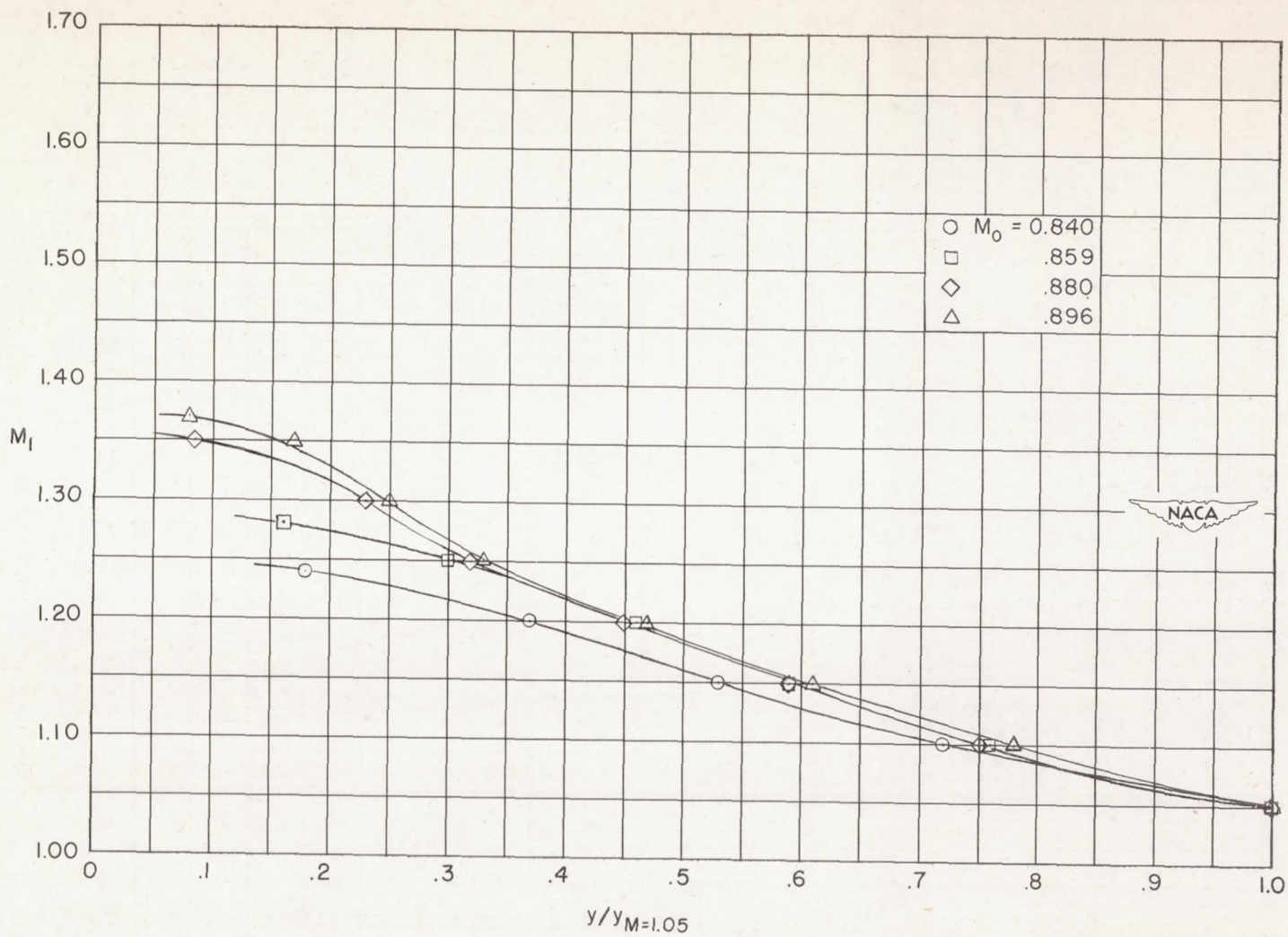


Figure 15.- Variation along shock wave of Mach number M_1 in front of shock wave.

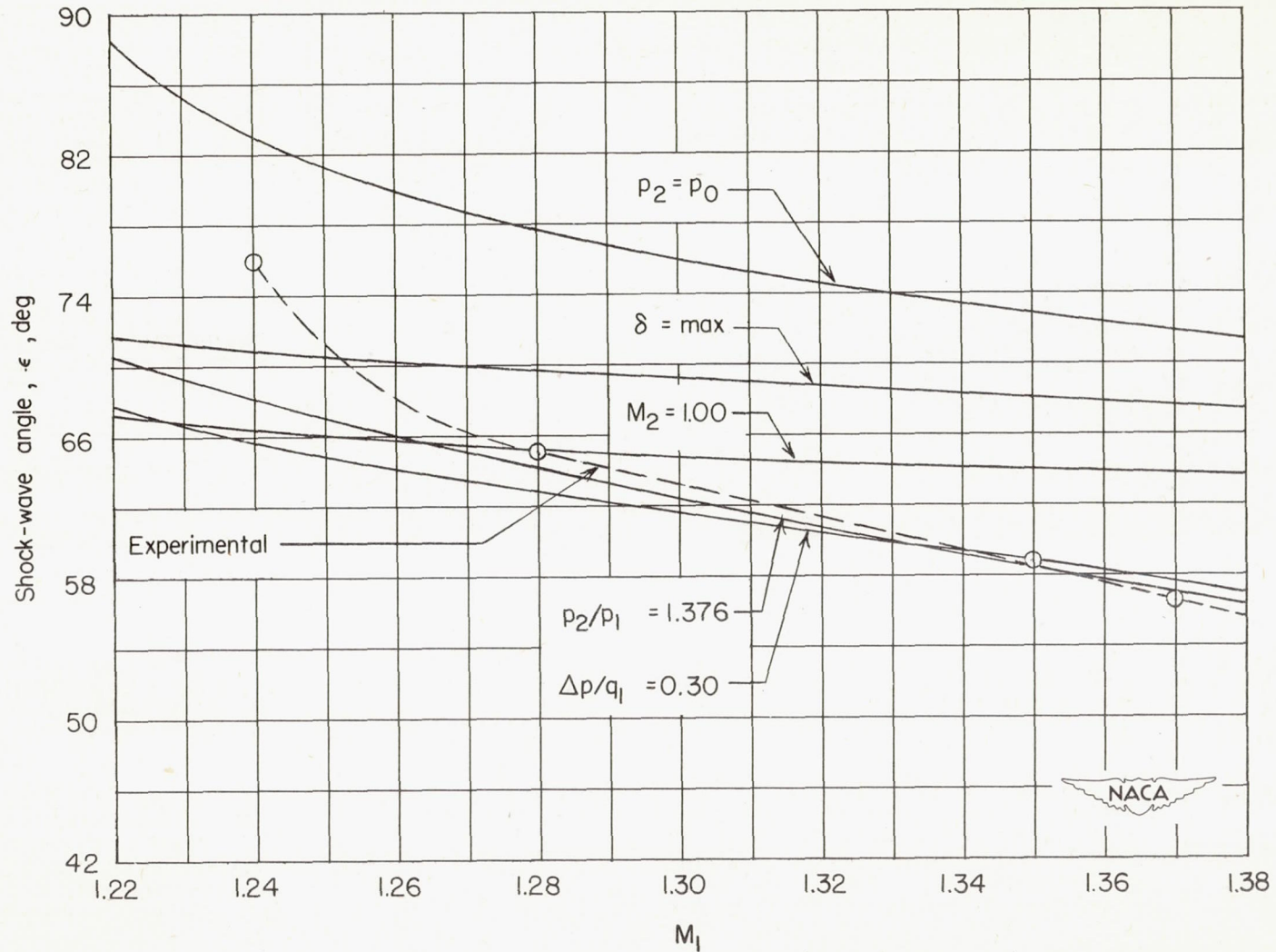


Figure 16.- Comparison of calculated results for various boundary conditions with experimental results.